Stochastic and Spatiotemporal Effects in T-Cell Signaling

by

Christopher C. Govern

B.S. in Chemical Engineering
with Minor in Applied Mathematics
University of Virginia, 2005

Submitted to the Department of Chemical Engineering in partial fulfillment of the requirements for the degree of

Doctor of Philosophy
in Chemical Engineering

at the

Massachusetts Institute of Technology

July 2011
[September 2011]

Signature of Author: _____
Department of Chemical Engineering
July, 2011

Certified by: _____
Arup K. Chakraborty
Robert T. Haslam Professor of Chemical Engineering
Professor of Chemistry and Biological Engineering
Thesis Supervisor

Accepted by: _____
William M. Deen
Carbon P. Dubbs Professor of Chemical Engineering
Graduate Officer of the Department

This doctoral thesis has been examined by a Committee of the Department of Chemical Engineering as Follows:

Professor Bernhardt Trout _____
Professor of Chemical Engineering
Committee Chair

Professor Arup Chakraborty _____
Robert T. Haslam Professor of Chemical Engineering
Professor of Chemistry and Biological Engineering
Thesis Supervisor

Professor Herman Eisen _____
Professor of Biology
Committee Member

Professor Mehran Kardar _____
Francis Friedman Professor of Physcis
Committee member

Abstract

T lymphocytes are key orchestrators of the adaptive immune response in higher organisms. This thesis seeks to apply different techniques from engineering and the physical sciences to understand how T cells balance the risks of autoimmunity and infection.

(1) What features of proteins do T cells search for that correlate with pathogenicity, distinguishing self from foreign? Two contrasting theories have emerged that attempt to describe T cell ligand potency, one based on the half-life ($t_{1/2}$) of the interaction between T cell receptors (TCR) and peptide-MHC complexes (pMHC), the second on the equilibrium affinity (K_D). We study an extensive set of TCR-pMHC interactions in CD4+ T cells which have differential K_D and kinetics of binding. The data indicate that ligands with short $t_{1/2}$ can be highly stimulatory if they have fast on-rates. Simple models suggest these fast-kinetic ligands are stimulatory because the pMHC bind and rebind the same TCR several times. Accounting for rebinding, ligand potency is K_D-based when ligands have fast on-rates and $t_{1/2}$-based when they have slow on-rates, unifying previous theories.

(2) How do T cells make optimal responses with the imperfect information they receive through their receptors? Recent experiments suggest that T cells sometimes make stochastic decisions. Biological systems without sensors and genetic diversity, such as some bacteria, make stochastic decisions to diversify responses in uncertain environments, thereby optimizing performance (e.g. growth). T cells, however, can draw on considerable environmental and genetic diversity to diversify their responses. Using T cell biology as a guide, we identify a new role for noise in such systems: it helps systems achieve complex goals with simple signaling machinery. With decision-theoretic techniques, we suggest necessary conditions for noise to be useful in this way.

(3) How can biological systems, like T cells, maintain desired responses in the presence of molecular noise, suppressing it or exploiting it as needed? We develop a semi-analytical technique to determine how small changes in the rate constants of different reactions or in the concentrations of different species affect the rate at which biological systems escape stable cellular states. A single deterministic simulation yields the sensitivities with respect to all reactions and species in the system. This helps to predict those species or interactions that are most critical for regulating molecular noise, suggesting those most promising as drug targets or most vulnerable to mutation.

These projects and others discussed in this thesis recruit techniques from random walks, statistical inference, and large deviation theory to understand problems ranging in scale from individual molecular interactions to the population of T cells acting in concert.

Acknowledgements

To the following my unprintable thanks:

For Mom and Dad, James, Kelly, Aiden, and baby-to-be.

For Carin, David, Neil, Jacob, Jools, Greg, Warefta, Gary, Daniel, Amy, Ben, Andre, Tom, Thomas, and Alex.

For Ming, Huan, Steve, Misha and Arvind.

For Mrs. Redmond and Arup Chakraborty.

For Eric Huseby, Mehran Kardar, Herman Eisen, Bernhardt Trout, Giorgio Carta and John Hudson.

For all the people who believed in me.

For all the people I believed in.

Table of Contents

Chapter 6

Chapter 1

Introduction

"seeing your bald intellect collywobbling on its feeble stem is
believing science=$(2b)^{-n}$ herr professor m"

e.e. cummings, XIX, *W [Viva]*

Nothing is like a living cell except a living cell, nor like a chemical reaction except a chemical reaction. The ability of models to elucidate biological systems is therefore necessarily limited. However, by focusing on small parts, models can suggest essential features, generating hypotheses that inform experiment. This thesis seeks to make a small progress into applying, by analogy, the techniques of the physical sciences and engineering to understand essential features of problems in biology.

The particular biological focus of this thesis is on immunology, specifically the role of T cells in immunological responses. T cells are among the key orchestrators of the adaptive immune response, tasked with identifying and clearing a diverse array of infections without causing collateral damage to self tissue (i.e. generating an autoimmune response).

1.1 Background and scope

T cells distinguish infectious agents from self tissue not by catching them in the act of being pathogenic (e.g. releasing virulent agents or high-jacking host replication machinery), but rather by scanning all proteins (protein fragments) indiscriminately, looking for features that correlate with a protein being foreign rather than self. In this respect, the T cell system is like a criminal profiling system; the infectious agents are the analogs of criminals.

Because the T cell system is based on profiling and not on direct evidence of pathogenicity, it confronts several challenges. The second and third chapters of this thesis consider two of these challenges.

First, what features of proteins can T cells search for that correlate with pathogenicity? There are no obvious structural differences between foreign and self proteins (contrary to the imagery in pharmaceutical advertisements). This question is the subject of Chapter 2.

In any case, whatever these correlative features are, they are unlikely to be perfect indicators of pathogenicity since they do not directly relate to the act of being pathogenic. The diversity of self and pathogenic proteins is so large that it likely complicates any attempt to find a feature that no self protein has but that all pathogenic proteins will always have. (This difficulty is highlighted by the inability of the innate immune system to clear all pathogens.) Furthermore, even if such features did exist, viruses mutate and evolve (sometimes, as in the case of HIV, on the time scale of the infection itself), just as criminals adapt to avoid getting profiled (e.g. screened at airports.) It is hard to imagine how correlations can be perfect against an adversarial agent.

That the correlative features are imperfect constitutes another challenge for T cells. How can T cells design an optimal response with imperfect information? When, in a criminal investigation, an enforcement agent witnesses a suspect *in flagrante delicto*, it is clear the enforcement agent should apprehend the suspect. However, when profiling based on imperfect correlation, it is not always clear how to best respond. In cases of uncertainty, law and order profiling systems typically follow a profiling step with an evidentiary step – people are profiled to be searched, but then are in fact searched, not just thrown in jail. T cells base their responses purely on the correlations. How can they best balance the risks of infection and autoimmunity? This question is the subject of Chapter 3.

The previous two challenges are faced by T cells as a profiling system. T cells also encounter challenges common to all types of cells. How do cells use the building blocks of biology (e.g. proteins) to engineer complex, sensitive, and speedy responses to diverse

inputs? Chapter 4 considers one aspect of the design of cellular signaling machinery, motivated by the work in Chapter 3 that suggests the optimal T cell response.

Finally, in Chapter 5, we consider different spatiotemporal effects in T cell signaling, extending the work of Chapter 2.

These questions span different scales of the immune system, from molecular interactions to the entire population of cells acting in concert, and recruit different techniques from the physical sciences and engineering to address them. The following sections provide more context for each question.

1.2 Correlative features in T cell profiling

Just as identifying features that correlate with guilt is an important question in criminal profiling, what features the T cell searches for in trying to uncover infection is a major question in immunology.

Addressing this question requires further details regarding the biology. T cells do not directly scan whole proteins; rather they scan protein fragments, known as peptides (p), that are presented on the surface of almost every cell in the body (1). (Why this should be the scheme is not a subject of this thesis.) Constantly, cells in the body chew up proteins that they find inside of them or that they scavenge from their environment. Misfolded proteins, for example, provide a source of proteins that the body will not miss if so chewed up, since such proteins are nonfunctional (or deleterious) anyway. The protein fragments are presented on the cell surfaces in the grooves of molecules known as MHC molecules. When the body is not infected, the peptides presented on cell surfaces are derived exclusively from self proteins, since no foreign proteins are present. However, when the body is confronting an infection, at least some of these protein fragments will be derived from the foreign pathogen, though many will still be self-derived.

A hint about what features of peptides T cells search for comes from work that has elucidated the development process of T cells. The human body generates many different T cells, each roughly with a different, randomly generated type of receptor on its surface (the T cell receptor, or TCR). It is with their TCRs that T cells "scan" peptides, as the receptors are able to bind to pMHC. The binding of pMHC and TCR is the first step in a sequence of molecular interactions (reactions) on the surface of the T cell and inside the T cell that leads to the T cell's response. In this sense, the bindings are the input to the T cell's response.

The nature of the interaction between a particular TCR and peptide depends on the unique random sequence of the TCR and the unique peptide. Specifically, the interactions can be described at a molecular scale by the kinetic parameters that govern them: the on-rate (how quickly the pMHC and TCR bind when near each other), the half life (how long they stay bound when they bind), and the equilibrium affinity (how frequently they are bound when they are nearby). (Note that only two of these three parameters are independent, as the third is a ratio of the first two.) Because of sequence diversity, different pairs of TCR and peptides have different on-rates, half-lives, and affinities of binding.

During a process in T cell development known as thymic selection, T cells serially scan many peptides that are guaranteed to be self (at least in the absence of a pathology). Those T cells that respond strongly to any of these self pMHC, because of their particular receptors and the particular combination of kinetic parameters describing their interactions with self peptides, are likely to be deleted from the host repertoire (negative selection) (2). This developmental process enables correlations between the binding features of a particular TCR and pMHC and whether that pMHC is self or foreign derived: since selection is against self, not foreign, those with TCR whose binding features to pMHC enable them to respond strongly when binding to pMHC post-selection (e.g. they bind strongly in some sense) are likely to be interacting with a foreign pMHC.

However, it has not been clear which of the three kinetic parameters that describe interactions between TCR and pMHC are actually involved in the correlation used in profiling (that is, lead to a "strong response") (3). All are plausible candidates for "strong binding" when they are large: empirically, while experiments have agreed that the binding must be strong in at least one of these senses, they have disagreed as to which sense or senses are most important; theoretically, each is supported by plausible intracellular signaling models.

Understanding how T cells profile peptides (that is, knowing which kinetic parameters actually correlate with T cell response) is important because each kinetic parameter suggests different mechanisms of intracellular signaling, fundamental knowledge which is useful in identifying drug targets, and each suggests different screening strategies for identifying immunogenic vaccines.

In the second chapter of this thesis, we utilize a new data set from Eric Huseby's lab, in concert with mechanistic models of binding events between pMHC and TCR, to try to understand which kinetic parameters correlate with T cell activation. The data set is particularly important because the variation in kinetic parameters among pMHC and TCR is significant enough to tease apart their potentially different effects when viewed in conjunction with macroscopic data on the T cell's response (e.g. T cell proliferation). (In many data sets, the different kinetic parameters have tended to trend similarly, or be constant, which has forestalled consideration of this debate; now it is clear they do not always go together).

A chief challenge in understanding how the different kinetic parameters affect T cell activation is understanding how the kinetic parameters interact with the different length and time scales that describe the cellular signaling machinery, since the signaling machinery determines the T cell's response. To do this, we constructed simple mechanistic models of the earliest stages of the T cell interaction. The models address various aspects of the interaction in space and in time. For example, the TCR and pMHC are both in membranes, diffusing through space (4). Additionally, it has been discovered

that key signaling molecules cluster on the surface of T cells (5). These length and time scales (among others) interact with length and time scales provided by the kinetic parameters to produce different responses.

In developing these models, we recruit a body of literature involved with random walks and diffusions and their properties in different dimensions. A notable fact, for example, is that a random walker (e.g. a drunkard moving randomly) will certainly return to wherever she started in one and two dimensions (on a line or in a plane), but not in three dimensions (6). (In one and two dimensions, however, the return may take, on average, forever.) This has implications for diffusing molecules on cell membranes (two dimensions) versus in the cytoplasm (three dimensions) versus on cytoskeletal filaments (one dimension). Importantly, it has implications for the problem of receptor-ligand binding on membranes, which are effectively two-dimensional on time scales shorter than membrane motion in the z-direction (4).

Finally, one practical difficulty in teasing apart the influence of different kinetic parameters using macroscopic experimental data (e.g. T cell activation) is the uncertainty about what it means for a T cell response (e.g. activation) to correlate with a particular parameter but not others. A comparison of linear fits will not do, as there is no reason to believe the response is linear in the parameters. Here we address this problem by looking for parameters whose values are one-to-one with the T cell's response. But future work will need to merge inquiries on the macroscopic scale with models of the T cell's signaling machinery more involved than those considered here in order to resolve the response at these two scales.

We demonstrate that a simple model accounting for multiple rebindings between the same pMHC and TCR can explain the new data set from Eric Huseby's lab, suggesting that fast on-rates can enable short half-life ligands to stimulate T cells. This model reconciles previous experiments suggesting that the affinity or the half-life are the most important parameters.

1.3 How T cells use imperfect information to make optimal responses

In intermediate summary, T cells look for features correlated with whether a peptide is self or foreign (the analog of "guilt" or "innocence" in criminal profiling) and one particular choice of feature they look for, empirically determined, is binding strength (a particular combination of kinetic parameters.) (Other correlative factors, not subjects of this thesis, include the number of pMHC presented on APC, their groupings into clusters, and, less specific to the interaction of a particular T cell, the cytokine environment (7, 8). In what follows, we use the generic term "stimulus" as a proxy for those features that correlate with a peptide being foreign (e.g. the activating binding kinetics.)

T cells use the information they obtain through their receptors to determine their responses. The responses of T cells include production of cytokines and T cell proliferation, which both contribute to clearing the infection. (Different types of T cells are specialized for different types of response.)

However, it is unclear how T cells should use the information, because the correlation between the stimulus (e.g. binding strength) and whether a peptide is foreign is not perfect, for reasons mentioned in Section 1.1. In addition, the details of the biology make it clear that the system by which T cells measure the correlative features is not perfect, introducing further uncertainty. Some T cells escape thymic selection, so that there are auto-reactive T cells in the periphery (9); and, because of limited resources (e.g. the amount of time allowed to scan the pMHC, the numbers of pMHC and TCR) there is some randomness in the stimulus a T cell receives when it scans another cell.

Thus, individual T cells face uncertainty about whether the pMHC they engage is really self or foreign. What should T cells do in cases of uncertainty? For example, T cells could balance this uncertainty by gradually increasing the magnitude of their response (e.g. gradually releasing more cytokines) as the likelihood the pMHC is foreign increases (that is, as the stimulus strength increases; see the discussion on thymic selection). However, recent experiments suggest that T cells make digital decisions about whether to

activate, at least as indicated by early markers of T cell signaling. That is, a given T cell is either fully active or fully inactive (e.g. there is a jump in cytokine release between the two states; though, as noted later, the decision may be stochastic) (10).

Another way to handle their uncertainty, given that they are constrained to either activate or not, is for T cells to err on the side of always activating whenever there is any uncertainty, and thereby protect against infection. But then they would frequently erroneously activate against self pMHC, potentially leading to autoimmune responses. However, if they took the opposite approach and never activated in such uncertainty, infections would sometimes spread unchecked. With imperfect information, there is no way for T cells to completely eliminate both the risk of infection and autoimmunity. Like a criminal justice system attempting to balance letting a criminal go free or an innocent go to jail, the T cell system must utilize the information on hand to delicately balance the risks of autoimmunity and infection. (This balancing is known as searching for Pareto optimal solutions.)

In the second chapter of the thesis, we consider two different ways T cells could balance (or "hedge") these risks. One possibility is that they could always activate whenever the stimulus exceeds some threshold (and thus the uncertainty favors it being foreign) and never activate below the threshold (the uncertainty favors it being self). Indeed, this seems to be a natural interpretation of the dictum that "strong stimuli" are correlated with foreign pMHC. Alternately, the probability a T cell activates could gradually increase form never activating for weak stimuli to always activating at strong stimuli; for intermediate stimuli, they would only sometimes activate (essentially flipping a coin). At an essential level, the difference between these two approaches is that the first is deterministic and the second is stochastic (random).

Interestingly, recent experiments suggest that T cells make their decisions in the second of these two ways (7, 10-12). For intermediate stimuli, they make stochastic, not deterministic, decisions. In the third chapter of this thesis, we try to understand the role of stochastic decisions in balancing the risk of autoimmunity and infection in the T cell

population. (How would the public respond if law enforcement sometimes arrested and sometimes did not when the same correlative features were present – and if they made this decision by flipping a coin? It is as though some T cells expended resources to measure the stimulus and then decided to discard information in the stimulus to make a stochastic decision anyway.)

The role of stochastic decisions in the T cell population has implications for more than just T cell biology directly, as it touches on a larger discussion in the literature about the role of stochasticity or randomness in biological systems (13). Randomness is ubiquitous at the molecular level of biological systems (14). Molecules move about randomly, buffeted by collisions with other molecules and with water (the random walks referred to in Section 1.2), and they bind and rebind randomly, due to these same thermal sources (15). Furthermore, concentrations of key molecules fluctuate from cell-to-cell (due to randomness, e.g., in transcription and translation processes) (16). Since biology often occurs with small number of molecules over finite times, these effects do not always average out on relevant scales. Thus, randomness at the molecular scale can manifest itself at the cellular scale, for example in stochastic decisions made by T cells.

Historically the manifestation of stochasticity at the cellular scale was considered deleterious, much as randomness in the function of engineered systems like computers is usually considered deleterious. Over the past several decades, however, researchers have begun to recognize constructive roles for noise in biological systems. It is in this latter spirit that we investigate whether stochasticity is beneficial for the T cell system.

Stochastic decisions also touch on literature in a variety of fields concerned with how humans should make decisions based on data, including decision theory, statistical inference, game theory, information theory, and economics. (John Nash won the Nobel Prize in part for showing that there is always an optimal strategy in a particular class of games so long as one is willing to sometimes flip a coin.) It is a testament to how confusing stochastic decisions can be that practical advice often counsels against making

a stochastic decision, even when it is optimal, since it can be hard to explain if the eventual decision turns out to be incorrect (17).

Connections between these applied fields and biological systems are in some ways still in their infancy (18), though potentially rich as interest in biological decision-making grows. We attempt to apply the techniques from the disciplines related to decision theory to understand stochastic decisions in a biological context, while respecting the unique features of biological systems.

One challenge in applying knowledge from these fields to biology is that much statistical inference is based on heuristics or assumptions. While these may be appropriate to understanding experimental data in the absence of alternatives, they are not necessarily applicable to the decisions biological systems make themselves (or we know too little about the biology to know what heuristics are appropriate). What is interesting in the biological context is to see what can be said qualitatively, independent of such unknown features. The problem of T cell stochastic decisions is such a qualitative problem in the field of biological decisions, and so it is an interesting problem to consider in terms of connection to these fields.

By studying T cell decisions, we find a new role for noise in complex biological systems. Stochastic decisions by individual components (T cells) allow the interacting population to achieve complex goals with simpler biochemical machinery (e.g., a simpler signaling network) than would be required to implement a deterministic response which achieves the same performance. This contrasts with the role of stochaticity in diversifying decisions in previously studied systems.

1.4 Sensitivity analysis of reaction networks

Previous sections have taken for granted T cells' ability to process information they obtain through their receptors to carry out cellular-scale responses. We have assumed,

for example, that machinery exists that can translate and transduce the binding of TCR-pMHC into activation.

Just as the building blocks of computers are circuits, the building blocks of cellular machinery are individual molecules (e.g. proteins, small molecules like calcium). Different molecules can interact with each other, binding and unbinding, modifying each other, and changing each other's conformation to expose or occlude functional surfaces. Work over the past several decades has shown how these simple interactions between molecules can achieve complex responses when they are incorporated in networks. In fact, it has been shown, for example, that gene transcription networks are capable of recapitulating the fundamental logical operations (like computers), so that any response is possible in principle (19).

Intriguingly, these biological machines function in the presence of randomness in the building-block molecular interactions, as described in Section 1.3. They are able to suppress noise to maintain stable cellular states or produce consistent responses to inputs; or, as in the previous section, they are able to constructively exploit noise to enable transitions between stable states or stochastic responses to inputs. Suppressed or exploited, the noise is controlled to enable biological function. Given that the randomness is so prevalent at the molecular scale, how is it controlled?

Previous work has uncovered qualitative design features of networks that affect their noise transmission properties (20, 21). In Chapter 4, we adopt a more empirical approach, complementing this theoretical work. That is, for given cellular signaling networks we seek to develop a procedure that identifies the particular reactions and species in that network that are most crucial in regulating stochastic transitions away from a stable cellular state – either to another stable cellular state or to (perhaps undesirable) distant states. These reactions and species are those that are most vulnerable to mutation (as in cancers) or most promising as drug targets.

If Chapter 3 is concerned with how unpredictable cellular signaling networks can be – T cells sometimes make stochastic decisions -- Chapter 4 is concerned with how surprisingly predictable they can be. Exactly when a transition occurs is quite unpredictable (up to a distribution), and whether it occurs in a biologically relevant time is unpredictable as a result. However, how the transition occurs when it occurs -- the particular sequence of reactions by which it occurs -- is often very predictable. This knowledge can be exploited to understand different properties of the transition, including how different reactions and species affect the expected time of the transition.

The methods by which such predictions can be made fall under the study of large deviation theory (LDT). Large deviation theory extends the results of the central limit theorem and the law of large numbers (22). The law of large numbers states, roughly, that sample averages converge to expectations; the central limit theorem describes how quickly this happens at the limit of large sample size. Large deviation theory describes how quickly the convergence happens at slightly smaller, but still large, sample size (that is, near the tails of distributions, where they converge most slowly.)

In networks of chemical reactions, what is often large is the number of molecular interactions required to change the state significantly ("large" and "significantly" must be more carefully defined.) In Chapter 4, we exploit an application of LDT to networks of chemical reactions in order to predict how the systems' ability to suppress or control noise is affected by perturbing the number of each type of species in the system or the rate constant of each reaction type. This approach leads to a semi-analytical formula. With this formula, only one deterministic simulation is required to determine the sensitivity of the transition time on all of the species and reactions in the system. We further exploit the semi-analytical nature of the formula to make qualitative conclusions about reactions that are important in regulating stochastic transitions.

1.5 Summary

This introduction has sought to situate the different projects constituting this thesis in the context of T cell immunology, which theme unifies them. The results, particularly those of Chapters 3 and 4, have a broader impact in the fields of biology and theoretical chemistry. The respective chapters introduce them in this context.

Chapters 2 through 4 span three different biological problems at three different scales of the immune system. In Chapter 2, we zoom in to the molecular level of interactions between individual molecules (TCR and pMHC). In Chapter 3, we focus on the population of T cells acting in concert. Finally in Chapter 4, we look at an intermediate scale, networks of chemical reactions.

The projects recruit three different techniques from engineering and physical sciences: random walks and diffusions (chapter 2), decision theory and statistical inference (chapter 3), and large deviation theory (chapter 4).

These different areas of inquiry present broad ideas for further study. Such ideas are explored in the conclusion. However, some of these ideas have already been explored as part of this thesis, but have been omitted from the main narrative flow. Chapter 5 contains two projects related to spatiotemporal aspects of signaling (which was also exploited in Chapter 2.)

1.6 Statement of Collaborations

Chapter 2 was the result of a close collaboration with Prof. Eric Huseby at the University of Massachusetts Medical School. All experimental results are from work in his lab. Theoretical results have been obtained jointly with him. The write up of this work was completed with him.

Chapter 4 was the result of another close collaboration with Ming Yang, a fellow Ph.D. student with Arup Chakraborty. The results in that chapter are all joint with him. The write up of the work was completed with him.

The work on T cell memory referenced in Chapter 5 was predominantly conducted by Jayajit Das, a postdoc with Arup Chakrabroty, and his experimental collaborators. The small part explicitly discussed in that chapter constitute my contribution to that endeavor.

References

1. Murphy K, Travers P, & Walport M (2007) *Janeway's Immunobiology* (Garland Science) 7 Ed.
2. Palmer E (2003) Negative selection - Clearing out the bad apples from the T-cell repertoire. *Nat. Rev. Immunol.* 3(5):383-391.
3. Stone JD, Chervin AS, & Kranz DM (2009) T-cell receptor binding affinities and kinetics: impact on T-cell activity and specificity. *Immunology* 126(2):165-176.
4. Bell GI (1978) Models for specific adhesion of cells to cells. *Science* 200(4342):618-627.
5. Lillemeier BF, *et al.* (2009) TCR and Lat are expressed on separate protein islands on T cell membranes and concatenate during activation. *Nat Immunol* 11(1):90-96.
6. Redner S (2001) *A guide to first-passage processes* (Cambridge University Press, New York).
7. Busse D, *et al.* (2010) Competing feedback loops shape IL-2 signaling between helper and regulatory T lymphocytes in cellular microenvironments. *Proc. Natl. Acad. Sci. U. S. A.* 107(7):3058-3063.
8. Malek TR (2008) The biology of interleukin-2. *Annu Rev Immunol* 26:453-479.
9. Mueller DL (Mechanisms maintaining peripheral tolerance. *Nat. Immunol.* 11(1):21-27.
10. Das J, *et al.* (2009) Digital Signaling and Hysteresis Characterize Ras Activation in Lymphoid Cells. *Cell* 136(2):337-351.
11. Feinerman O, Veiga J, Dorfman JR, Germain RN, & Altan-Bonnet G (2008) Variability and robustness in T cell activation from regulated heterogeneity in protein levels. *Science* 321(5892):1081-1084.
12. Altan-Bonnet G & Germain RN (2005) Modeling T cell antigen discrimination based on feedback control of digital ERK responses. *PLoS. Biol.* 3(11):1925-1938.
13. Raj A & van Oudenaarden A (2008) Nature, Nurture, or Chance: Stochastic Gene Expression and Its Consequences. *Cell* 135(2):216-226.
14. Swain PS, Elowitz MB, & Siggia ED (2002) Intrinsic and extrinsic contributions to stochasticity in gene expression. *Proc. Natl. Acad. Sci. U. S. A.* 99(20):12795-12800.

15. Gillespie DT (1977) Exact stochastic simulation of coupled chemical-reactions. *J. Phys. Chem.* 81(25):2340-2361.
16. Choi PJ, Cai L, Frieda K, & Xie S (2008) A stochastic single-molecule event triggers phenotype switching of a bacterial cell. *Science* 322(5900):442-446.
17. Resnik MD (1987) *Choices: An Introduction to Decision Theory* (University of Minnesota Press, Minneapolis).
18. Perkins TJ & Swain PS (2009) Strategies for cellular decision-making. *Mol. Syst. Biol.* 5:15.
19. Buchler NE, Gerland U, & Hwa T (2003) On schemes of combinatorial transcription logic. *Proc. Natl. Acad. Sci. U. S. A.* 100(9):5136-5141.
20. Thattai M & van Oudenaarden A (2002) Attenuation of noise in ultrasensitive signaling cascades. *Biophys. J.* 82(6):2943-2950.
21. Lestas I, Vinnicombe G, & Paulsson J (2010) Fundamental limits on the suppression of molecular fluctuations. *Nature* 467(7312):174-178.
22. Touchette H (2009) The large deviation approach to statistical mechanics. *Phys. Rep.-Rev. Sec. Phys. Lett.* 478(1-3):1-69.

Chapter 2

"Fast on-rates allow short dwell time ligands to activate T cells" [1]

"We have the idea that our hearts, once broken, scar over with
an indestructible tissue that prevents their ever breaking again
in quite the same place; but as Sammy watched Joe,
he felt the heartbreak of that day in 1935 when
the Mighty Molecule had gone away for good."

Michael Chabon, *The Amazing Adventures of Kavalier and Clay*

Two contrasting theories have emerged that attempt to describe T cell ligand potency, one based on the half-life ($t_{1/2}$) of the interaction, the second on the equilibrium affinity (K_D). Here we have identified and studied an extensive set of TCR-pMHC interactions in CD4+ cells which have differential K_D and kinetics of binding. Our data indicate that ligands with short $t_{1/2}$ can be highly stimulatory if they have fast on-rates. Simple models suggest these fast-kinetic ligands are stimulatory because the pMHC bind and rebind the same TCR several times. Rebinding occurs when the TCR-pMHC on-rate outcompetes TCR-pMHC diffusion within the cell membrane, creating an "aggregate $t_{1/2}$" that can be significantly longer than a single TCR-pMHC encounter. Accounting for aggregate $t_{1/2}$, ligand potency is K_D-based when ligands have fast on-rates and $t_{1/2}$-dependent when they have slow on-rates. Thus, TCR-pMHC on-rates allow high affinity, short $t_{1/2}$ ligands to follow a kinetic proofreading model.

2.1 INTRODUCTION

T cell receptors (TCRs) expressed on T cells bind host-MHC proteins presenting both self and foreign pathogen-derived peptides (pMHC). Depending on the signal emanating

[1] This work has appeared in the Proceeding of the National Academies of Science as "Fast on-rates allow short dwell time ligands to activate T cells" (C. C. Govern, M. K. Paczosa, A. K. Chakraborty, E. S. Huseby, *Proc. Natl. Acad. Sci. U. S. A.* **107**, 8724 (2010)). Experimental results in this chapter are from Eric Huseby's lab.

from these interactions, diverse biological outcomes ensue. In the thymus, these TCR-pMHC mediated signals shape the specificity of the mature T cell repertoire and prevent overtly self-reactive T cells from escaping (1). In the periphery, naïve T cells require continual TCR engagement with self-pMHC complexes to receive a homeostatic survival signal, while engagements with foreign peptides induce rapid T cell division and the acquisition of effector functions (2). How T cells interpret the interaction between their TCR and pMHC ligand leading to these different biological outcomes is greatly debated.

Two competing models of T cell activation have been proposed, with ligand potency being a function of TCR-pMHC equilibrium affinity (K_D) (3-7) or half-life ($t_{1/2}$) (8-11). Evidence supporting K_D-based receptor occupancy models of TCR signaling comes from sets of ligands which show a correlation between K_D and ligand potency (3, 5) and from the fact that ligands induce qualitatively distinct biological outcomes depending upon their concentration (12).

In sharp contrast to receptor occupancy models, $t_{1/2}$-based kinetic proofreading models hypothesize that TCR must be engaged long enough to complete a series of signaling events, including co-receptor recruitment and TCR phosphorylation (13). Increases in the $t_{1/2}$ of the TCR-pMHC engagement raise the probability that any single TCR-pMHC engagement will surpass the threshold amount of time required to initiate T cell activation (14). Recently this threshold amount of time has been predicted to be at least 2 sec (9, 15). Whether there is, in addition, an optimal $t_{1/2}$ that balances these kinetic proofreading requirements and the serial triggering of TCRs has been debated (16, 17)

Further evidence supporting $t_{1/2}$-based kinetic proofreading models arises from the discovery of antagonist pMHC ligands (18). TCR antagonists induce partial but not complete phosphorylation of the TCR complex and fail to fully activate T cells at any ligand concentration (18). The subsequent discovery that antagonist ligands bind TCRs with shorter $t_{1/2}$ than stimulatory agonist-pMHC complexes further suggests that activating ligands must engage a specific TCR for a long enough period of time to allow a series of signaling events to occur (19, 20).

As compelling as the arguments are for $t_{1/2}$-models of T cell activation, discoveries of highly potent T cell ligands with short $t_{1/2}$ suggest that T cell activation may not be solely dependent on the dwell time (4-6, 21, 22). In an attempt to reconcile why neither K_D nor $t_{1/2}$ fully predicts ligand potency, we have identified low, medium and high potency T cell ligands which have medium and fast binding kinetics. The potency of these ligands fails to be described by either a K_D or $t_{1/2}$-based model. By mathematically modeling the biophysical mechanisms leading to T cell activation using standard assumptions, our results indicate that fast on-rates allow individual TCRs to bind and rebind rapidly to the same pMHC several times prior to diffusing away. The rebindings lead to aggregate $t_{1/2}$ that can be significantly longer than individual TCR-pMHC interactions. Importantly, ligand potency correlates closely with this aggregate $t_{1/2}$ regardless of whether the ligands have fast or slow on-rates or $t_{1/2}$. These findings demonstrate that K_D and $t_{1/2}$ models of T cell activation are not mutually exclusive, since both emerge from an aggregate $t_{1/2}$ model. In particular, the aggregate $t_{1/2}$ depends on the $t_{1/2}$ or K_D alone when on-rates are low or high, respectively. Aggregate $t_{1/2}$ allows strong K_D /fast binding kinetic ligands to follow a kinetic proofreading model of activation.

2.2 RESULTS

2.2.1 Identification of high, medium and low K_D TCR – pMHC interactions with fast rates of association and disassociation

During our previous study of TCRs specific for IA^b/3K, we noticed that several of these TCRs bound IA^b/3K with strong K_D using very fast binding kinetics (22, 23). However, because some of the off-rates were exceptionally fast, with loss of all specific binding for some occurring in less than 1 sec, the original measurement had a significant error range. Using surface plasmon resonance focusing on obtaining TCR-pMHC disassociation rates, we measured the binding kinetics of the B3K506 and B3K508 TCRs interacting with the previously reported and additional IA^b/3K APLs (Fig. 1).

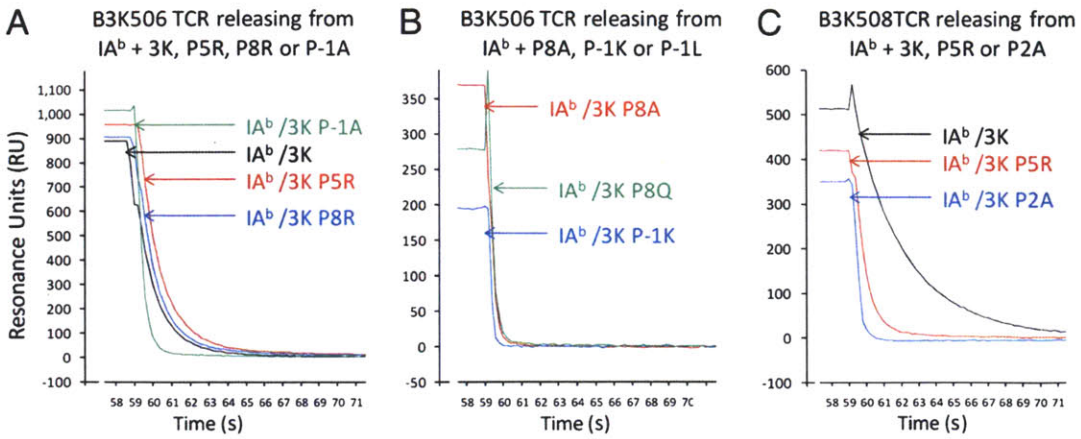

Fig. 1. Release of soluble IA^b/3K and APLs from immobilized B3K506 or B3K508 TCR, monitored SPR. (**A**) Soluble IA^b/3K, P5R, P8R or P-1A or (**B**) P8A, P5Q, P-1K loaded onto B3K506 TCRs, or (**C**) IA^b/3K, P5R or P2A loaded onto B3K508 TCRs were allowed to disassociate for 60 sec at a flow rate of 20μl/min at 25°C. Data was collected at 0.2 sec intervals and fit to a 1:1 Langmuir binding model to determine the dissociation rate (k_d) and half life ($t_{½}$) of the MHC/TCR complex. Curves are examples of three independent experiments.

Although the B3K506 and B3K508 TCRs interact with the IA^b/3K complex with conventional K_D for agonist ligands (7μM for the B3K506; 29μM for the B3K508), the binding kinetics of the interaction of the B3K506 TCR with IA^b/3K is extremely fast; k_a = 101,918/M*sec and k_d = 0.7/sec leading to a $t_{1/2}$ of 0.9 sec (Table S1 and Fig. S1). The K_D of other B3K506 and B3K508 TCR ligands range from 7 – 175 μM, all with fast or medium binding kinetics.

2.2.2 B3K506 and B3K508 CD4 T cells proliferate in response to high, medium and low K_D ligands with very short $t_{1/2}$

To determine the potency of high, medium, and low K_D ligands with differing binding kinetics, mature CD4 T cells from B3K506 and B3K508 Rag1$^{-/-}$ TCR Tg mice were incubated with titrating concentrations of peptides and assessed for proliferation (Fig. 2). Because the peptides with K_D or $t_{1/2}$ beyond the SPR detection limit failed to induce significant activation, we do not consider them in our subsequent analysis. Of critical importance, except for a two-fold increase in binding by the 3K P2A peptide to IA^b, the

peptides all bind similarly to IA^b proteins (24). Furthermore, mature B3K506 and B3K508 CD4 T cells are equally sensitive to anti-CD3 mediated T cell signaling, suggesting that the responses of these different T cells to stimulatory ligands can be directly compared (Fig. S2). Our data confirm that fast-kinetic ligands can signal, suggesting the 2 sec limit on $t_{1/2}$ is not absolute. Notably, the B3K506 undergo proliferation at sub-μM peptide concentrations by the 3K, P5R, P8R and P-1A ligands ($t_{1/2}$ = 0.9, 0.9, 0.8 and 0.3 sec, respectively) (Table S1).

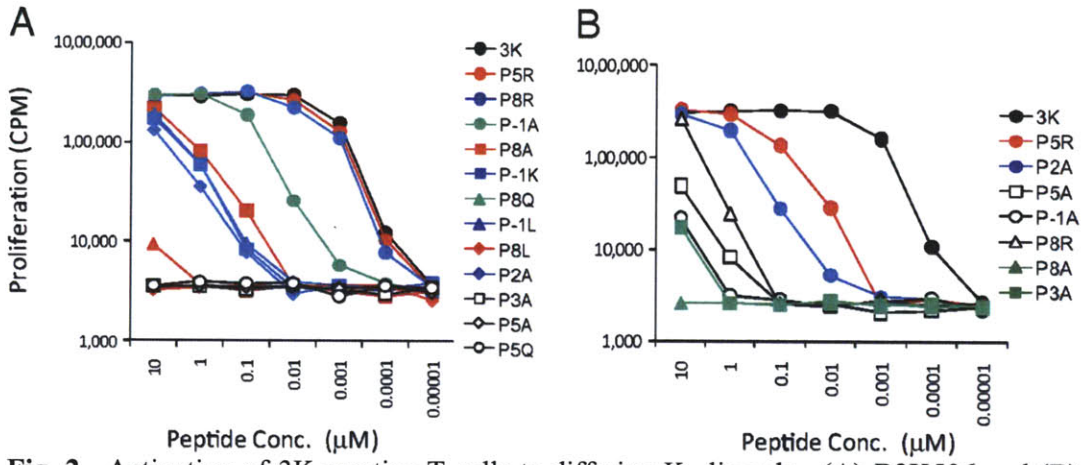

Fig. 2. Activation of 3K-reactive T cells to differing K_D ligands. (**A**) B3K506 and (**B**) B3K508 T cells proliferate when challenged with 3K and APLs. 3K APLs are listed next to each panel top to bottom by increasing K_D. Data are representative of at least three independent experiments.

Some T cell ligands with shorter $t_{1/2}$ than the immunizing ligand can induce super-agonist or partial T cell effector functions if the TCR complex is not efficiently ubiquitinated (18, 25). To determine whether B3K506 and B3K508 T cells undergo complete activation in response to fast kinetic ligands, we chose two additional cellular functions to explore: 1) ligand-induced TCR downregulation as a measure of receptor phosphorylation, ubiquitination and degradation by Cbl-b (26) and 2) cytokine production by T cells. Consistent with inducing complete phosphorylation of the TCR complex and T cell activation, fast kinetic ligands induce TCR downregulation and TNFα production (Fig. S3 and Table S1).

2.2.3 Ligand potency of 3K or APLs fails to obey straight-forward K_D or $t_{1/2}$ models

Individually, ligand potency for the B3K506 or the B3K508 T cells loosely follows the overall trend of both K_D- and $t_{1/2}$-based models. However, when B3K506 and B3K506 T cell activation data are compared neither model suffices (Fig 3 and Table S1). In regards to K_D, the B3K508 T cells are activated too well. For example, the 3K ligand induces proliferation of B3K506 and B3K508 T cells at a similar nanomolar range concentration, despite having significantly different K_D (7 versus 29μM). In another example, the B3K506 TCR binds IA^b/ P-1A (26μM) with similar K_D as the B3K508 TCR binding IA^b/3K (29μM), yet the B3K506 T cells proliferate at an EC_{50} that is 23-fold less than the B3K508 T cells. A failure of K_D to define the ligand potency is further apparent when additional 3K APLs are tested (Fig 3A and Table S1).

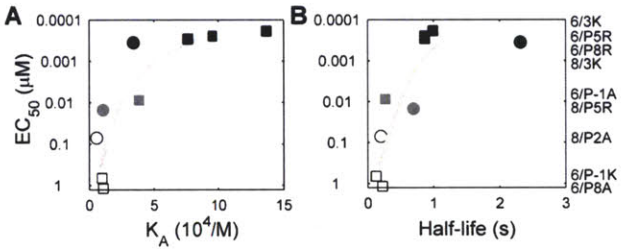

Fig. 3. Failure of K_D or $t_{1/2}$-based models to predict ligand potency. EC_{50} values, based on proliferation, are shown with respect to (**A**) K_A; (**B**) $t_{1/2}$. Data points are labeled by T cell, B3K506 (square) or B3K508 (circle) and grouped by ligand potency: highest (black), intermediate (grey), and lowest (white). Specific TCR-pMHC pairs are listed to the right ordered according to EC_{50}. The EC_{50} values are averaged over three measurements.

In reverse correlation from K_D, ligand potency does not correlate with $t_{1/2}$ as the B3K506 T cells are activated too well. The 3K ligand induces similar proliferation of the B3K506 T cells ($t_{1/2}$ = 0.9 sec) as the B3K508 T cells ($t_{1/2}$ = 2.2 sec) (Table S1). In addition, the P5R ligand is significantly less potent in activating the B3K508 T cells than the 3K ligand is in activating the B3K506 T cells, despite having a similar $t_{1/2}$ (0.7 and 0.9 sec, respectively). Multiple discrepancies can be observed when comparing other 3K APLs (Fig. 3B and Table S1). The finding that each T cell in isolation loosely follows both K_D and $t_{1/2}$-based models appears to be an artifact of limited variation in the kinetics among the ligands for each T cell. A failure of K_D or $t_{1/2}$ to predict ligand potency is true for

cytokine production as well, suggesting the proliferation response is not anomalous (Fig. 3 and Table S1).

Consistently, activating ligands for B3K506 T cells use fast on-rates or strong K_D to compensate for short $t_{1/2}$. (Since there is a simple relation among them, only two of the three parameters describing the interaction are independent.) Vice versa, B3K508 T cells compensate for a weak K_D by engaging IA^b/3K ligands for a longer $t_{1/2}$. These results suggest that ligand potency is determined by an interplay between the TCR-pMHC on-rate and $t_{1/2}$ (or K_D and $t_{1/2}$) in a way that allows for enhanced signaling by fast-kinetic ligands.

2.2.4 Does a combined $K_D/t_{1/2}$ model or serial triggering predict T cell ligand potency?

In an attempt to reconcile how the interplay of K_D and binding kinetics influences T cell activation, we evaluated whether a straightforward merging of the two predicts ligand potency. A combined K_D and $t_{1/2}$ model suggests that increasing the frequency or total number of TCRs engaged by pMHC would stochastically result in an increase in the number of uncharacteristically long TCR-pMHC interactions. To test this we identified the change in receptor occupancy required for a strong K_D, fast kinetic ligand to be bound to an equal number of TCRs, on average, for at least 2 sec as compared to a medium kinetic, medium K_D ligand.

To approximate how frequently each pMHC ligand is bound to a TCR, we assume that a quasi-equilibrium between TCR and pMHC occurs on the time scale of cell-cell contact and that TCR are far in excess of the relevant pMHC. The probability that a pMHC is bound to TCR then depends on the equilibrium association affinity (K_A) through a simple saturation curve (3):

$$\frac{c_{pMHC-TCR}}{c^0_{pMHC}} = \frac{K_A c^0_{TCR}}{1 + K_A c^0_{TCR}} \qquad (1)$$

The parameter c^0_{pMHC} denotes the concentration of pMHC on the APC, c^0_{TCR} denotes the concentration of TCR in the interface, and $c_{\text{pMHC-TCR}}$ denotes the concentration of bound

pMHC. c^0_{TCR} was estimated to be 20 TCR/μm^2 (10,000 TCR per T cell / 500μm^2 surface area of a T cell; Supp. Tests). Within TCR islands, c^0_{TCR} can be locally much higher (80-430/μm^2) (27), however increasing this value had little effect on our results. To convert the measured K_A of TCR-pMHC in solution to K_A when the TCR and pMHC are membrane bound, we have used a confinement length measured for the 2B4 TCR interacting with the MCC88-103 ligand (1.2 nm, corresponding to a conversion factor of 0.262 nm) (8).

The TCR-pMHC saturation curve from Equation 1 contains a threshold K_D, K*, above which pMHC ligands are bound at least 50% of the time. Using the above approximations, K* is 130μM and pMHC ligands with a 43μM K_D are bound 75% of the time (Fig. 4). These values mirror measurements made by Grakoui and colleagues, in which the majority of a 60 μM K_D pMHC ligand was bound to a TCR when located within the interface of T cells and APCs (8). Due to ligand saturation, increasing K_D above 100μM has only a modest effect on the overall frequency of TCRs bound to pMHC. This saturation curve can be used to show that changes in TCR-pMHC occupancy do not describe ligand potency (Supp. Tests).

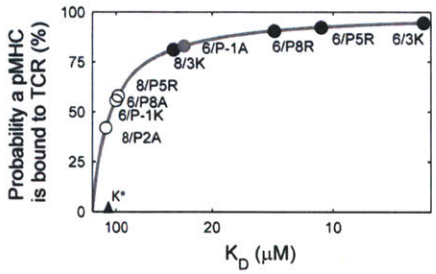

Fig. 4. Receptor occupancy depends only weakly on K_D for pMHC ligands with K_D stronger than 130μM. The receptor occupancy predicted by Equation 1 is plotted according to the parameter estimates in the text, on a scale that is linear in K_A ($1/K_D$). The predictions for the actual pMHC-TCR pairs in our experiments are superimposed on the plot, colored according to their actual activity as described in the caption to Fig. 3.

By comparing ligands with similar EC_{50} of proliferation yet different $t_{1/2}$, we tested whether a merged $K_D/t_{1/2}$ model describes ligand potency. Specifically, the tests evaluate

whether a stronger K_D for the B3K506 TCR engaging pMHC generates enough additional bindings to overcome the lower probability of their bindings being long-lived. One comparison is the B3K506 TCR interacting with 3K/P-1A peptide (K_D = 26μM, $t_{1/2}$ = 0.3 sec, EC_{50} = 9nM) and the B3K508 TCR interacting with the 3K/P5R peptide (K_D = 93μM, $t_{1/2}$ = 0.7 sec, EC_{50} = 15nM). Assuming TCRs bind pMHC with exponentially distributed dwell times, the B3K506 TCR would have to bind 26-fold more IA^b/P-1A ligand than the B3K508 TCR binding IA^b/P5R to generate an equal number of 2 sec engagements. However, the 3.6 fold difference in K_D between the two TCR-pMHC pairs leads to only a 1.5 fold difference in receptor occupancy. The effect is qualitatively similar for other comparisons (Fig. S4A) and is largely robust to assumptions about the parameters (Supp. Tests). Thus a merged $K_D/t_{1/2}$ model does not properly account for ligand potency. Based on similar reasoning the effects of serial triggering cannot contribute significantly to ligand potency (Fig S4B-C and Supp. Tests). It appears that the role of the on-rate and affinity in our data is not to increase the number of bindings, either at any given time (receptor occupancy) or over time (serial triggering).

2.2.5 Could rebinding of TCRs to pMHC expand the dwell time for fast kinetic ligands?

The failure of K_D, $t_{1/2}$ or serial triggering models indicates other mechanisms must underlie ligand potency. The hypothesis of serial triggering, that individual pMHC can sequentially bind multiple TCRs led us to wonder whether a pMHC can bind multiple times to the same TCR. The ability of a receptor/ligand pair to associate, disassociate and re-associate in a finite amount of time prior to complete disengagement is termed rebinding. Although TCR-pMHC interactions are usually thought of as single binding events, it is theoretically possible ligands with fast on-rates may be able to rebind TCRs (28), especially since they are bound on membranes where diffusivities are typically slower than in solution. If it occurred, TCR-pMHC rebinding would generate an aggregate dwell time of interaction, assuming the rebindings occur faster than the TCR signaling complex disassembles.

To investigate whether TCR-pMHC rebindings are plausible, we have followed an extensive set of work analyzing diffusion-influenced reactions (29, 30). Our approach has been to apply the particular estimate of the aggregate binding time, including rebindings, provided by Bell (31) because of its simplicity and to suggest that the qualitative results are robust to the choice of model (see below and Supp. Tests). In applying Bell's model, we assume that pMHC and TCR move purely diffusively on flat, stiff membranes. Neglecting membrane forces is potentially in conflict with emerging work indicating the role of the actin cytoskeleton in breaking TCR-pMHC bonds, decreasing their $t_{1/2}$ (32). However, when on-rates are fast enough for rebinding to occur, they happen very quickly, so it is unclear how much membrane forces could intervene.

The model also assumes that all rebindings occur at the same rate, which neglects any stabilization of binding that may be provided by coreceptors. Stabilization would have the effect of increasing the propensity of rebinding. Furthermore, the model counts only those rebindings that occur almost immediately, before the TCR and pMHC separate by more than a molecular length scale (e.g. 100 Å), on the order of 1 ms using the parameters below. Though the molecular details of TCR activation are not entirely understood (33, 34), TCR activation is not expected to be appreciably reversed on such short time scales.

Within this framework, Bell's result for the total dwell time, summing the duration of any rebindings that occur, is;

$$t_a = t_{1/2} + \left[\frac{\ln(2)}{2\pi\left(D_{TCR} + D_{pMHC}\right)}\right] \cdot K_A \qquad (2)$$

The parameters D_{TCR} and D_{pMHC} represent the diffusivities of TCR and pMHC, respectively. From Bell's result it can be seen that the total aggregate half-life (t_a) is dependent upon the individual $t_{1/2}$ and the equilibrium affinity. The first term in Equation 2 accounts for the duration of the first binding, whereas the second affinity-dependent term accounts for any subsequent rebindings. Noting that every individual binding event lasts, on average, as long as any other, the expected number of rebindings between a particular pMHC-TCR pair is:

$$\overline{N} = \frac{k_{on}}{2\pi\left(D_{pMHC} + D_{TCR}\right)} \quad (3)$$

The parameter k_{on} denotes the on-rate of the pair on the membrane. The system has qualitatively different dependence on the $t_{1/2}$ and K_D when on-rates are small and large. When on-rates are fast relative to the diffusion rates, pMHC binds and rebinds the same TCR many times reaching a quasi-equilibrium before diffusing away. As a result, the equilibrium affinity dominates the duration of the interaction when on-rates are high. However, when on-rates are slow, rebinding does not occur and $t_{1/2}$ dominates. Because Equation 2 can be independently motivated by simple arguments such as these, it is qualitatively robust to the choice of model (Supp. Tests).

More generally, Equation 3 suggests that there is a threshold on-rate above which rebindings are relevant:

$$k_{on}^{*} = 2\pi\left(D_{TCR} + D_{pMHC}\right) \quad (4)$$

Whenever the on-rate exceeds this threshold (also known as the diffusion-limited rate), at least one rebinding is expected to occur. Importantly, the specific parameter values are important only insofar as they influence this threshold and not the underlying biophysical event.

2.2.6 Rebinding of TCRs to pMHC uniquely explains how fast kinetic ligands induce T cell activation

To evaluate whether rebinding could impact the dwell time of B3K506 or B3K508 TCRs engaging pMHC ligands, we applied Equation 2 to our data set. The diffusivity for a TCR and pMHC were estimated at 0.04 μm^2/sec and 0.02 μm^2/sec respectively, corresponding to midrange measured values (see Supp. Tests). On-rates measured using SPR were converted to on-rates on the membrane by assuming 1) that off-rates of membrane bound TCRs binding pMHC are identical to SPR measurements and 2) that the K_D of membrane bound TCRs engaging pMHC are proportional to SPR-measured affinities, as done in our analysis of receptor occupancy. Because of limited data, it is

generally difficult to directly convert SPR-measured on-rates to on-rates on the membrane (35, 36). We discuss sensitivity to the assumptions in the supplement.

Using these parameter values, rebinding likely occurs for TCR-pMHC pairs with fast binding kinetics (Fig. 5). Specifically, this initial model predicts that the threshold on-rate for rebinding is 60,000/M*sec. As a result, the number of rebindings increases from almost none to 1.7 as the on-rate increases in our sample from 11,000/M*sec to 102,000/M*sec. Since T cell activity is generally thought to be very sensitive to $t_{1/2}$, a factor of 2 or 3 can be important. When rebindings are accounted for, the highly potent B3K506 T cell ligands 3K, P5R and P8R change from $t_{1/2}$ of 0.9 or 0.8 sec to aggregate $t_{1/2}$ of 2.7, 1.9 and 1.8 sec, and the medium potent P-1A ligand converts from a $t_{1/2}$ of 0.27 sec, to an aggregate $t_{1/2}$ of 0.72 sec. Importantly, aggregate $t_{1/2}$ is significantly better at predicting ligand potency than K_D or $t_{1/2}$ (Fig. 6C, S4, S7 and S8).

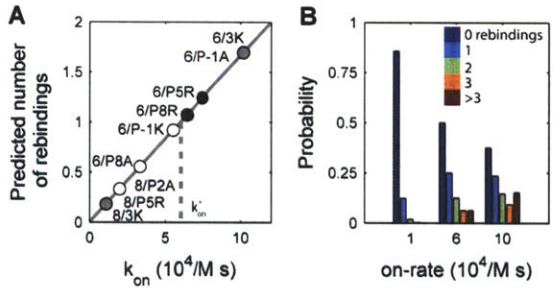

Fig. 5. Fast on-rates lead to rebinding. (**A**) The average number of rebindings predicted by Equation 3 is plotted, versus the on-rate. The threshold for rebinding, k_{on}*, separates pairs expected to rebind at least once from those that rarely rebind. (**B**) The probability of 0, 1, 2, 3, or more than 3 rebindings between TCR-pMHC, according to their on-rate, as predicted from Equation 2 (Supp. Tests).

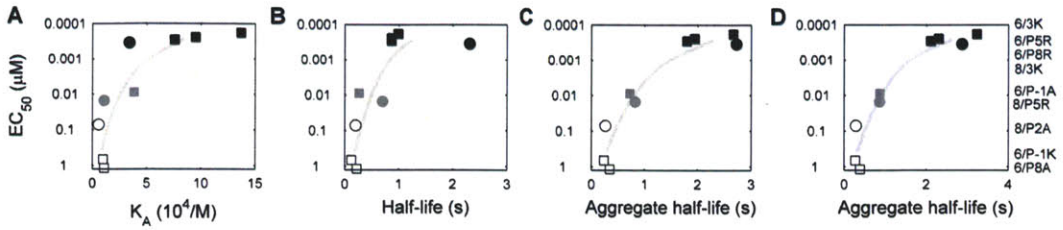

Figure 6. Aggregate $t_{1/2}$ is the best predictor of ligand potency for 3K-reactive T cells. EC_{50} values, based on proliferation, are shown with respect to **(A)** K_D; **(B)** $t_{1/2}$; **(C)** aggregate $t_{1/2}$, with rebinding threshold set at 60,000/M*sec; and **(D)** aggregate $t_{1/2}$, with rebinding threshold set at 45,000/M*sec.

Within the data set two groups of high or medium potency ligands arise from different TCR-pMHC binding parameters (Table S1). Using these groups, the competing models can be quantitatively evaluated. The four high potency ligands (3K, P5R, P8R binding the B3K506 TCR and 3K binding the B3K508 TCR), have K_D and $t_{1/2}$ that vary widely by factors of 4.0 and 2.7, but aggregate $t_{1/2}$ that only vary by a factor of 1.5 (Fig. 6C). The two ligands in the second most-potent group (B3K506 TCR binding P2A, B3K508 TCR binding P5R) have K_D and $t_{1/2}$ that vary by factors of 3.6 and 2.6, respectively, but aggregate $t_{1/2}$ that are almost identical, varying only by a factor of 1.1.

Though our aggregate $t_{1/2}$ model was generated without empirically fitting the data, our estimate for the rebinding threshold, 60,000/M*sec, is near the best fit for minimizing the variation in the aggregate $t_{1/2}$ of the most potent group of ligands (Fig. S5). Quite similarly, for the medium potent ligands, the best-fit threshold is 45,000/M*sec (Fig. 6D). The convergence of the aggregate $t_{1/2}$ model with empirical data suggests the assumptions and underlying biophysical process are correct.

2.3 Discussion

Binding of two proteins is governed by the K_D, on-rate and $t_{1/2}$, any two of which suffice to describe the interaction since the three are simply related. Though ligand potency could be dependent upon each of these binding characteristics, research over the past two decades has suggested that only the K_D or $t_{1/2}$ matter. Mechanistically these two mutually exclusive models have been interpreted to mean that T cells are either: 1) sensitive to the

number of TCRs simultaneously bound to pMHC (3-6); or 2) sensitive to ligands that produce a long enough interaction to fully phosphorylate the TCR complex (8-11, 13). In seeming contradiction to both theories, data presented here suggests neither the K_D nor $t_{1/2}$ determines the potency of T cell ligands.

A plethora of data suggests that T cells are increasingly sensitive to long-lived TCR-pMHC engagements, with $t_{1/2}$ of 2 sec being near the shortest allowable time (9, 15). Additionally, T cell responses are dependent upon ligand concentration, suggesting T cells are also responsive to the frequency of these long-lived bonds. With this as a starting point, we asked how changes in the on-rate or K_D might allow T cells to be equally reactive to ligands with different $t_{1/2}$. The IA^b/3K model system is particularly well suited for this analysis because each of the 3K APLs bind IA^b similarly, and the relatively large number of TCR – IA^b/3K APL pairs contain several which have similar potency while using different K_D and binding kinetics. These controlled combinations of T cells and pMHC ligands allowed a direct comparison of the different theories of T cell activation.

Because high potency T cell ligands with short $t_{1/2}$ all have fast on-rates, we hypothesized TCR-pMHC interactions may be influenced by diffusion rates. Although rebinding is potentially relevant for any binding event, it will be less important for cytosolic reactions because diffusivities in the cytoplasm are relatively high (31). However, when both receptor and ligand are anchored on membranes, the rates of diffusion are drastically reduced. A recent study of the interaction between membrane-bound CD2 and CD58 using FRAP suggests that the fast-binding pair may rebind 100 times prior to separating, significantly increasing the duration of the bonds (37) and potentially explaining the pair's physiological activity (38).

Modeling TCR-pMHC interactions when both are membrane bound shows that fast on-rates allow rebinding to occur. Depending upon the on-rates, this effect can greatly extend bond durations, allowing medium potency ligands with measured $t_{1/2}$ of 0.3 and 0.7 sec to generate aggregate $t_{1/2}$ near 1 sec. As an independent example , the LCMV-

specific P14 TCR has been shown to bind its cognate H-2D^b-gp33 ligand with a low $t_{1/2}$ of 0.7 sec (21). Due to a fast on-rate of 400,000/M*sec, our rebinding model predicts the P14 TCR would have an aggregate $t_{1/2}$ of 5.5 sec, fully consistent with kinetic proof-reading models of activation.

Most importantly, rebinding-mediated aggregate $t_{1/2}$ uniquely predicts ligand potency for B3K506 and B3K508 T cells (Fig. 6). Although our data initially appear to be in conflict with both K_D and $t_{1/2}$-based activation models, the aggregate $t_{1/2}$ model is consistent with reports that either $t_{1/2}$ or K_D can be the better predictor of ligand potency. T cell ligands with slow on-rates are predicted to follow a strict $t_{1/2}$-based reactivity pattern because rebinding does not occur and the aggregate $t_{1/2}$ is equal to the $t_{1/2}$ of a single binding event. The canonical $t_{1/2}$-dependent systems, such as the 2B4-IE^k/MCC and 3L.2-IE^k/Hb TCR-pMHC pairs, have slow on-rates compared to the rebinding threshold we have estimated (45,000-60,000/M*sec) (10, 11, 19). Because most T cell activation studies have been done using these systems, $t_{1/2}$-based models have appeared sufficient and rebindings have not been required to understand ligand potency. For example, the on-rates for the $t_{1/2}$-dependent 2B4/MCC system studied by Krogsgaard et al. are all less than 6,670/M*sec, so that almost no rebindings (less than 0.15) are predicted to occur (10).

In contrast to the canonical $t_{1/2}$-models, most T cell activation studies which suggest K_D is a better predictor of ligand potency have on-rates larger than or close to the rebinding threshold (5, 6). Our data suggest these correlations with K_D occur because of rebinding. For example, the K_D-dependence of the two peptides studied by Ely (6) is consistent with a dependence on the aggregate half-life, the more potent peptide having a 14-fold faster on-rate and a predicted 1.3- to 1.4-fold longer aggregate half-life, according to our model. Thus, observations that ligand potency is dependent upon K_D or $t_{1/2}$ are not in conflict with each other, but rather are different manifestations of the interaction between the T cell and APC when the on-rate is very fast or very slow. With the continuing emergence of T cell ligands with very fast on-rates (4), our findings are likely to impact a large repertoire of T cells.

Upon completion of this work, we have become aware of results for CD8+ T cells that are in harmony with our conclusions (39).

Materials and Methods

Mice and Peptides

C57BL/6 mice were purchased from The Jackson Laboratory (Bar Harbor, ME). $Rag1^{-/-}$ B3K506 and $Rag1^{-/-}$ B3K508 TCR Tg mice have been previously described (22). All mice were maintained in a pathogen-free environment in accordance with institutional guidelines in the Animal Care Facility at the University of Massachusetts Medical School. Peptides were purchased from the MRC at National Jewish Medical Center.

References

1. Palmer E (2003) Negative selection - Clearing out the bad apples from the T-cell repertoire. *Nature Reviews Immunology* 3(5):383-391.
2. Tanchot C, Lemonnier FA, Perarnau B, Freitas AA, & Rocha B (1997) Differential requirements for survival and proliferation of CD8 naive or memory T cells. *Science* 276(5321):2057-2062.
3. Sykulev Y, Cohen RJ, & Eisen HN (1995) The law of mass action governs antigen-stimulated cytolytic activity of CD8(+) cytotoxic T lymphocytes. *Proc. Natl. Acad. Sci. U. S. A.* 92(26):11990-11992.
4. Stone JD, Chervin AS, & Kranz DM (2009) T-cell receptor binding affinities and kinetics: impact on T-cell activity and specificity. *Immunology* 126(2):165-176.
5. Tian S, Maile R, Collins EJ, & Frelinger JA (2007) CD8(+) T cell activation is governed by TCR-Peptide/MHC affinity, not dissociation rate. *J. Immunol.* 179(5):2952-2960.
6. Ely LK, *et al.* (2005) Antagonism of Antiviral and Allogeneic Activity of a Human Public CTL Clonotype by a Single Altered Peptide Ligand: Implications for Allograft Rejection. *J. Immunol.* 174(9):5593-5601.
7. Alam SM, *et al.* (1996) T-cell-receptor affinity and thymocyte positive selection. *Nature* 381(6583):616-620.
8. Grakoui A, *et al.* (1999) The immunological synapse: A molecular machine controlling T cell activation. *Science* 285(5425):221-227.
9. Qi SY, Krogsgaard M, Davis MM, & Chakraborty AK (2006) Molecular flexibility can influence the stimulatory ability of receptor-ligand interactions at cell-cell junctions. *Proc. Natl. Acad. Sci. U. S. A.* 103(12):4416-4421.
10. Krogsgaard M, *et al.* (2003) Evidence that structural rearrangements and/or flexibility during TCR binding can contribute to T cell activation. *Mol. Cell* 12(6):1367-1378.
11. Kersh GJ, Kersh EN, Fremont DH, & Allen PM (1998) High- and low-potency ligands with similar affinities for the TCR: The importance of kinetics in TCR

signaling. *Immunity* 9(6):817-826.
12. Ashton-Rickardt PG, *et al.* (1994) Evidence for a differential avidity model of T-cell selection in the thymus. *Cell* 76(4):651-663.
13. McKeithan TW (1995) Kinetic Proofreading in T-Cell Receptor Signal-Transduction. *Proc. Natl. Acad. Sci. U. S. A.* 92(11):5042-5046.
14. George AJT, Stark J, & Chan C (2005) Understanding specificity and sensitivity of T-cell recognition. *Trends Immunol.* 26(12):653-659.
15. Altan-Bonnet G & Germain RN (2005) Modeling T cell antigen discrimination based on feedback control of digital ERK responses. *PLoS. Biol.* 3(11):1925-1938.
16. Kalergis AM, *et al.* (2001) Efficient cell activation requires an optimal dwell-time of interaction between the TCR and the pMHC complex. *Nat. Immunol.* 2(3):229-234.
17. Holler PD & Kranz DM (2003) Quantitative analysis of the contribution of TCR/pepMHC affinity and CD8 to T cell activation. *Immunity* 18(2):255-264.
18. Sloan-Lancaster J & Allen PM (1996) Altered peptide ligand-induced partial T cell activation: Molecular mechanisms and role in T cell biology. *Annu. Rev. Immunol.* 14:1-27.
19. Alam SM, *et al.* (1999) Qualitative and quantitative differences in T cell receptor binding of agonist and antagonist ligands. *Immunity* 10(2):227-237.
20. Lyons DS, *et al.* (1996) A TCR binds to antagonist ligands with lower affinities and faster dissociation rates than to agonists. *Immunity* 5(1):53-61.
21. Boulter JM, *et al.* (2007) Potent T cell agonism mediated by a very rapid TCR/pMHC interaction. *Eur. J. Immunol.* 37(3):798-806.
22. Huseby ES, *et al.* (2005) How the T cell repertoire becomes peptide and MHC specific. *Cell* 122(2):247-260.
23. Huseby ES, Crawford F, White J, Marrack P, & Kappler JW (2006) Interface-disrupting amino acids establish specificity between T cell receptors and complexes of major histocompatibility complex and peptide. *Nat. Immunol.* 7(11):1191-1199.
24. Liu XQ, *et al.* (2002) Alternate interactions define the binding of peptides to the MHC molecule IA(b). *Proc. Natl. Acad. Sci. U. S. A.* 99(13):8820-8825.
25. Cemerski S, *et al.* (2007) The stimulatory potency of T cell antigens is influenced by the formation of the immunological synapse. *Immunity* 26(3):345-355.
26. Naramura M, *et al.* (2002) c-Cbl and Cbl-b regulate T cell responsiveness by promoting ligand-induced TCR down-modulation. *Nat. Immunol.* 3(12):1192-1199.
27. Dushek O & Coombs D (2008) Analysis of serial engagement and peptide-MHC transport in T cell receptor microclusters. *Biophys. J.* 94(9):3447-3460.
28. Dushek O, Das R, & Coombs D (2009) A role for rebinding in rapid and reliable T cell responses to antigen. *PLoS Comput Biol* 5(11):e1000578.
29. Freeman DL & Doll JD (1983) The Influence of Diffusion on Surface-Reaction Kinetics. *J. Chem. Phys.* 78(10):6002-6009.
30. Melo E & Martins J (2006) Kinetics of bimolecular reactions in model bilayers and biological membranes. A critical review. *Biophys. Chem.* 123(2-3):77-94.
31. Bell GI (1978) Models for specific adhesion of cells to cells. *Science*

200(4342):618-627.
32. Huppa JB, *et al.* (2010) TCR-peptide-MHC interactions in situ show accelerated kinetics and increased affinity. *Nature* 463(7283):963-U143.
33. Davis SJ & van der Merwe PA (2006) The kinetic-segregation model: TCR triggering and beyond. *Nat Immunol* 7(8):803-809.
34. Call ME & Wucherpfennig KW (2005) The T cell receptor: Critical role of the membrane environment in receptor assembly and function. *Annu. Rev. Immunol.* 23:101-125.
35. Dustin ML, Bromley SK, Davis MM, & Zhu C (2001) Identification of self through two-dimensional chemistry and synapses. *Annu. Rev. Cell Dev. Biol.* 17:133-157.
36. Robert P, Benoliel AM, Pierres A, & Bongrand P (2007) What is the biological relevance of the specific bond properties revealed by single-molecule studies? *J. Mol. Recognit.* 20(6):432-447.
37. Tolentino TP, *et al.* (2008) Measuring diffusion and binding kinetics by contact area FRAP. *Biophys. J.* 95(2):920-930.
38. Kaizuka Y, Douglass AD, Vardhana S, Dustin ML, & Vale RD (2009) The coreceptor CD2 uses plasma membrane microdomains to transduce signals in T cells. *J. Cell Biol.* 185(3):521-534.
39. Aleksic M, *et al.* (2010) Dependence of T Cell Antigen Recognition on T Cell Receptor-peptide MHC Confinement Time. *Immunity* 32(2):163-174.

2.A Appendix for Chapter 2

Table S1. TCR-ligand K_D, binding kinetics, and T-cell effector functions

TCR	IA^b + 3K mutation	K_D (μM)	k_{on} (1/M·s)	k_{off} (1/s)	$t_{1/2}$ (s)	Proliferation EC_{50} (nM)	TNF-α EC_{50} (nM)
B3K506	WT	7	101,918	0.7	0.9	0.2	3.1
B3K506	P5R	11	74,654	0.8	0.9	0.2	6
B3K506	P8R	13	64,318	0.8	0.8	0.3	7
B3K506	P-1A	26	101,731	2.6	0.3	9	68
B3K506	P8A	92	33,370	3.1	0.2	1,200	2,210
B3K506	P-1K	101	55,149	5.6	0.1	660	5,500
B3K506	P8Q	114	ND	>5	<0.2	9,800	>10,000
B3K506	P-1L	122	ND	>5	<0.2	710	3,600
B3K506	P8L	256	ND	>5	<0.2	>10,000	>10,000
B3K506	P2A	278	ND	>5	<0.2	750	5,500
B3K506	P3A	>550	ND	ND	ND	>10,000	>10,000
B3K506	P5A	>550	ND	ND	ND	>10,000	>10,000
B3K506	P5Q	>550	ND	ND	ND	>10,000	>10,000
B3K508	WT	29	10,887	0.3	2.2	0.4	6
B3K508	P5R	93	11,048	1.0	0.7	15	87
B3K508	P2A	175	19,914	3.5	0.2	71	530
B3K508	P5A	>550	ND	ND	ND	5,700	>10,000
B3K508	P-1A	>550	ND	ND	ND	>10,000	>10,000
B3K508	P8R	>550	ND	ND	ND	980	>10,000
B3K508	P8A	>550	ND	ND	ND	>10,000	>10,000
B3K508	P3A	>550	ND	ND	ND	>10,000	>10,000

Scatchard analysis of binding data data were used to determine the dissociation constant (K_D). The k_{on} was calculated from the K_D and k_{off} ($k_{on} = k_{off}/K_D$). The $t_{1/2}$ values were calculated using first-order reaction kinetics: $t_{1/2} = \ln(2)/k_{off}$. ND, not determined.

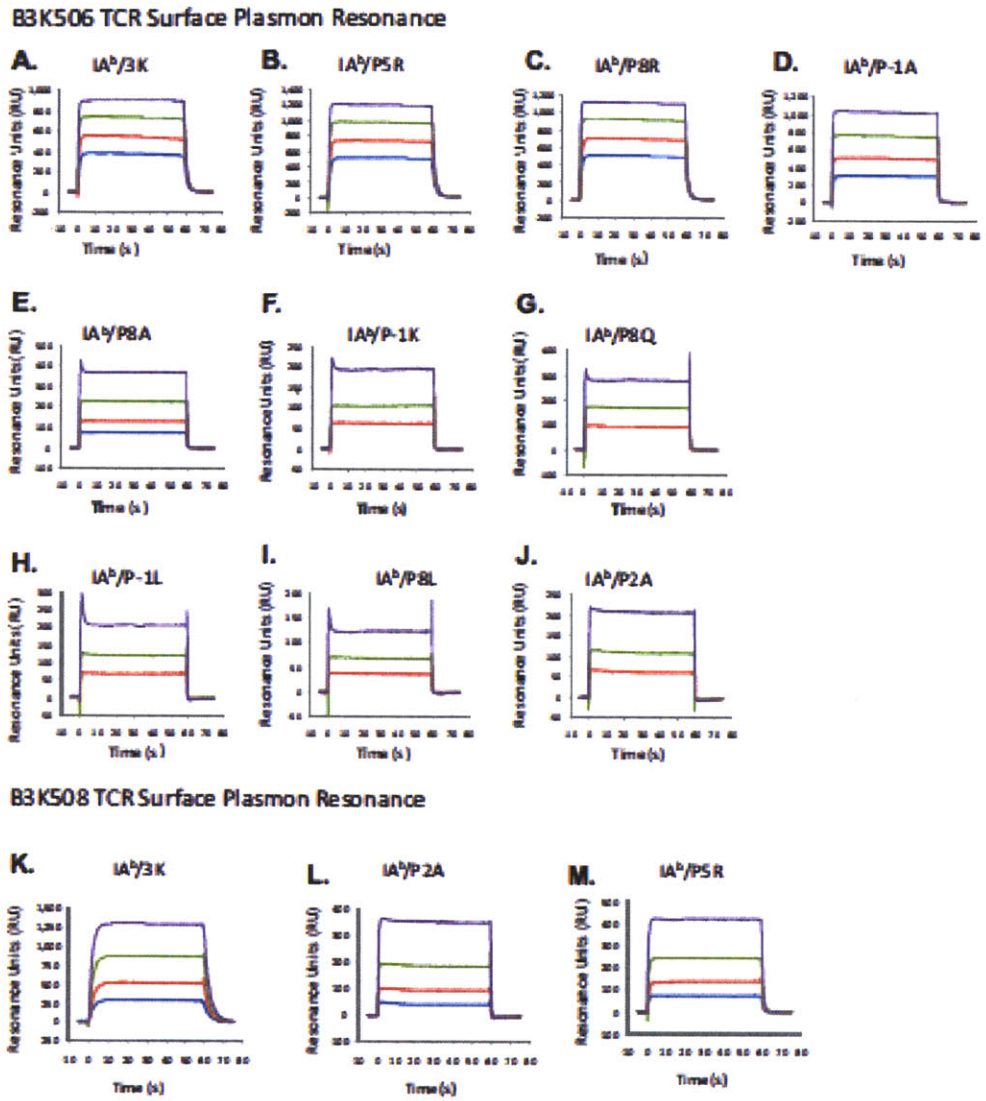

Fig. S1. The B3K506 and B3K508 TCRs interact with IA^b/3K and peptide variants with differing rates of association and disassociation. The affinity and kinetics of soluble, monomeric IA^b-3K or variant peptide ligands binding to immobilized B3K506 and B3K508 TCRs were analyzed by surface plasmon resonance using a BIAcore 2000 and BIAcore 3000 instrument (BIAcore AB, Uppsala, Sweden). Approximately 2000 RU of soluble B3K506 TCR was captured on the surface of a CM5 biosensor flowcell by an immobilized anti-Cα mAb, ADO-304. For the B3K506 T cells, soluble IA^b/3K or variant peptides were injected at 20μl/min for 60sec through a CM5 biosensor flow cell at a concentration of (**A**) 3K WT (4, 8, 16, 32 μM), (**B**) P5R (5.6, 11.2, 22.5, 45 μM), (**C**) P8R (8, 16, 32, 64 μM), (**D**) P-1A (8, 16, 32, 64 μM), (**E**) P8A (8, 16, 32, 64 μM), (**F**) P-1K (12.9, 25.7, 51.4 μM), (**G**) P8Q (13, 26, 52 μM), (**H**) P-1L (16, 32, 64 μM), (**I**) P8L (4, 8, 16, 32 μM), (**J**) P2A (4, 8, 16, 32 μM). No specific binding was detected for the P3A, P5A and P5Q ligands interacting with the B3K506 TCR. For the B3K508 T cells, soluble IA^b/3K or variant peptides were injected at 20ml/min for 60sec through a CM5 biosensor flow cell at a concentration of (**K**) 3K WT (4, 8, 16, 32 μM), (**L**) P5R (5.6, 11.2, 22.5, 45 μM) and (**M**) P2A (4, 8, 16, 32 μM). Limited binding was detected for the P5A ligand binding the B3K508 TCR at the 32 and 64μM. No specific binding was detected for the P-1A, P8R, P8A and P3A ligands interacting with the B3K508 TCR. As a control for bulk fluid phase refractive index the IA^b-3K preparations was also injected through a

fourth flow cell with an immobilized irrelevant TCR Ani 2.3 specific for HLA-DR52c. All samples reached equilibrium binding within 10 sec. The complex was allowed to dissociate for 60 sec between injections. Raw data were corrected for the bulk signal from buffer and IA^b-3K by performing identical injections through a flow cell in which an irrelevant abTCR was immobilized. The data were further corrected for the loss of captured αβTCR during the series of injections based on the observed dissociation rate (k_d) of the abTCR from the anti-Cα mAb (~ 4.5 x 10^{-4}/sec). The data were analyzed with BIAcore Bioeval 4.1 software.

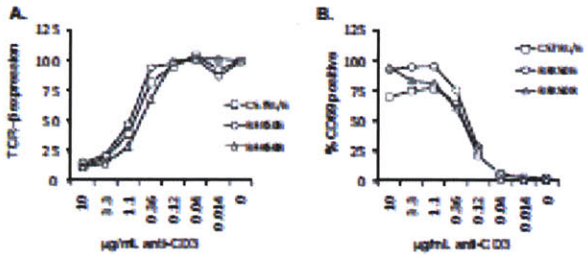

Fig. S2. C57BL/6, B3K506 and B3K508 $CD4^+$ T cells downregulate TCR expression and upregulate CD69 expression equivalently in response to titrating amounts of anti-CD3 cross-linking. CD4 T cells were incubated in plates coated with 10μg/ml of anti-CD28, titrating amounts of anti-CD3 for 18 hours and analyzed by flow cytometry for (**A**) TCRβ expression and (**B**) CD69 expression. TCRβ expression is normalized for each T cell population to the expression at which no activation occurs. Data are the average of three wells per variability and are representative of two independent experiments.

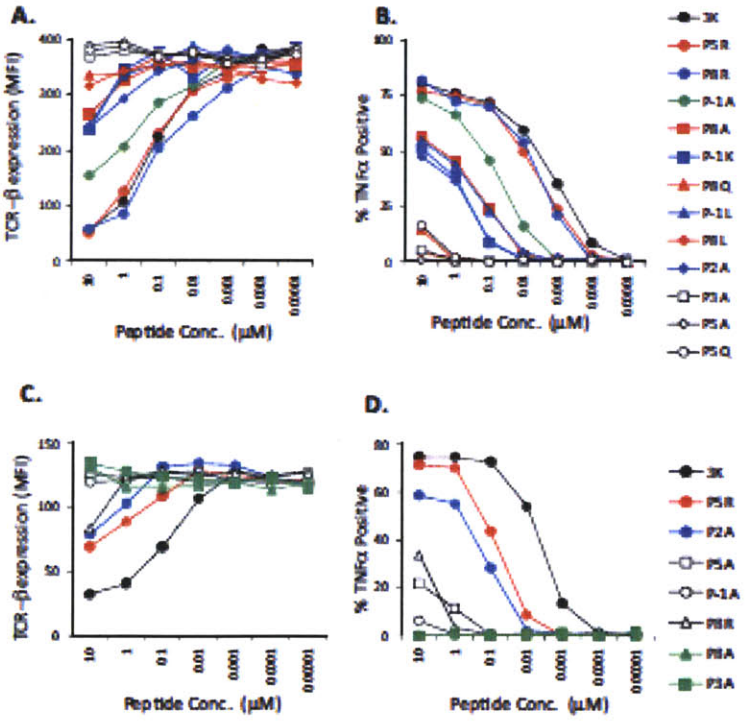

Fig. S3. B3K506 and B3K508 T cells downregulate TCR expression and produce TNFα when challenged with high, medium and low K_D ligands. Naïve B3K506 CD4 T cell (**A**) downregulate TCR expression and

(**B**) produce TNFa to 3K and APL ligands. Peptide ligands are listed top to bottom by decreasing K_D with the 3K peptide having the strongest K_D and the P5Q peptide the weakest (undetectable) K_D. (**C**) Naïve B3K508 CD4 T cell downregulate TCR expression and (**D**) produce TNFa to 3K and APL ligands. Peptide ligands are listed top to bottom by decreasing K_D. Data is representative of at least three independent experiments.

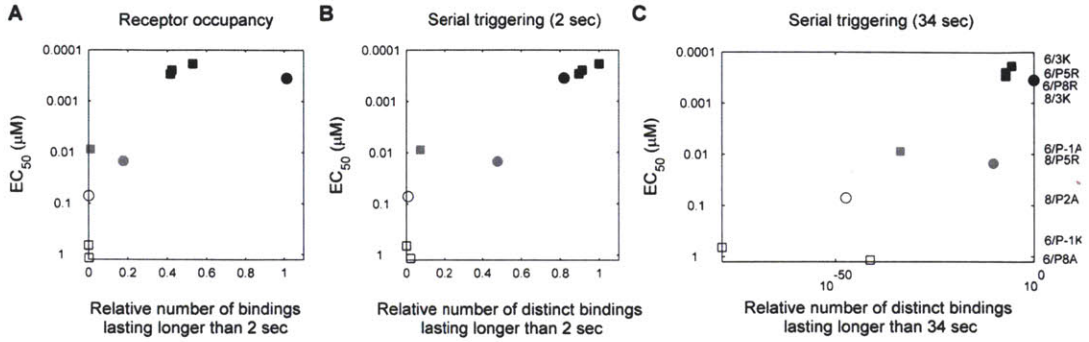

Fig. S4: Evaluating models that correlate ligand potency with the number of long-lived bonds between the pMHC and TCR. (**A**) A model merging receptor occupancy and dwell time does not explain the activities of the pMHC-TCR pairs. The pMHC-TCR pairs are ranked according to the average number of interactions between them, at any given time, that have lasted longer than 2 sec. This average number was calculated as the product of two quantities: (1) the fraction of peptides bound at any given time, as given in Equation 1, and (2) the fraction of such bindings that last longer than 2 sec, assuming exponentially distributed binding times. The result has been normalized by the B3K508 peptide interacting with the 3K peptide, which is the most active. The results are fairly insensitive to the parameter estimates due to the strong (exponential) dependence on the half-life and the weak (sublinear) dependence on the affinity. (**B-C**) A model merging serial triggering and dwell time does not explain the activities of the pMHC-TCR pairs. The pMHC-TCR pairs are ranked according to the number of distinct interactions between them that last longer than a threshold time. The number of interactions is normalized by the number of interactions for the B3K506 TCR interacting with the 3K peptide, which is predicted to be most active. The threshold time required to activate a TCR is assumed to be: (**B**) 2 sec and (**C**) 34 sec. Note that panel (**C**) is on a log scale.

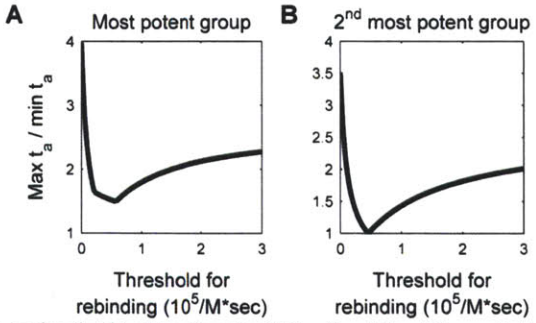

Fig. S5. Determining the optimal rebinding threshold for the data. The variation in aggregate half-lives (t_a) within groups of similar activity is plotted against different rebinding thresholds for (**A**) the most potent group of peptides and (**B**) the second most potent group of peptides. The optimal thresholds are (**A**) 60,000/(M*sec) and (**B**) 45,000/(M*sec).

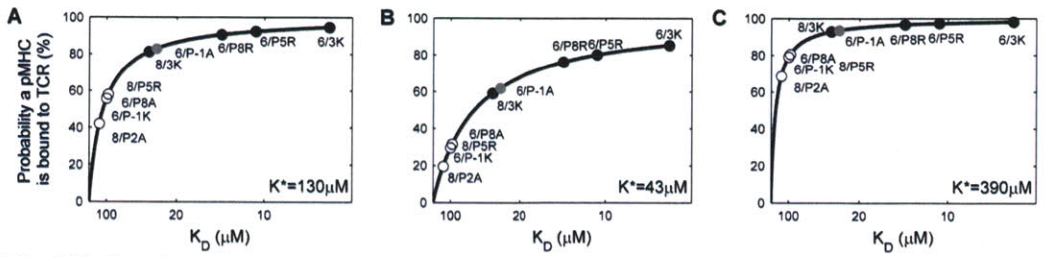

Fig. S6. Sensitivity of receptor occupancy to parameter estimates. The predicted receptor occupancy for each pMHC-TCR pair is plotted, according to Equation 1, (**A**) using a threshold affinity, K_D*, of 130μM as estimated in the main text, and (**B**) with an affinity threshold three times stronger (43μM) and (**C**) three times weaker (390μM). The different affinity thresholds model uncertainty in the concentration of TCR on the surface of the cell and the conversion between SPR-measured affinities and affinities on the membrane.

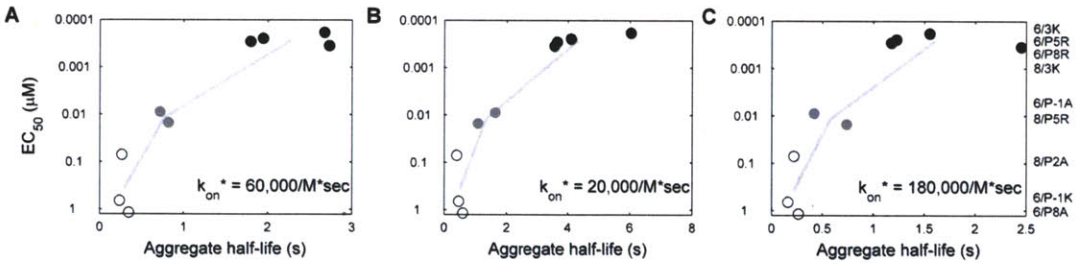

Fig. S7. Sensitivity of rebinding to parameter estimates. Correlations between peptide potency and the aggregate half-life are plotted (**A**) with a rebinding threshold, k_{on}*, of 60,000/M*sec, as estimated in the main text and with rebinding thresholds (**B**) three times lower (20,000/M*sec) and (**C**) three times higher (180,000/M*sec). The aggregate half-lives were determined according to Equation 2. The different rebinding thresholds model uncertainty in the diffusivities of the pMHC and TCR and the conversion between SPR-measured on-rates and on-rates on the membrane.

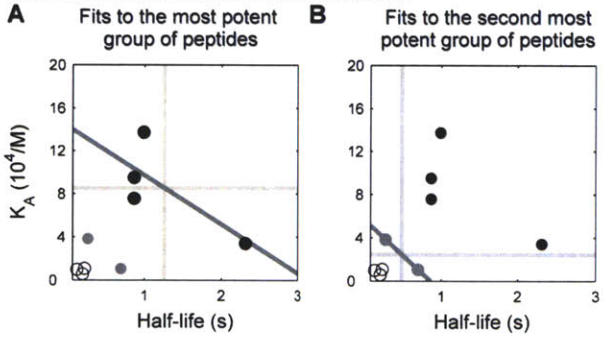

Fig. S8. The models are compared according to their ability to account for peptides with equal activity but different affinities, on-rates, and half-lives. (**A**) The models are fit to the most potent group of peptides, which all have similar potency. The vertical, horizontal, and diagonal lines correspond to best-fits for the half-life, affinity, and rebinding models, respectively. (**B**) The models are fit to the second most potent group of peptides. The best-fits for the rebinding model correspond to rebinding thresholds, k_{on}^{*}, of (**A**) 32,000/M s and (**B**) 45,000/M s. These are similar to the best-fits obtained using the techniques in Fig. S5.

2.A.1 Supplemental Materials and Methods

2.A.1.1 T cell proliferation

T cell proliferation was assessed by incubating 1 x 10^5 naïve $Rag1^{-/-}$ B3K506 or B3K508 $CD4^+$ T cells for 48 hr with 5 x 10^5 irradiated C57BL/6 spleen cells and titrating amounts of 3K or 3K variant peptides in 200μl of RPMI, pulsed with 1mC [^{3}H] thymidine/well for 18hr, harvested and counted on a Wallac scintillation counter.

2.A.1.2 TCR downregulation

1 x 10^5 B3K506 and B3K508 $Rag1^{-/-}$ $CD4^+$ T cells were incubated with 5 x 10^4 bone marrow derived dendritic cells pulsed with titrating amounts of 3K or variant peptides for 16 hrs in 200ml RPMI. Cells were then washed, and labeled with anti-TCRb-FITC (HAM597), anti-CD69-PE, anti-CD4-PerCP and anti-Thy1.2-APC. TCRb expression was assessed by flow cytometry (FACScaliber, BD biosciences) on $CD4^+$ $Thy1.2^+$ cells and analyzed using FlowJo version 8.3 (TreeStar).

2.A.1.3 Intracellular cytokine production

3x10^5 CD4 B3K506 or B3K508 $Rag1^{-/-}$ $CD4^+$ T cells were stimulated with 1x10^5 C57BL/6 BM-DC pulsed with titrating concentrations of 3K or variant peptides in the presence of GolgiPlug (1μl/ml BD biosciences) for 5 hrs at 37°C. T cells were then surface stained with anti-CD4, anti-CD8, washed, fixed in 4% formaldehyde (Fischer Scientific) and stained for intracellular TNFa using a Cytofix/Cytoperm kit (BD biosciences) using manufacturer's protocol. TNFa expression was assessed by flow cytometry (FACScaliber, BD biosciences) on $CD4^+$ T cells and analyzed using FlowJo version 8.3 (TreeStar).

2.A.1.4 Surface plasmon resonance measurements of TCR–pMHC kinetics and affinities

Soluble IA^b/3K and IA^b/3K peptide variants were expressed and produced using the baculovirus expression system as previously described (1, 2). K_D and binding kinetics for TCRs binding to IA^b/3K and APLs were obtained on BIAcore 2000 and 3000 instruments (BIAcore AB, Uppsala, Sweden). Data points were collected at 0.2 sec intervals and analyzed with BIAcore Bioeval 4.1 software. Scatchard Analyses of the equilibrium data were used to determine the dissociation constant (K_D). The kinetic data were used to determine the dissociation rate and the association rate (k_a) was calculated from the K_D and k_d ($k_a=k_d/K_D$).

2.A.2 Tests of different models of ligand potency and sensitivity to model parameters

2.A.2.1 Tests to determine if T ligand potency correlates with TCR-pMHC occupancy when TCR and pMHC are membrane bound

T cell ligand potency does not correlate with the measured K_D (Fig.3A). Even though the K_D measurement of soluble proteins does not describe ligand activity, it is possible changes in receptor occupancy when TCRs and pMHC are membrane bound do describe our data. In this section, we provide an alternate argument against receptor-occupancy (K_D) based theories. In the main text, we concluded that the affect of K_D on receptor occupancy is weak due to saturation effects (Fig. 4). Thus, for a K_D–based model to explain the wide range of activities seen in our data set, the effect of receptor occupancy on activity would have to be quite strong.

To directly assess whether changes in receptor occupancy can account for ligand potency, we have compared two quantities: 1) the dose response of a T cell to different concentrations of ligand; and 2) the response of the T cell, at fixed concentrations of ligand, to ligands with different K_D. Because changes in concentration and K_D lead independently to changes in receptor occupancy, the dose response curves and the mutation studies provide independent measures of the effect of receptor occupancy on

activity. By comparing K_D-based changes in receptor occupancy (comparing different ligands) to concentration-based changes (comparing the same ligand at different concentrations), the impact of K_D can be directly assessed. To do so, we posited that changes in peptide concentration lead directly to changes in receptor occupancy, assuming TCR are in great excess and that the additional peptide binds MHC (this is at least true for low peptide concentrations). For example, we assume that a two-fold increase in peptide concentration leads to a two-fold increase in pMHC-TCR engagement.

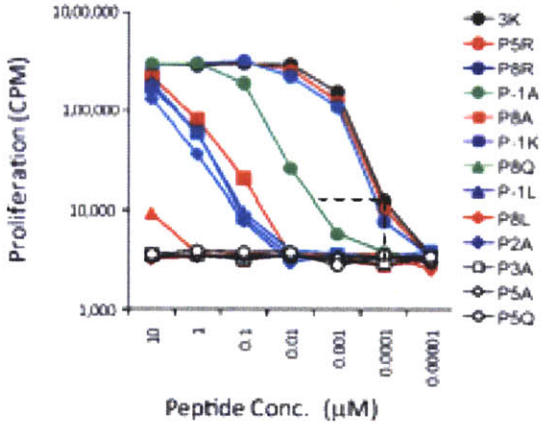

Figure S9: **Comparing changes in peptide concentration with changes in equilibrium affinity**. Changes in peptide concentration affect T cell proliferation far less than an affinity-based receptor occupancy theory would require.

Consonant with our arguments against a pure K_D theory in the main text, the data indicate that that the effect of receptor occupancy on activity is not strong enough to explain our data. The dose response curves indicate that large changes in receptor occupancy are required to increase activity, far larger than the difference in receptor occupancies between two peptides with different K_D. This can be seen in particular by examining the responses of the B3K506 TCR to two different peptides, IA^b/3K and IA^b/P-1A. The IA^b/3K peptide is more stimulatory for the B3K506 TCR than the IA^b/P-1A peptide at every concentration of peptide. In particular, at a concentration of 0.0001μM, the 3K peptide induces 14% more proliferation, on a log scale, than the P-1A peptide. The 3K

peptide also has a stronger K_D (7μM and 26μM, respectively), in apparent agreement with a K_D theory. Its four-fold higher affinity can lead at most, though, to a four-fold higher receptor occupancy at each concentration of peptide (Equation 1). Because of saturation, the actual increase is probably less. In fact, using estimates of relevant parameters, we predicted in the main text that its receptor occupancy is only 12% higher than the receptor occupancy of the P-1A peptide (Fig. 4).

For the K_D model to explain the differential activity of these two peptides, a 4-fold increase in receptor occupancy must be able to generate a 14% increase in proliferation. A 4-fold increase in the concentration of P-1A from 0.0001μM, though, barely increases its proliferation (2% on a log scale). In fact, the concentration of the P-1A ligand must be increased over 50 fold to recapitulate the activity of the 3K peptide at 0.0001μM. Even if a 50-fold increase in concentration leads to a smaller increase in receptor occupancy, the gap is quite large.

Since the different affinities in our data set lead to only small differences in receptor occupancy and peptide activity is not very sensitive to receptor occupancy, K_D theories do not explain our data.

2.A.2.2 Testing the impact of Serial Triggering

Because neither K_D nor $t_{1/2}$ models, independently or combined, explained the T cell activation data, we assessed whether serial triggering could influence ligand potency. The serial triggering hypothesis postulates that an individual pMHC can sequentially trigger multiple, distinct TCR (3, 4). Thus, the faster on-rate of IA^b/3K binding B3K506 TCRs would lead to a greater number of distinct binding events over the course of the T cell-APC interaction. Serial triggering of many more TCRs by fast kinetic ligands versus slow kinetic ligands could lead to an increase in the probability of generating uncharacteristically long-lived interactions.

To test whether serial triggering accounts for the ligand potency of IA^b/3K-reactive T cells, we determined how many more binding events would be required for a strong K_D, fast kinetic ligand to bind an equal number of TCRs for at least 2 sec as a medium kinetic, medium K_D ligand. We followed the analysis conducted by Coombs and colleagues (5). In this model, the number of distinct TCR bound by a pMHC is:

$$N = \frac{\ln(2)}{t_{1/2}}\left(\frac{K_A c_{TCR}}{1 + K_A c_{TCR}}\right)T$$

The parameter T denotes the total time a pMHC is present in the APC-TCR interface. Since the number of distinct TCR a pMHC binds depends on the affinity and on-rate in exactly the same way as the receptor occupancy, the conclusion that serial triggering also does not account for our data is not surprising.

As an example, we compared the responses of the fast-kinetic B3K506 TCR binding the IA^b/P-1A ligand and the B3K508 TCR binding IA^b/P5R. These two peptides induce similar activity but have different K_D and binding kinetics. If we assume TCRs binding pMHC have exponentially distributed dwell times, as in the main text, then to have a similar probability of engaging pMHC for 2 sec, the B3K506 TCR would have to generate 26-fold more distinct binding events to the IA^b/P-1A ligand than the B3K508 TCR binding IA^b/P5R. However, the 3.6 fold difference in K_D between the two TCR-pMHC pairs leads to only a 6.5 fold difference in the in number of distinct bound TCRs. The impact of serial triggering on equalizing half-lives becomes worse when a higher $t_{1/2}$ threshold is assumed (Fig. S4C), further suggesting that serial triggering cannot lead to significant increases in uncharacteristically long-lived TCR-pMHC interactions. Most importantly, both the B3K506 and B3K508 T cells demonstrate enhanced activity to ligands with increasing $t_{1/2}$. These data indicate that for fast kinetic, medium and strong K_D ligands, T cell activation is negatively correlated with increasing numbers of binding events.

2.A.2.3 Model and parameter sensitivity analysis

2.A.2.3.1 Model merging receptor occupancy and dwell time

In the main text, we estimated parameters in Equation 1 to evaluate whether receptor occupancy and dwell time models could jointly explain our data. Recent arguments suggest that the relevant TCR concentration in Equation 1 is the effective concentration of TCR in the synapse, averaged over TCR-rich and TCR-sparse regions, assuming that the TCR can move freely in between the two regions (6). Thus, the concentration of the TCR in the interface between the T cell and APC, c^0_{TCR}, was estimated in the main text by dividing the total number of TCR on a T cell (10,000 TCR per T cell) by the total surface area of a T cell (500 μM^2), leading to an estimate of 20 TCR/μM^2 (7). Within TCR-rich regions (e.g. islands), c^0_{TCR} is locally much higher (80-430/um^2) (8). Though we have used the lower effective concentration of TCR, higher concentrations would only improve the robustness of our conclusions, as we demonstrate below.

To convert the measured K_A of TCR-pMHC in solution to K_A when the TCR and pMHC are membrane bound, we have used a confinement length measured for the 2B4 TCR interacting with the MCC88-103 ligand (1.2 nm, corresponding to a conversion factor of 0.262 nm) (7). Although this conversion has precedent, it is uncertain, as recent research reveals (9, 10). The need for more direct measurements of membrane kinetics has long been acknowledged (11). In particular, one recent study of pMHC-TCR kinetics on the membrane has suggested that on-rates and off-rates are faster on the membrane than solution-based measurements suggest and that actin-cytoskeleten-driven membrane motion has a role in tearing apart bonds (10). The role of the membrane in breaking apart bonds as short-lived as those in this paper is unclear.

Since the parameters involved in our models are uncertain, we checked that our conclusions were robust to parameter variations. First, we checked the validity of our conclusion that the receptor occupancy is saturated. To do so, we varied the threshold affinity, K*, modeling uncertainty both in the concentration of TCR on the T cell and likely errors in converting SPR-measured affinities to affinities on the membrane (Fig. S6). If the threshold K_D is weaker than our estimate, even weakly binding peptides will almost always be bound, and the conclusion is robust. As the threshold K_D becomes

much stronger than our estimate, some of the weaker binding peptides in our sample become unsaturated. Even in these cases, however, it is unlikely that changes in K_D could compensate for changes in $t_{1/2}$ in a merged receptor occupancy/dwell time model. The dwell time depends strongly (exponentially) on the $t_{1/2}$, whereas the receptor occupancy depends weakly (sublinearly) on the K_D, even if the system is not saturated (see the arguments in the tests of the pure affinity model).

2.A.2.3.2 Rebinding

2.A.2.3.2.1 Model sensitivity

In the main text, we applied Bell's model to estimate the importance of rebinding on the membrane. Here, we briefly motivate rebinding models to suggest that our qualitative conclusions are robust to the choice of model.

Once a ligand and receptor debind, we assume there is some probability they will rebind within a given time interval. Suppose we knew this probability (p). Then, the number of rebindings would be a geometrically distributed random variable with parameter 1- p, assuming that every rebinding is independent, and the expected number of rebindings would be p/(1-p).

What is the probability p? Clearly, it depends on the time interval over which rebindings are counted. In the case of the interaction between TCR and pMHC, we are only interested in those rebindings that occur relatively quickly, before the TCR signaling complex disassembles. Since it is unclear how quickly the TCR signaling complex disassembles, however, models must choose a different measure of "quickness." (Analytically, other measures are also more tractable.) One reasonable approach is to count only those rebindings that occur before the pMHC binds another TCR for the first time.

In a different approach, Bell's model can be interpreted to count only those rebindings that occur almost immediately, before the receptor and ligand are ever separated by more than a molecular distance. To see this, consider the probability that a pMHC binds to a TCR before diffusing away when it is within a molecular distance of the TCR. For simplicity, we can model the reaction and diffusion as competing exponential processes with rates corresponding to their characteristic rates, which scale as k_{on}/L^2 and D/L^2, respectively, where L is the molecular distance. (Note that k_{on} is expressed on a per molecule basis.) Applying this simple analysis to determine the probability p (12), it is possible to obtain Bell's model (Equation 2), within a constant factor.

How sensitive are the conclusions to the particular choice of model? Clearly, the choice of which rebindings to count will affect the quantitative results. Allowing more time for the pMHC and TCR pair to rebind, for example, will lead to larger predictions for the aggregate $t_{1/2}$. The qualitative prediction of the model, however, is robust. Independent of the choice of model, the aggregate $t_{1/2}$ will depend on the $t_{1/2}$ and K_D when on-rates are low or high, respectively, and on a combination of the two when on-rates are intermediate. The robustness of this conclusion stems from the fact that it can be motivated independently by simple arguments. When on-rates are slow, rebindings will not occur and the aggregate $t_{1/2}$ will depend on the single-interaction half-life. Conversely, when on-rates are fast, a pMHC and TCR will rebind many times, essentially equilibrating. As a result, the aggregate $t_{1/2}$ will depend only on the K_D when on-rates are large.

2.A.2.3.2.2 Parameter estimates and sensitivity

To evaluate whether rebinding could impact the dwell time of B3K506 or B3K508 TCRs engaging IA^b/3K and APL ligands, we estimated the parameters in Equation 2. The diffusivity for a TCR and pMHC was estimated using published experimental measurements. We used 0.04 um^2/sec and 0.02 um^2/sec as typical estimates of the diffusivities of pMHC (13-15) and TCR, respectively (16-18). The range of reported diffusivities is from 0.01 to 0.1 um^2/sec for pMHC, with measurements concentrated

toward the lower end, and from 0.01 to 0.12 um^2/sec for TCR, though the higher estimates may apply to TCR outside lipid rafts. We converted our SPR measurements of on-rates to on-rates on the membrane by assuming that affinities on the membrane are proportional to SPR-measured affinities, as in our analysis of receptor occupancy, and further, by assuming that off-rates on the membrane are identical to those measured by SPR. Because of limited data, it is generally difficult to convert SPR-measured on-rates to on-rates on the membrane (11, 19). A recent study of pMHC-TCR kinetics on the membrane has suggested that on-rates and off-rates are faster on the membrane than solution-based measurements suggest and that actin-cytoskeleten-driven membrane motion has a role in tearing apart bonds (10). The role of the membrane in breaking apart bonds as short-lived as those in this paper is unclear. Additionally, since faster on-rates promote rebinding but membrane motion driving the pair apart inhibits rebinding, it is too early to understand how our qualitative results would be affected.

Because of the uncertainty in these parameters, we checked the robustness of our conclusion that rebinding explains the potency of the peptides in our data set. To do so, we varied the threshold for rebinding, k_{on}*, which models uncertainties in the diffusivities of the TCR and pMHC and errors in converting SPR-measured on-rates to on-rates on the membrane. It is also a rough way of accounting for other factors that might increase or decrease the likelihood of rebinding, such as membrane motion, as well as uncertainty in the model itself. Three-fold differences in the threshold on-rate do not qualitatively affect our conclusions (Figs. S5 and S7). As the threshold for rebinding increases, rebindings become less likely for any given pMHC-TCR pair and the effect of rebinding on the aggregate $t_{1/2}$ weakens. As long as the rebinding threshold falls within or near the range of on-rates in our data, it will explain at least part of the difference between the B3K506 and B3K508 TCR, balancing their K_D and $t_{1/2}$.

Independent of the parameter estimates, we also provided best-fit values in the main text, which, being close to our estimates, reinforced our conclusions. We provide another type of best-fit analysis, based on fitting the models to groups of peptides with similar activity, in Fig. S8 to show this conclusion in another way.

Supplemental References

1. Huseby ES, *et al.* (2005) How the T cell repertoire becomes peptide and MHC specific. *Cell* 122(2):247-260.
2. Huseby ES, Crawford F, White J, Marrack P, & Kappler JW (2006) Interface-disrupting amino acids establish specificity between T cell receptors and complexes of major histocompatibility complex and peptide. *Nat. Immunol.* 7(11):1191-1199.
3. Valitutti S, Muller S, Cella M, Padovan E, & Lanzavecchia A (1995) Serial Triggering of Many T-Cell Receptors by a Few Peptide-Mhc Complexes. *Nature* 375(6527):148-151.
4. Wofsy C, Coombs D, & Goldstein B (2001) Calculations show substantial serial engagement of T cell receptors. *Biophys. J.* 80(2):606-612.
5. Coombs D, Kalergis AM, Nathenson SG, Wofsy C, & Goldstein B (2002) Activated TCRs remain marked for internalization after dissociation from pMHC (vol 3, pg 926, 2002). *Nat. Immunol.* 3(11):1109-1109.
6. Zhu DM, Dustin ML, Cairo CW, & Golan DE (2007) Analysis of two-dimensional dissociation constant of laterally mobile cell adhesion molecules. *Biophys. J.* 92(3):1022-1034.
7. Grakoui A, *et al.* (1999) The immunological synapse: A molecular machine controlling T cell activation. *Science* 285(5425):221-227.
8. Dushek O & Coombs D (2008) Analysis of serial engagement and peptide-MHC transport in T cell receptor microclusters. *Biophys. J.* 94(9):3447-3460.
9. Tolentino TP, *et al.* (2008) Measuring diffusion and binding kinetics by contact area FRAP. *Biophys. J.* 95(2):920-930.
10. Huppa JB, *et al.* (2010) TCR-peptide-MHC interactions in situ show accelerated kinetics and increased affinity. *Nature* 463(7283):963-U143.
11. Dustin ML, Bromley SK, Davis MM, & Zhu C (2001) Identification of self through two-dimensional chemistry and synapses. *Annu. Rev. Cell Dev. Biol.* 17:133-157.
12. DeGroot MH (2002) *Probability and Statistics* (Addison-Wesley, Boston) 3 Ed p 816.
13. Wade WF, Freed JH, & Edidin M (1989) Translational Diffusion of Class-Ii Major Histocompatibility Complex-Molecules Is Constrained by Their Cytoplasmic Domains. *J. Cell Biol.* 109(6):3325-3331.
14. Edidin M, Kuo SC, & Sheetz MP (1991) Lateral Movements of Membrane-Glycoproteins Restricted by Dynamic Cytoplasmic Barriers. *Science* 254(5036):1379-1382.
15. Pecht I & Gakamsky DM (2005) Spatial coordination of CD8 and TCR molecules controls antigen recognition by CD8(+) T-cells. *FEBS Lett.* 579(15):3336-3341.
16. Sloan-Lancaster J, *et al.* (1998) ZAP-70 association with T cell receptor zeta (TCR zeta): Fluorescence imaging of dynamic changes upon cellular stimulation. *J. Cell Biol.* 143(3):613-624.

17. Favier B, Burroughs NJ, Wedderburn L, & Valitutti S (2001) TCR dynamics on the surface of living T cells. *Int. Immunol.* 13(12):1525-1532.
18. Gakamsky DM, *et al.* (2005) CD8 kinetically promotes ligand binding to the T-cell antigen receptor. *Biophys. J.* 89(3):2121-2133.
19. Robert P, Benoliel AM, Pierres A, & Bongrand P (2007) What is the biological relevance of the specific bond properties revealed by single-molecule studies? *J. Mol. Recognit.* 20(6):432-447.

Chapter 3

Stochastic decisions enable T lymphocytes to achieve complex immunological goals with a simple signaling network[1]

"The first story is about what the Constitution is like.
It's going to show that the Constitution is no simple contract,
not because it uses a certain amount of open-ended
language that a contract draftsman would try to avoid, but
because its language grants and guarantees many good things,
and good things that compete with each other and
can never all be realized, all together, all at once."
--Justice David Souter

Biological systems without sensors and genetic diversity, such as some bacteria (at least as modeled), make stochastic decisions to diversify responses with the aim of optimizing performance (e.g., growth) in uncertain environments. T lymphocytes, a key part of the adaptive immune system in higher organisms, are an example of a genetically diverse population of cells with sensors for diverse environments which co-exist in the host and perform complex biological functions. In such a system, each cell should not need to make stochastic decisions to diversify responses. But, T cells do make stochastic decisions. With the biology of this system as a guide, we use a decision-theoretic framework to obtain general necessary conditions for stochastic responses to be beneficial for function in systems with sensors and great genetic diversity. By studying a specific model that satisfies these conditions, we find a new role for noise in complex biological systems. Stochastic decisions by individual components (T cells) allow the interacting population to achieve complex goals with simpler biochemical machinery (e.g., a simpler signaling network) than would be required to implement a deterministic response which achieves the same performance. Thus, while not required for

[1] The work in this chapter has been submitted for publication as "Stochastic decisions enable T lymphocytes to achieve complex immunological goals with a simple signaling network."

diversification, noise provides a simpler solution to a complex challenge confronted by populations of cells in higher organisms.

3.1 Introduction

Stochastic effects in cell decision processes have been observed in varied biological contexts (*1-5*). Most studies to determine their role have focused on systems where the inputs received by individual cells are not diverse because they lack sensors or because of limited or no genetic and environmental diversity. In such cases, stochastic decisions by individual cells diversify responses to help a population of cells achieve certain system-specific objectives (*6-13*). For example, stochastic decisions enhance survival of sensorless bacteria in a varying environment (*9-13*).

Diverse stimuli provide varying inputs to a population of cells with sensors in complex organisms, and the resulting responses can draw on considerable genetic variation between cells (since cells in higher organisms with different genotypes or epigenetic markers can co-exist to perform complex functions). One important example is the response of a population of T lymphocytes (T cells), orchestrators of adaptive immunity, to diverse infections. Each T cell has a receptor (or sensor), the T cell receptor (TCR), and most T cells express a unique TCR. T cells respond to peptides (p) derived from pathogenic proteins which are expressed on infected cells in complex with host major histocompatibility (MHC) proteins (*14*). A particular T cell can respond to a pMHC if its TCR binds sufficiently strongly to it. A pathogen expresses many pMHCs, each binding to individual TCRs with different affinities. This system, therefore, is one where a genetically diverse population of cells, each with a sensor, receives diverse inputs to which it responds to clear infections. Over a range of TCR-pMHC binding affinity, or strength of other stimuli such as that provided by cytokines, some T cells fire and others do not, due to internal and/or external noise (*15-18*). The role of noise in regulating the function of such systems is not known (*1*). We consider a model of T cell interactions and their outcomes which abstracts general features observed in experiments to address this issue in the context of a specific biological system.

3.2 Model development

Given a stimulus strength, x, each T cell makes a binary decision to either activate or not. The decisions, determined by the T cell's signaling network, are observed to be stochastic. Thus, the probability of activation ($\sigma(x)$ in Fig. 1A) increases from approximately zero to approximately one over a finite range of stimulus strength; in contrast, for deterministic decisions, $\sigma(x)$ is always either 0 or 1. Self peptides derived from host proteins are also expressed on cells, and they are more likely to stimulate TCRs on T cells weakly due to developmental processes. The outcomes of decisions made by a collection of T cells can be quantified by a cost for the host, which depends upon the decisions in two ways: 1] Whether the responses to self or pathogenic pMHC are correct or not. If too many T cells activate upon interactions with self pMHC, autoimmunity would ensue. If too few T cells activate in response to a pathogen's pMHC molecules, persistent infection or death could result. 2] There are also costs to the host regardless of whether decisions are correct. Examples are: a decision to activate incurs a metabolic cost; when there are resource (e.g., cytokine) limitations, the decision to activate costs more if several T cells have already been activated.

The dependence of the cost, C, on the factors above is denoted by $C(\vec{e},\vec{d})$. Each element (d_i) of the vector, $\vec{d}$, lists the decision made upon a specific T cell-pMHC interaction ($d_i = 1$ and $d_i = 0$ denote a decision to activate and not activate, respectively). The vector, $\vec{e}$, is a list describing whether each decision is correct or not (Fig. 1B). The cost can also depend upon the stimulus strength (supporting online text). Our goal is to understand whether the decision rule for individual T cells, $\sigma^*(x)$, that optimizes the outcome for the host involves stochastic decisions. For all decision rules, the ultimate outcome (or cost to the host) of T cell decisions is uncertain because diverse processes pertinent to an immune response are intrinsically stochastic. For example, two individuals may have varying success clearing infection and avoiding autoimmunity even though their T cells adopt the same decision rule. Therefore, we optimize the following expected (average) cost to a host:

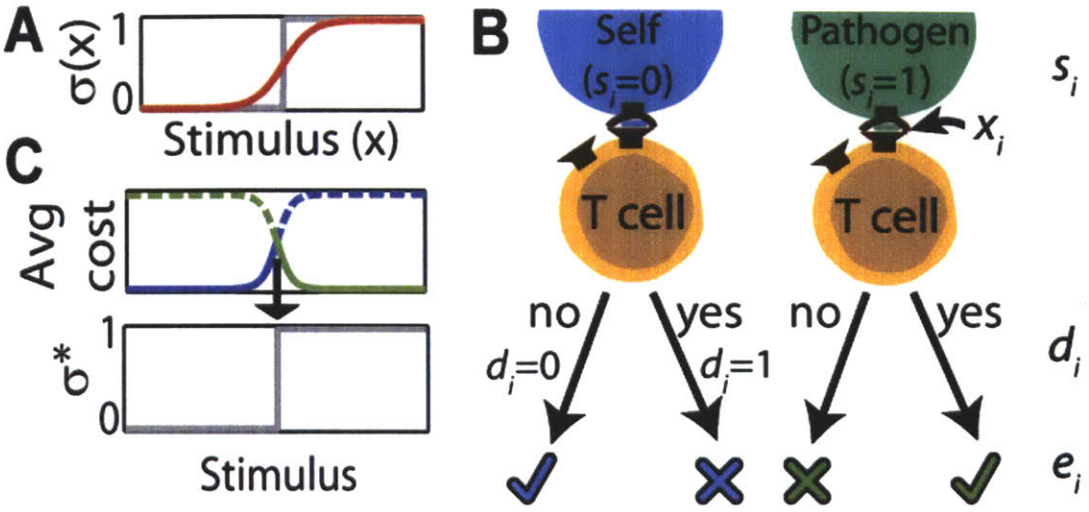

Figure 1: T cells make stochastic decisions. (A) A T cell's activation probability, σ, is governed by a stochastic decision rule (red), not a sharp deterministic threshold (grey; (15-18). (B) The variable s_i denotes whether the interaction is with self or pathogenic pMHC; x_i is the stimulus strength (e.g. TCR-pMHC binding strength); d_i is the actual decision made (yes, activate; no, remain inactive); and e_i specifies whether the decision is correct (✓) or not (⊠) against self (blue) or pathogenic (green) pMHC (four possibilities). (C) An isolated T cell should activate whenever the expected or average cost of not activating (e.g. blue) is greater than the expected cost of activating (green), corresponding to an optimal deterministic decision rule, σ^*, where activation occurs above a sharp threshold stimulus strength.

$$E[C(\vec{e},\vec{d})] = \sum_{\vec{s},\vec{d},N} \int d\vec{x} C(\vec{e},\vec{d}) P(\vec{s},\vec{x},\vec{d},N) \qquad (1)$$

$\vec{s}$ is a vector that lists whether each interaction is with self (s_i=0) or pathogenic (s_i=1) pMHC, N is the total number of interactions, and P indicates a probability model describing the diverse stochastic effects in the immune system when a particular decision-rule σ is used; note that $\sigma(x_i) = P(d_i = 1|x_i)$ by definition, as $P(d_i = 1|x_i)$ is the probability of activation given the stimulus, x_i. The variables $\vec{s}$, $\vec{x}$, $\vec{d}$, and N, must be explicitly included to study genetically diverse cells with sensors in an uncertain environment. (Note that e_i is fully determined by the decision d_i and s_i.) The coarse-grained treatment of the details of all other stochastic processes in terms of a probability model enables us to make widely-applicable statements about this class of systems. The optimal decision rule, σ*, minimizes the expected cost (*19, 20*).

3.3 Results

3.3.1 Isolated T cell

Consider the simplest case of an isolated T cell interacting once with a single stimulus (x, e, d, and s are scalars). For a given stimulus, x, the expected cost is the expected cost of activating weighted by the probability of activation ($\sigma(x)$), and the expected cost of not activating weighted by the probability of not activating ($1-\sigma(x)$):

$$E[C(e,d) \mid x] = E[C(e,d) \mid x, d = 1]\sigma(x) + E[C(e,d) \mid x, d = 0](1 - \sigma(x)) \qquad (2)$$

As noted, self-peptides are less likely to stimulate T cells very strongly; so, the expected cost of activating for very weak stimuli is high, and vice versa. So, the expected cost for activation is a strictly decreasing function of x, and that for not activating increases with x (Fig. 1C). So, the expected cost for not activating exceeds that of activating at a single stimulus strength. Eq. 2 shows that the choice of σ that minimizes the expected cost is $\sigma = 0$ if the expected cost of activation is greater than expected cost of not activating, and $\sigma = 1$ if the opposite is true. Therefore, the optimal decision rule for isolated T cells is a deterministic sharp switch from not activating to activating and could be implemented by the existing T cell signaling machinery if noise was suppressed (e.g., with more molecules). Given the importance of T cell decisions on the host's health, why have evolutionary forces not led to this situation?

3.3.2 Coupling at the population level

Function is determined by the response of the T cell population. Individual T cell responses are coupled to each other in a number of ways. The cost incurred by a T cell's decision depends on the decisions of other T cells (Fig. 2A). The cost of a T cell not activating in response to a pathogenic pMHC is lower if many T cells have been activated in response to the infection since only a certain level of activation can clear infections. Also, the cost of activating against self pMHC is higher if similar events have already occurred since peripheral tolerance mechanisms can tolerate only some autoimmune

responses. Resource (e.g., cytokine) limitations also couple the costs incurred by individual T cell decisions. Coupling of T cell responses through incurred costs means that the cost to the host is not the sum of costs incurred in individual interactions; i.e.,

$$C(\vec{e},\vec{d}) \neq \sum_{i=1}^{N} \overline{C}(e_i,d_i) \tag{3}$$

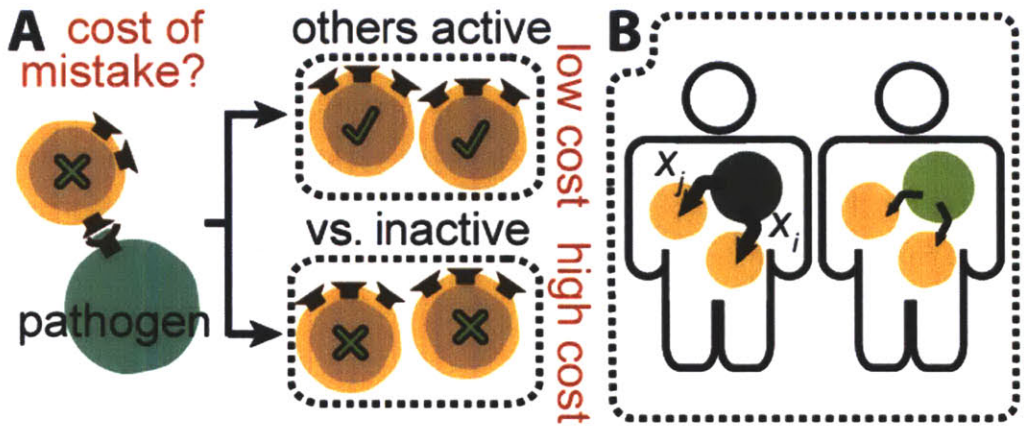

Figure 2: T cells are coupled at the population level. (A) T cell decisions are coupled through their costs for the host. For example, the cost of a T cell mistakenly not activating (✖) against a pathogenic pMHC depends on the correctness of other T cells' decisions. If enough others activate (✔) in response to this pathogen, the mistake has minimal impact since the infection will be cleared (low cost). Conversely, if other T cells have not been activated, there is a high cost for the T cell not activating as the pathogen will proliferate unchecked. (B) T cell decisions are coupled through their observations, because T cells are in the same host confronting the same infection. For example, if a particular infection results in the expression of pathogenic pMHC with which some T cell clone in a host interacts particularly strongly (indicated by a dark green color in the host on the left), then there will be many strong interactions over the course of that infection. In contrast (right), if an infection results in the strongest interaction being weak (light green color in the host on the right), there will be many weak interactions. T cell decisions are also coupled because the decisions T cells make can affect others' observations, but this is not illustrated.

The observations made by individual T cells via their sensors are coupled because the T cells are in the same host and confronting the same infections (Fig. 2B). For example, if a particular infection results in the expression of pathogenic pMHC with which a T cell clone interacts particularly strongly, the interactions of each T cell of this clonotype (and other similar ones) with this pMHC will result in a strong stimulus as well. Thus, the

observations made in individual T cell-pMHC interactions are not independent. This coupling through T cells' observations means that the joint probability of the observations is not the product of probabilities of individual observations:

$$P(\vec{s},\vec{x},\vec{d} \mid N) \neq \prod_{i=1}^{N} P(s_i,x_i)P(d_i \mid x_i) \tag{4}$$

The decision of one T cell can also affect the observations of other T cells. For example, if a T cell activates in response to a particular pMHC expressed upon infection by a fast–mutating virus, the resulting immune pressure will cause the outgrowth of a mutant strain that will present pMHC that may strongly stimulate another T cell. This type of coupling implies that the probability of the observations and the decisions jointly is not the product of the probabilities of the observations and the decisions:

$$P(\vec{s},\vec{x},\vec{d} \mid N) \neq P(\vec{s},\vec{x})\prod_{i=1}^{N} P(d_i \mid x_i) \tag{5}$$

3.3.3 Necessary conditions for stochastic decisions to be beneficial

If T cells are coupled only through their costs, each T cell makes an error (activates against self or does not activate against pathogens) independently. The probabilities of making an error are:

$$p_0 = P(s=0)\int dx P(x \mid s=0)\sigma(x) = \text{probability of incorrectly activating} \tag{6a}$$

$$p_1 = P(s=1)\int dx P(x \mid s=1)(1-\sigma(x)) = \text{probability of incorrectly not activating} \tag{6b}$$

Eq. 6a is the product of the probability of seeing a self pMHC averaged over all conditions ($P(s = 0)$) and the probability of activating to a stimulus strength, x, given that it is a self pMHC ($s = 0$). A similar logic leads to Eq. 6b. The Neyman-Pearson lemma (*21*) states that the decision rule jointly minimizing the probabilities of error in Eq. 6 is a single deterministic sharp threshold, when the likelihood of one action being correct increases with the stimulus, as for T cells (supporting online text).

If T cells were coupled only through their observations, the inequality in Eq. 3 would not hold, and the resulting linearity makes treating the coupling through the observation probabilities (Eq. 4) easy (supporting online text). We find that the expected cost (Eq. 1) is:

$$E\left[C\left(\vec{e},\vec{d}\right)\right] = \int a(x)\sigma(x)dx \qquad (7)$$

where a is a function that depends on the probability model and cost function but not on the decision rule. Arguments analogous to those for the isolated T cell (supporting online text) suggest that the optimal decision rule for T cells is a single sharp threshold (not stochastic).

Our arguments provide general necessary conditions for stochasticity to be useful in systems with sensors and access to abundant environmental or genetic diversity: (1) the population-level response is important (isolated T cells do not require stochastic decisions); and (2) biological features of the system must strongly couple the population of cells (T cells must be coupled through more than the cost alone or the observations alone). For populations of cells which lack environmental or genetic diversity, coupling through the cost alone is sufficient for stochastic decisions to be beneficial (*3, 8, 22*). Thus, the conditions above are more stringent (though observations might be considered trivially coupled if no cell has sensors). T cells satisfy these necessary conditions as they are not coupled through costs or observations alone.

3.3.4 A simple model of the T cell population in which stochastic decisions are beneficial

To explore the minimal sufficient conditions for stochastic decisions to emerge as an optimal solution for a population of T cells, we considered a simple model of coupling between T cell decisions via incurred costs and observations. Coupling through the costs is treated by noting that the cost incurred by the host over the course of a single infection decreases nonlinearly with the fraction of pathogenic pMHC to which T cells activate (f_1), and increases with the fraction of self pMHC that stimulate activation (f_0). Thus:

$$C(\vec{e},\vec{d}) = \left(\frac{1}{1+c_1 f_1(\vec{e})}\right) + c_2\left(e^{c_3 f_0(\vec{e})} - 1\right) \quad (8)$$

which satisfies Eq. 3. Our qualitative conclusions do not depend on the values of the constants c_1, c_2, and c_3, or the specific nonlinear form of Eq. 8 (supporting online text).

Coupling through the observations is treated by choosing a probability model that satisfies Eq. 4. It incorporates many possible infections, I_k, each of which correspond to different distributions, $P(x_i|s_i=1,I_k)$, of strong stimuli for the host's T cell repertoire (Fig. 3A). Independent of the infection, self pMHC lead primarily to weak stimuli as described by $P(x_i|s_i=0)$ (Fig. 3A). Then, the probability model (consistent with Eq. 4) is:

$$P(\vec{s},\vec{x},\vec{d} \mid N) = \sum_k P(I_k) \prod_{i=1}^{N} P(s_i,x_i \mid I_k) P(d_i \mid x_i) \quad (9)$$

The probability that the infection confronted is the k^{th} one, $P(I_k)$, is chosen so that it is unlikely that the immune system confronts an infection that leads only to weak stimuli. We assume that the number of encounters is large enough to sample the probability distributions well during any particular infection.

By numerical optimization, we find that a stochastic decision rule outperforms one characterized by a single sharp threshold which would be obtained by suppressing noise (Fig. 3B). Just including coupling between T cell decisions via the incurred costs and observations in a simple way results in stochastic decisions being beneficial, suggesting that this would definitely be so if additional sources of coupling between T cells were included. A single sharp threshold stimulus strength separating decisions to activate or not enforces all-or-nothing immune pressure over different regions of stimulus strength. This is unlikely to be the appropriate balance between the risk that some self-peptides will generate strong stimuli or that some infections will lead only to relatively weak stimuli (Fig. 3C). A stochastic decision rule achieves this balance, critical for the host's survival, more readily.

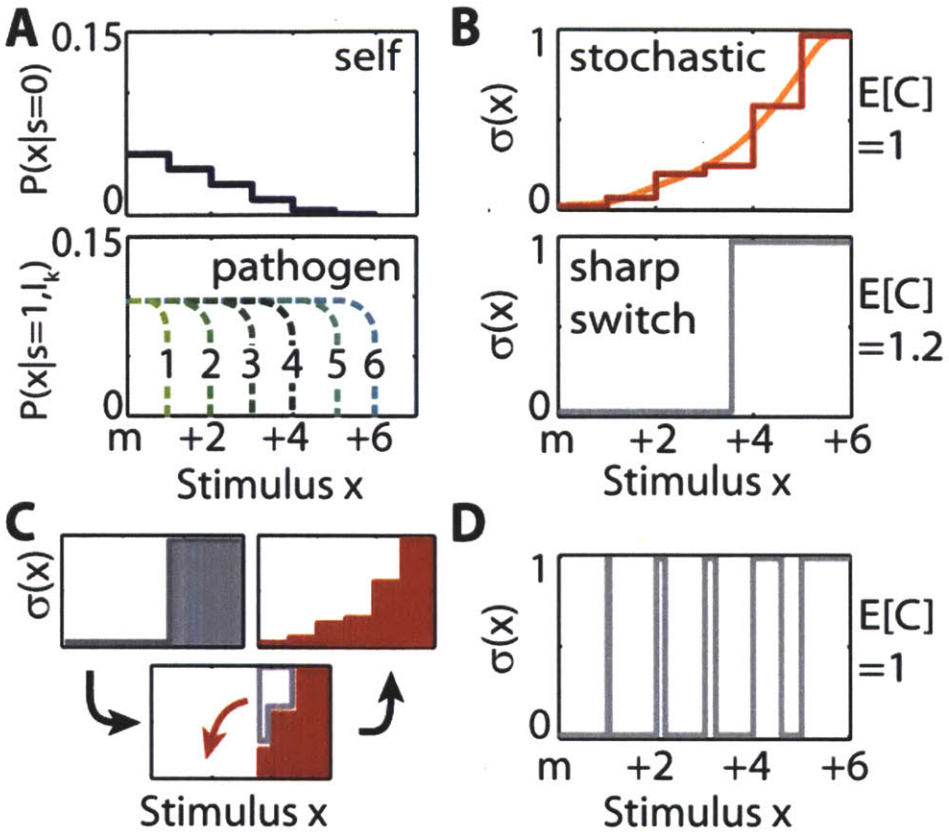

Figure 3: A simple model demonstrates that stochastic decisions can enable T cells to achieve complex goals with a simpler signaling network than that required for an optimal deterministic decision rule. (A) The probability distributions for the stimuli T cells receive from self ($P(x|s=0)$, upper) and pathogenic ($P(x|s=1,I_k)$, lower) pMHC, where I_k denotes the k^{th} infection. For weak stimulus strengths, these probability distributions are expected to be similar for self and pathogenic pMHC with high values for P; m denotes an intermediate stimulus strength, above which these probability distributions are different. The numbers on the abscissa are in arbitrary units. The six possible infections (distributions of pathogenic stimuli) occur with probability 0.001, 0.049, 0.15, 0.25, 0.3, and 0.25, from I_1 to I_6, so that infections which lead only to relatively weak stimuli are unlikely. Similarly, strong stimuli from self are unlikely. (B) For the probability and cost models in the main text, the best single sharp threshold (grey) has a higher expected cost (E[C]) than a stochastic decision rule (red). Reported E[C] is normalized by the expected cost of the stochastic decision rule. The optimal decision rules reflect the discretization of the probability distributions describing stimulus strengths (see panel A); the orange curve helps visualize the stochastic solution. (C) The best stochastic decision rule (red) can be created from a sharp threshold (grey) by shifting immune pressure (red arrow) from strong stimuli to weaker stimuli. This shift helps balance the risk that some self pMHC lead to strong stimuli and some pathogens lead only to relatively weak stimuli. (D) A complex deterministic decision rule that alternates between never activating ($\sigma=0$) and always activating ($\sigma=1$) performs as well as the best stochastic one (panel B). Implementing this decision rule would require a complex signaling network.

3.3.5 The role of stochastic decisions in systems with access to environmental and genetic diversity

Are there deterministic decision rules, albeit more complicated than a single sharp switch, which are as good as the optimal stochastic solution? The Dvoretzky-Wald-Wolfowitz (DWW) theorem suggests that it is always possible to find such a deterministic solution, for a model such as that described by Eqs. 8 and 9, as long as the probability distributions of stimuli observed by T cells are continuous (*23, 24*). The latter should be true because two T cells are unlikely to see exactly the same stimulus due to abundant genetic (different TCRs) and environmental (different pathogens, different levels of pMHC expression) diversity. By searching for optimal deterministic solutions that are not restricted to being a single sharp switch (supporting online text), we obtain a deterministic optimal decision rule (Fig 3D) that performs as well as the stochastic solution.

The DWW theorem makes precise the intuition that stochasticity may not be needed for diversification of the response when there is considerable genetic or environmental diversity to draw on, as for the T cell population. However, Fig. 3D shows that the optimal deterministic decision rule that exploits the environmental and genetic diversity is not a simple sharp threshold. Thus, it could not be obtained using the existing T cell signaling machinery and suppressing noise. Because of coupling between T cell decisions, the optimal deterministic decision rule is far more complicated, and could only be implemented by a complex signaling network (e.g. many coordinated feedback loops to generate many sharp thresholds.) By making stochastic decisions, T cells can perform just as well with a far simpler signaling network, which may be easier to control and evolve.

3.4 Discussion

The role of noise in biological decisions has been viewed in two ways. First, as a nuisance that is costly to suppress (*25*). Second, as a way for populations with limited

environmental or genetic diversity to diversify their responses, which, in turn, optimizes some function (e.g. population growth in a varying environment (*11*)). We have considered a biological system that is comprised of genetically and environmentally diverse cells with sensors. In this system, noise is not necessary for diversification. Our results uncover a new role for noise in complex biological systems. Stochasticity enables a population of cells to achieve complex goals with simpler biochemical machinery (e.g., signaling networks) than would be required in the absence of noise. By abstracting the features of the T cell response to pathogens, we have identified general necessary conditions that proscribe when stochasticity is useful in this way. A remarkable implication for T cell biology is that to understand the design of an individual T cell's signaling network it is necessary to analyze the behavior of the T cell population.

References

1. Raj A & van Oudenaarden A (2008) Nature, Nurture, or Chance: Stochastic Gene Expression and Its Consequences. *Cell* 135(2):216-226.
2. McDonnell MD & Abbott D (2009) What Is Stochastic Resonance? Definitions, Misconceptions, Debates, and Its Relevance to Biology. *PLoS Comput. Biol.* 5(5):9.
3. Perkins TJ & Swain PS (2009) Strategies for cellular decision-making. *Mol. Syst. Biol.* 5:15.
4. Spencer SL, Gaudet S, Albeck JG, Burke JM, & Sorger PK (2009) Non-genetic origins of cell-to-cell variability in TRAIL-induced apoptosis. *Nature* 459(7245):428-U144.
5. Tay S, *et al.* (2010) Single-cell NF-kappa B dynamics reveal digital activation and analogue information processing. *Nature* 466(7303):267-U149.
6. Wolf DM, Vazirani VV, & Arkin AP (2005) Diversity in times of adversity: probabilistic strategies in microbial survival games. *J. Theor. Biol.* 234(2):227-253.
7. Avlund M, Dodd IB, Szabolcs S, Sneppen K, & Krishna S (2009) Why Do Phage Play Dice? *J. Virol.* 83(22):11416-11420.
8. Paszek P, *et al.* (2010) Population robustness arising from cellular heterogeneity. *Proc. Natl. Acad. Sci. U. S. A.* 107(25):11644-11649.
9. Thattai M & van Oudenaarden A (2004) Stochastic gene expression in fluctuating environments. *Genetics* 167(1):523-530.
10. Balaban NQ, Merrin J, Chait R, Kowalik L, & Leibler S (2004) Bacterial persistence as a phenotypic switch. *Science* 305(5690):1622-1625.
11. Kussell E & Leibler S (2005) Phenotypic diversity, population growth, and information in fluctuating environments. *Science* 309(5743):2075-2078.
12. Acar M, Mettetal JT, & van Oudenaarden A (2008) Stochastic switching as a survival strategy in fluctuating environments. *Nature Genet.* 40(4):471-475.
13. Beaumont HJE, Gallie J, Kost C, Ferguson GC, & Rainey PB (2009) Experimental evolution of bet hedging. *Nature* 462(7269):90-U97.
14. Murphy K, Travers P, & Walport M (2007) *Janeway's Immunobiology* (Garland Science) 7 Ed.
15. Das J, *et al.* (2009) Digital Signaling and Hysteresis Characterize Ras Activation in Lymphoid Cells. *Cell* 136(2):337-351.
16. Feinerman O, Veiga J, Dorfman JR, Germain RN, & Altan-Bonnet G (2008) Variability and robustness in T cell activation from regulated heterogeneity in protein levels. *Science* 321(5892):1081-1084.
17. Altan-Bonnet G & Germain RN (2005) Modeling T cell antigen discrimination based on feedback control of digital ERK responses. *PLoS. Biol.* 3(11):1925-1938.
18. Busse D, *et al.* (2010) Competing feedback loops shape IL-2 signaling between helper and regulatory T lymphocytes in cellular microenvironments. *Proc. Natl. Acad. Sci. U. S. A.* 107(7):3058-3063.
19. Bertsekas D (2005) *Dynamic Programming and Optimal Control* (Athena Scientific, Belmont, MA) 3 Ed.

20. Resnik MD (1987) *Choices: An Introduction to Decision Theory* (University of Minnesota Press, Minneapolis).
21. Lehmann (1959) *Testing Statistical Hypotheses* (John Wiley & Sons, New York).
22. Paulsson J, Berg OG, & Ehrenberg M (2000) Stochastic focusing: Fluctuation-enhanced sensitivity of intracellular regulation. *Proc. Natl. Acad. Sci. U. S. A.* 97(13):7148-7153.
23. Dvoretzky A, Wald A, & Wolfowitz J (1950) ELIMINATION OF RANDOMIZATION IN CERTAIN PROBLEMS OF STATISTICS AND OF THE THEORY OF GAMES. *Proc. Natl. Acad. Sci. U. S. A.* 36(4):256-260.
24. Feinberg EA & Piunovskiy AB (2005) On the Dvoretzky-Wald-Wolfowitz theorem on nonrandomized statistical decisions. *Theory Probab. Appl.* 50(3):463-U461.
25. Lestas I, Vinnicombe G, & Paulsson J (2010) Fundamental limits on the suppression of molecular fluctuations. *Nature* 467(7312):174-178.

3A Appendix for Chapter 3

3A.1 Motivation for the coarse-grained model

In the main text, we noted that Eq. 1 results from a coarse-grained model of the immune system. In this section, we provide details about this coarse graining and show how the cost can formally depend explicitly on the stimulus strengths.

Let the vector $\vec{u}(t)$ indicate the value of all the variables necessary to describe the immune system and any infections at a fixed time t. For example, $\vec{u}(t)$ contains as elements the positions of all T cells in the body, the number of TCR on their surfaces bound to pMHC, and the spatial distribution of cytokines, among many other variables. The function $\vec{u}(t)$ defines a temporal trajectory of the system.

Let $P[\vec{u}(t)]$ be the probability (density) of a specific trajectory $\vec{u}(t)$. This probability depends on the probability distribution of initial conditions for the immune system (e.g. the particular infection(s) encountered, the T cell repertoire) and the dynamics of the immune response and infection. This probability also depends on the T cells' decision rule, $\sigma(x)$, since the decision rule affects the dynamics of the immune response.

Let $\hat{C}[\vec{u}(t)]$ be the cost to the host incurred during a specific realization of the immune system's trajectory. Here we allow the cost to depend on all possible variables necessary to describe the immune system and their values over the course of the host's immune response.

The expected cost to the host is $E\left[\hat{C}[\vec{u}(t)]\right]$, where the expectation is taken with respect to the probability model $P[\vec{u}(t)]$. The coarse graining noted in the main text is then:

$$E\left[\hat{C}[\vec{u}(t)]\right] = E_{\vec{s},\vec{x},\vec{d},N}\left[E\left[\hat{C}[\vec{u}(t)]\middle|\vec{s},\vec{x},\vec{d},N\right]\right] \qquad \text{(S1)}$$

The inner expectation is taken with respect to all trajectories consistent with particular values of $\vec{s}$, $\vec{x}$, $\vec{d}$, and N. The outer expectation is then taken with respect to the uncertainty in these 4 variables.

From Eq. S1 we can identify the coarse-grained cost introduced in the main text as:

$$C\left(\vec{s},\vec{x},\vec{d},N\right) = E\left[\hat{C}\left[\vec{u}(t)\right]\middle|\vec{s},\vec{x},\vec{d},N\right] \tag{S2}$$

In the main text, we have suppressed the argument N, since it is implied by the vector arguments, replaced $\vec{s}$ by $\vec{e}$ (since, given $\vec{d}$, they are one-to-one) and suppressed the argument $\vec{x}$, leading to $C\left(\vec{e},\vec{d}\right)$. We address the dependence on $\vec{x}$ in proofs in the following sections of the supplement.

Note that the probability $P\left(\vec{s},\vec{x},\vec{d},N\right)$ required in the coarse-grained model is just derived from $P\left[\vec{u}(t)\right]$ by integrating over all trajectories consistent with $\vec{s}$, $\vec{x}$, $\vec{d}$, and N. In the main text and the supplement, whenever arguments to the probability P are suppressed, they have been integrated over.

3A.2 Necessary conditions for stochastic decisions to be beneficial

In the main text, we described necessary conditions for stochastic decisions to be useful in systems with environmental and genetic diversity. We argued that when these conditions do not hold, a single deterministic sharp threshold is best. (More carefully, stochasticity can be useful only at the single stimulus value corresponding to the threshold stimulus.) In the next two subsections, we elaborate the proofs for these necessary conditions.

The proofs recruit the property, argued in the main text, that the likelihood of a T cell seeing a particular stimulus from a pathogenic pMHC versus a self PMHC increases with the magnitude of the stimulus. That is,

$$\frac{P(x,s=1)}{P(x,s=0)} \text{ is strictly increasing with } x \tag{S3}$$

This statement is closely related to the statement that stronger stimuli are more likely to be from pathogenic pMHC than self pMHC.

Note that, in addition to the three forms of coupling mentioned in the main text, the level of coarse graining adopted in the paper admits one more form of coupling. Under this fourth form of coupling, the actual decisions d_i or the observations x_i or c_i are not independent from the total number N of encounters the population will have. This form of coupling is most vivid in systems with exponential growth (e.g. bacteria), where the growth of the population, dependent on its decisions, affects the number of cells and therefore the number of encounters that occur. For T cells, correct decisions against pathogenic pMHC lead to speedy clearance of an infection, and therefore fewer total interactions in an infectious context than when there are incorrect decisions. When we refer to systems being coupled through the cost or the observations alone, we implicitly mean that they are not coupled in this way or in the other ways mentioned in the main text.

3A.2A The population must be coupled through more than just the observations alone for stochastic decisions to be beneficial.

In this section, we show that a sharp threshold is best if the members of the population are coupled only through their observations (i.e. the inequality in Eq. 4 holds but Eqs. 3 and 5 hold with equality).

Under coupling through the observations alone, the expected cost in Eq. 1 can be simplified. The following steps, resulting in Eq. S4, consist of simple algebraic manipulations, exploiting: (1) the linearity of the cost function, so that any dependencies in the observations are integrated out in the expectation; and (2) the independence of the i^{th} decision from all observations other than the i^{th} observation, so that the decision rule $\sigma(x)$ can be isolated from the probability $P(x,s)$.

First we consider N to be fixed (given). Let (*) denote the conditional expectation:

$$(*) = E_{\vec{s},\vec{x},\vec{d}|N}\left[C(\vec{e},\vec{d})\middle|N=n\right]$$

Then, using the assumed linearity of the cost function (from Eq. 3 with equality):

$$(*) = E_{\vec{s},\vec{x},\vec{d}|N}\left[\sum_{i=1}^{N}\overline{C}(e_i,d_i)\middle|N=n\right]$$

where $\overline{C}$ is defined in Eq. 3. Bringing the expectation inside the summation (since N is given):

$$(*) = \sum_{i=1}^{n} E_{\vec{s},\vec{x},\vec{d}|N}\left[\overline{C}(e_i,d_i)\middle|N=n\right]$$

Then, because $\overline{C}$ depends only on one interaction (the i^{th}), the expectations can be taken trivially over all variables other than those associated with the i^{th} interaction:

$$(*) = \sum_{i=1}^{n} E_{s_i,x_i,d_i|N}\left[\overline{C}(e_i,d_i)\middle|N=n\right]$$

Expanding the expectation as a sum/integral over the variables x_i, s_i, and d_i, weighted by their probabilities:

$$(*) = \sum_{i=1}^{n}\int dx_i \sum_{s_i=0,1}\sum_{d_i=0,1}\overline{C}(e_i,d_i)P(x_i,s_i,d_i \mid N=n)$$

Recruiting the assumption that the observations and the total number of interactions are independent, since the population is coupled only through its costs:

$$(*) = \sum_{i=1}^{n}\int dx_i \sum_{s_i=0,1}\sum_{d_i=0,1}\overline{C}(e_i,d_i)P(x_i,s_i,d_i)$$

Because, by assumption, the decisions do not affect the observations (Eq. 5 with equality, integrated over all variables but those corresponding to the i^{th} interaction):

$$(*) = \sum_{i=1}^{n}\int dx_i \sum_{s_i=0,1}\sum_{d_i=0,1}\overline{C}(e_i,d_i)P(s_i,x_i)P(d_i|x_i)$$

Expanding the summation over d_i:

$$(*) = \sum_{i=1}^{n}\int dx_i \sum_{s_i=0,1}\overline{C}(e_i,d_i=1)P(s_i,x_i)P(d_i=1|x_i)+\overline{C}(e_i,d_i=0)P(s_i,x_i)P(d_i=0|x_i)$$

Applying the definition of σ(x):

$$(*) = \sum_{i=1}^{n}\int dx_i \sum_{s_i=0,1}\overline{C}(e_i,d_i=1)P(s_i,x_i)\sigma(x_i)+\overline{C}(e_i,d_i=0)P(s_i,x_i)(1-\sigma(x_i))$$

Grouping terms according to $\sigma(x)$ and compacting the notation (the dependence on i comes only because the probability may depend on i):

$$(*) = \sum_{i=1}^{n} \int dx \sum_{s_i=0,1} \left(\overline{C}(e,d=1) - \overline{C}(e,d=0)\right) P_i(s,x)\sigma(x) + \sum_{i=1}^{n} \int dx \sum_{s=0,1} \overline{C}(e,d=0) P_i(s,x)$$

The second term does not depend on $\sigma(x)$ and therefore does not affect the optimization over $\sigma(x)$. For compactness, we suppress it in what follows:

$$(*) = \int dx \sum_{s=0,1} \left(\overline{C}(e,d=1) - \overline{C}(e,d=0)\right) \left(\sum_{i=1}^{n} P_i(s,x) \right) \sigma(x)$$

To derive this last equation, we assumed N was given. This assumption can be relaxed:

$$E_{\vec{s},\vec{x},\vec{d},N}\left[C(\vec{e},\vec{d})\right] = E_N\left[E_{\vec{s},\vec{x},\vec{d}|N}\left[C(\vec{e},\vec{d})\middle|N\right]\right]$$

Substituting the expression that was derived for (*) into the right hand side:

$$E_{\vec{s},\vec{x},\vec{d},N}\left[C(\vec{e},\vec{d})\right] = \int dx \sum_{s=0,1} \left(\overline{C}(e,d=1) - \overline{C}(e,d=0)\right) \left(E_N\left[\sum_{i=1}^{N} P_i(s,x) \right] \right) \sigma(x)$$

In principle, $P_i(s,x)$ can depend on i in two ways: through $P_i(x|s=0)$ and $P_i(x|s=1)$ or through $P_i(s=0)$ and $P_i(s=1)$. In the following we assume that the dependence comes at most through $P_i(s=0)$ and $P_i(s=1)$; that is, the stimuli from self and pathogenic pMHC come from stationary processes (since the initial conditions are also averaged over). We make this assumption because more complicated behavior in the coarse grained model would seem to implicate one of the other forms of coupling (e.g. decisions affecting observations), which we have excluded in this proof by assumption.

When P_i does not depend on i, this previous equation can be simplified to the following, which is the main result of the preceding manipulations:

$$E\left[C(\vec{e},\vec{d})\right] = \int dx a(x)\sigma(x) + b \qquad \text{(S4)}$$

$$a(x) = E[N] \sum_{s=0,1} P(x,s)\left[\overline{C}(e,d=1) - \overline{C}(e,d=0)\right]$$

$$b = E[N] \sum_{s=0,1} \int dx P(x,s)\overline{C}(e,d=0)$$

When P_i depends on i, but as above, the proof below follows similarly. Recall that e is a function of d and s, and so is fully determined in the expressions for $a(x)$ and b.

Because Eq. S4 is a linear functional of $\sigma(x)$, the optimization of $\sigma(x)$ in Eq. S4 can be done at each value of x separately. Specifically,

$$\sigma^*(x) = \begin{cases} 1 & a(x) < 0 \\ 0 & a(x) > 0 \end{cases} \tag{S5}$$

Note that for *a(x)* exactly equal to 0, $\sigma^*(x)$ can take any value. We have assumed here that the set of such x is insignificant (e.g. a set of 0 measure.) With simple algebra, the requirement that a is negative corresponds to:

$$\frac{P(x,s=1)}{P(x,s=0)} > \frac{\overline{C}(e_{01},d=1)-\overline{C}(e_{00},d=0)}{\overline{C}(e_{10},d=0)-\overline{C}(e_{11},d=1)} \tag{S6}$$

where the notation e_{sd} denotes the value of e when the correct decision is s and the actual decision is d. (The numerical value of e_{sd} is arbitrary, so long as $\overline{C}$ is defined consistently.) As noted in Eq. S3, the left hand side in Eq. S6 is strictly increasing with x. Therefore, if $\overline{C}$ is independent of x, as in the main text, Eq. S5 corresponds to a single sharp threshold, as described for an isolated T cell in the main text. When $\overline{C}$ depends on x, it is harder to draw general conclusions. However, the best solution will still be a single sharp threshold as long as the difference in the expression for *a(x)* in S4 changes sign only once. The arguments in this section recall the Neyman-Pearson lemma (21).

3A.2B The population must be coupled through more than just the costs alone for stochastic decisions to be useful.

In this section, we show that a single sharp threshold is best if members of the population are coupled only through their costs (i.e. the inequality in Eq. 3 holds but Eqs. 4 and 5 hold with equality). We assume the cost does not depend explicitly on the stimuli $\vec{x}$, noting the discussion in the previous section.

Since the observations are not coupled (by assumption), the probability that a particular encounter leads to an error (or correct decision) is independent of errors in other encounters. Specifically, the probabilities of correct and incorrect decisions in any encounter are, for a given probability model:

$$p_0 = P(s=0)\int dx P(x \mid s=0)\sigma(x) = \text{probability of incorrectly activating} \quad \text{(S7)}$$

$$p_1 = P(s=1)\int dx P(x \mid s=1)(1-\sigma(x)) = \text{probability of incorrectly not activating}$$

$$p_0^c = P(s=0) - p_0 = \text{probability of correctly not activating}$$

$$p_1^c = P(s=1) - p_1 = \text{probability of correctly activating}$$

The probability of activating, correctly or incorrectly, is just $p_1^c + p_0$. Note that the form of the probabilities in Eq. S7 is like the form considered in the Neyman-Pearson lemma (e.g. type 1 and type 2 errors; 21)

Any candidate decision rule leads to particular values of these probabilities. Consider a particular candidate decision rule that is not of a single sharp threshold form. According to the Neyman-Pearson lemma, one can find a single sharp threshold decision rule that has the same probability of incorrectly not activating but a lower probability of incorrectly activating. This single sharp threshold, therefore, will have a lower cost due to errors, on average. Furthermore, the single sharp threshold has a lower probability of activating (since it activates correctly just as often, but activates incorrectly less often), and so incurs a lower cost due to resource consumption, on average. Regardless of the structure of the cost function, then, the single sharp threshold will have a lower cost, on average. Since this is true regardless of the candidate decision rule, the optimal decision rule must have the form of a single sharp threshold. The particular location of the threshold will depend on the exact form of the cost function and the probabilities.

3A.3 Simple model of the T cell population

3A.3.1 Optimization of the simple T cell model

In the main text, we considered a simple model in which the host encounters a single infection. Which particular infection the host encounters is uncertain. The cost function in Eq. 8 and probability model in Eq. 9 set up an optimization problem for the decision rule. To simplify the calculation, we made the assumption in the main text that the

number of encounters in each infection is large enough so that, within a particular infection, the distributions of stimuli from self and pathogenic pMHC are well-sampled. In the main text, we introduced the notation f_0 and f_1 for the fractions of encounters with self and pathogenic pMHC that activate T cells. When the distributions are well sampled, the fractions f_0 and f_1 converge to probabilities:

$$f_0(\vec{e}) \to \int dx P(x \mid s=0)\sigma(x) \qquad \text{(S8)}$$

$$f_1(\vec{e}) \to \int dx P(x \mid s=1, I_k)\sigma(x)$$

That is, the probability a T cell activates in an encounter with self pMHC is just the probability the T cell activates given the stimulus x ($\sigma(x)$) times the probability the stimulus is actually x in an encounter with self pMHC ($P(x|s=0)$), integrated over all possible stimuli x; Eq. S8b follows similarly. Then, the only uncertainty in the expectation in Eq. 1 is which particular infection the immune system confronts (out of 6), since the many values of $\vec{s}$, $\vec{x}$, and $\vec{d}$ that might be encountered during the infection are now integrated out in Eq. S8. Note that, because the optimization depends separately on f_0 and f_1, the relative probability of pMHC being self or pathogenic ($P(s=0)$ vs. $P(s=1)$) in Eq. 9 is irrelevant.

The simple probability model we have chosen is constant over unit intervals of the stimulus (Fig. 3A), in order to simplify computation of the optimal decision rule. As a result, the optimization problem can be transformed from a functional optimization over all σ to an optimization over vectors $\vec{v}$ where:

$$v_i = \int_{\text{ith unit interval}} \sigma(x)dx \qquad \text{(S9)}$$

Each v_i is constrained to be between 0 and 1, inclusive (because each interval is of unit length and the decision rule falls between 0 and 1, inclusive, for all x).

If more than one element of the optimal solution $\vec{v}$ is not strictly 0 or 1, then a stochastic strategy is strictly better than a single sharp threshold, since sharp thresholds have v_i equal to 0 or 1 (no or complete activation) on all intervals except the one the threshold falls in.

In general, the optimum decision rule σ^* corresponding to the optimal solution $\vec{v}$ is degenerate, since Eq. S9 is not invertible. The stochastic decision rule plotted in Fig. 3B was obtained by letting σ(x) be constant over each interval. The deterministic decision rule plotted in Fig. 3D was obtained by taking σ(x)=1 over the first part of each interval, and then σ(x)=0 over the second part of each interval, such that the appropriate value for v_i was obtained. Though slightly simpler deterministic decision rules can be found by varying the choice of σ(x), they are still more complicated than the stochastic decision rule or a single sharp threshold. The best single sharp threshold (Fig. 3B) was obtained by explicitly searching over all possible threshold locations.

3A.3.2 Variations of the simple T cell signaling model

In the main text, our simple model consisted of the cost function in Eq. 8, with c_1=50, c_2=0.2, and c_3=40, and the probability model in Eq. 9 with distributions in Fig. 3A. (These parameters weight the cumulative mistakes against self and pathogenic pMHC roughly equally.) In this section, we show that a different cost function with different probability distributions leads to the same qualitative results as the example in the main text, suggesting the results do not particularly depend on the choices of these model inputs. The cost function and probability model presented here have the same qualitative properties motivated in the main text. In particular, they couple the T cells through the cost to the host and their observations, satisfying the necessary conditions for useful stochastic decisions. The cost function is:

$$C(\vec{e},\vec{d}) = e^{-c_1 f_1(\vec{e})} + c_2\left(e^{c_3 f_0(\vec{e})} - 1\right) \qquad \text{(S10)}$$

c_1=35

c_2 =0.1

c_3=150

The probability distributions for encounters with self and pathogenic pMHC are presented in Fig. S1A. As in the main text, we model only an intermediate range of stimulus, since it is assumed T cells will not activate at very weak stimulus.

As with the model in the main text, the best stochastic solution outperforms the best single sharp threshold (Fig S1B). The percentage change is small, but suffices to confirm that stochastic decisions outperform single sharp thresholds. (Because of the simplifications, the model is not quantitative.)

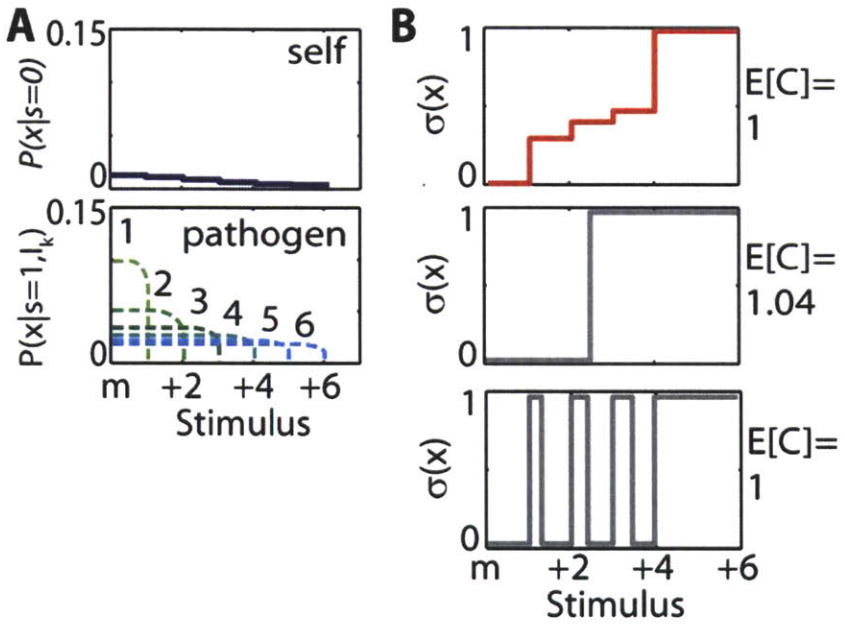

Figure S1: Varying the cost function and probability distributions does not change the qualitative results in the main text. (A) An alternate model for the probability distributions for the stimuli T cells receive from self ($P(x|s=0)$, upper) and pathogenic ($P(x|s=1,I_k)$, lower) pMHC, where I_k denotes the k^{th} infection. For weak stimulus strengths, these probability distributions are expected to be similar for self and pathogenic pMHC with high values for P; m denotes an intermediate stimulus strength, above which these probability distributions are different. The numbers on the abscissa are in arbitrary units. The six possible infections (distributions of pathogenic stimuli) occur with probability 0.001, 0.099, 0.2, 0.2, 0.25, and 0.25, from I_1 to I_6, so that infections which lead only to relatively weak stimuli are unlikely. Similarly, strong stimuli from self are unlikely. (B) For the probability and cost models, the best single sharp threshold (grey) has a higher expected cost (E[C]) than a stochastic decision rule (red). Reported E[C] is normalized by the expected cost of the stochastic decision rule. The optimal decision rules reflect the discretization of the probability distributions describing stimulus strengths (see panel A). A complex deterministic decision rule that alternates between never activating ($\sigma=0$) and always activating ($\sigma=1$) performs as well as the best stochastic one. Implementing this decision rule would require a complex signaling network.

Chapter 4

Identifying the Reactions and Species that Regulate Stochastic Transitions in Biological Systems[1]

"Maybe I shall meet him Sunday,
Maybe Monday, maybe not;
Still I'm sure to meet him one day --
Maybe Tuesday
Will be my good news day."

George and Ira Gershwin

4.1 Introduction

Randomness is ubiquitous at the molecular level of biochemical reactions, due to fluctuations in reaction rates and cell-to-cell variability in protein concentrations (1). Cells harness this randomness by organizing individual molecular interactions into complex reaction networks, which suppress noise to maintain stable cellular states or exploit it to enable stochastic transitions between them (2-4). Discovering the key mechanisms in these reaction networks that are responsible for regulating stochastic fluctuations is important to uncovering design principles of biological signaling networks (5, 6) and, practically, to identifying the species that are most vulnerable to mutations or are promising as drug targets.

As a particular measure of the importance of different reactions and species in regulating stochastic fluctuations away from stable cellular states, we focus on how they affect the average time it takes for a biologically meaningful stochastic transition to occur. Specifically, we focus on the percentage change in the transition time when the

[1] The work in this chapter was conducted in close collaboration with my colleague Ming Yang, and the writing in this chapter is also joint with him. A manuscript based on this chapter is in preparation.

concentrations of each species or the reaction rate constants associated with each reaction are perturbed by a small amount.

Determining these sensitivities can be computationally complex for two main reasons. First, direct simulations to determine transition times can be computationally costly, because transitions away from a stable state can be rare and therefore hard to sample (7-9). Second, realistic biochemical networks often involve many reactions and species, which each must be perturbed to determine if they significantly affect the transition.

Here we develop a semi-analytical technique for calculating sensitivities when the transitions are rare and thus most difficult to study by explicit simulation. The technique exploits the fact that the rarer the transition, the more predictable it is, as addressed by the large deviation theory (10-16); this utilizes an approach that has been successfully applied to other problems in reaction networks (16-19). We demonstrate with a nontrivial biological model that our technique gives results quantitatively consistent with trajectory-based simulation results. Computationally, the advantage of our approach is that it requires only a single deterministic simulation to determine the effect of perturbing all rate constants and concentrations, as long as the transitions are rare and the perturbations are small and do not lead to a phase transition. Conceptually, our semi-analytical expressions unveil qualitative features that characterize the key components that affect network stability.

4.2 Model development

Consider a system of N_S different chemical species, whose copy numbers evolve stochastically according to a network of reactions, characterized by a stoichiometric matrix $\mathbf{E}$ (of dimension N_S by N_R, where N_R is the number of reaction types) and rate constants $\boldsymbol{k}$ (of dimension N_R) according to pre-defined rate laws (e.g. mass action). The system may have one or more stable steady states for the species concentrations, corresponding to different stable cellular states. We consider cases when the volume V is large enough that a continuum approximation for species concentrations is valid and large

excursions away from any particular fixed point are rare relative to the time scale of relaxation to the fixed point. In this limit, the transitions away from a fixed point $\mathbf{c}_A^{FP}$, as specified by species concentrations, to another fixed point $\mathbf{c}_B^{FP}$ or to some other biologically relevant (set of) states, can be described by a rate K (8). The percentage change in this transition rate K when the rate constant k_i is perturbed by a small percentage can be quantified by $\frac{\partial \ln K}{\partial \ln k_i}$. Similarly, the percentage change in K when the concentration of the i^{th} species is perturbed by adding molecules of it to the system is $\frac{\partial \ln K}{\partial c_i}$. (The unperturbed rate constants serve as a natural scale for rate constant perturbations, but the scale for concentration perturbations is not as unique, since the concentrations evolve with time.)

We first focus on transitions between stable steady states $\mathbf{c}_A^{FP}$ and $\mathbf{c}_B^{FP}$. There are many possible paths that the system can take. Any particular path that starts at $\mathbf{c}_A^{FP}$ can be described by the time evolution of the concentration of each species, i.e. $\mathbf{c}(t)$. Alternatively, the path can be described by the actual reaction propensities at each time $\boldsymbol{\upsilon}(t)$ (that is, the number of reactions of each type that occur per volume per time). Given the starting point $\mathbf{c}(0)$ (e.g. $\mathbf{c}_A^{FP}$), $\mathbf{c}(t)$ is uniquely defined by $\boldsymbol{\upsilon}(t)$ through the following equation:

$$\mathbf{c}(t) = \mathbf{c}(0) + \mathbf{E}\int_0^t \boldsymbol{\upsilon}(t)dt \qquad (1)$$

Since $\mathbf{c}(t)$ does not uniquely define $\boldsymbol{\upsilon}(t)$ when $\mathbf{E}$ is non-invertible, the latter is more fundamental. $\mathbf{E}$ is noninvertible, for example, whenever there are reversible reactions in the system.

Not all transition paths are equally probable. Suppose a system is evolving according to a particular path $\boldsymbol{\upsilon}(t)$ and that the system is therefore at a particular point $\mathbf{c}(t)$ at time t. Over the next differential time interval $[t,t+\Delta t]$, the actual number of reactions of type i that occur is $n_i = \upsilon_i V \Delta t$. However, the expected number of reactions of type i is

$\lambda_i = \overline{\upsilon}_i V\Delta t$, as determined by the deterministic reaction propensities, $\overline{\upsilon}_i$, at the state $\mathbf{c}(t)$, according to the pre-defined rate law $\overline{\upsilon}_i(t;\mathbf{k},\mathbf{c})$. The probability of observing n_i reactions of type i over the differential time Δt follows a Poisson distribution characterized by λ_i. Hence, the probability of observing $\mathbf{n} = \boldsymbol{\upsilon} V\Delta t$ reactions is:

$$P(\mathbf{n}) = \prod_{i=1}^{N_R} \frac{\lambda_i^{n_i}}{n_i!} e^{-\lambda_i} = \prod_{i=1}^{N_R} \frac{(\overline{\upsilon}_i V\Delta t)^{\upsilon_i V\Delta t}}{(\upsilon_i V\Delta t)!} e^{-\overline{\upsilon}_i V\Delta t} \tag{2}$$

The first equality holds assuming the time interval is sufficiently small so that the species concentrations do not change significantly over the interval. By Stirling's approximation,

$$\lim_{V\to\infty} \frac{\ln P}{V} = -\sum_{i=1}^{N_R} \Delta t \left(\upsilon_i \ln \frac{\upsilon_i}{\overline{\upsilon}_i} - \upsilon_i + \overline{\upsilon}_i \right) \tag{3}$$

Hence at the continuum limit, the probability density of the path $\boldsymbol{\upsilon}(t)$, not necessarily a transition path, with t from 0 to τ, is proportional to $\exp\left(-VS(\boldsymbol{\upsilon},\tau)\right)$, where:

$$S(\boldsymbol{\upsilon},\tau) = \sum_{i=1}^{N_R} \int_0^{\tau} dt \left(\upsilon_i \ln \frac{\upsilon_i}{\overline{\upsilon}_i} - \upsilon_i + \overline{\upsilon}_i \right) \tag{4}$$

From the large deviation theory, $S(\boldsymbol{\upsilon},\tau)$ serves as the action (or rate function) of the path $\boldsymbol{\upsilon}$ over *[0,τ]*. Therefore, we have shown that for reaction networks, the action of the path can be defined by Eq. 4. This expression has been derived in a different way by Liu (20). Eq. 4 parses the total action into contributions from individual types of reactions, and hence it holds promise for identifying important reactions that can most effectively slow down or speed up rare transitions.

The minimum action S^* for the transition, and the corresponding most probable (least action) transition path $\boldsymbol{\upsilon}^*$, can be formally expressed by minimizing Eq. 4 over all the paths that originate from $\mathbf{c}_A^{FP}$ and reach $\mathbf{c}_B^{FP}$ at a time τ later and then minimizing over the time τ: $S^* = \min_{\tau} \min_{\boldsymbol{\upsilon}} S(\boldsymbol{\upsilon},\tau)$ (10).

The minimum action provides a connection to the transition rate K, because the transition rate of a rare event is, from large deviation theory (e.g. WKB approximation; (10)):

$$K = A\exp(-VS^*) \tag{5}$$

where A depends sub-exponentially on the volume and both A and S^* depend on the parameters describing the system (e.g. $\boldsymbol{k}$). At the limit of large V, simple calculation yields, $\frac{\partial \ln K}{\partial \ln k_i} \approx -V \frac{\partial S^*}{\partial \ln k_i}$ and $\frac{\partial \ln K}{\partial c_i} \approx -V \frac{\partial S^*}{\partial c_i}$. Hence, to determine the sensitivities of the transition rate on the different parameters, we only need to compute $\frac{\partial S^*}{\partial \ln k_i}$ or $\frac{\partial S^*}{\partial c_i}$.

4.3 Results

4.3.1 Perturbation of $\boldsymbol{k}$

Perturbing the rate constant k_i by Δk_i changes the minimal action S^*, because: (a) the steady states change (since the steady states depend on k_i); (b) the optimal path $\boldsymbol{\upsilon}^*$ changes (not only because its steady-state endpoints change); and (c) individual path actions change, because the deterministic propensities $\overline{\boldsymbol{\upsilon}}^*$ along paths change with k_i according to the rate law. The changes in S^* due to (a) and (b) are $O(\Delta k_i^2)$, whereas the change due to (c) is $O(\Delta k_i)$ (supplement). Hence, to compute $\frac{\partial S^*}{\partial \ln k_i}$, and therefore $\frac{\partial \ln K}{\partial \ln k_i}$, we only have to evaluate the change of action along the unperturbed optimal path $\boldsymbol{\upsilon}^*$ when k_i changes:

$$\frac{\partial \ln K}{\partial \ln k_i} = \int_0^{\tau^*} \frac{\delta S}{\delta \overline{\upsilon}_i} \frac{\partial \overline{\upsilon}_i}{\partial \ln k_i}\bigg|_{\boldsymbol{\upsilon}^*} dt = k_i \int_0^{\tau^*} \left(1 - \frac{\upsilon_i^*}{\overline{\upsilon}_i^*}\right) \frac{\partial \overline{\upsilon}_i^*}{\partial k_i} dt \qquad (6)$$

where we substitute Eq. 4 to obtain the second equality. If $\overline{\upsilon}_i$ is linear with k_i, as in mass action kinetics, the sensitivities can be further simplified:

$$\frac{\partial \ln K}{\partial \ln k_i} \approx -V \frac{\partial S^*(\mathbf{k})}{\partial \ln k_i} = V \int_0^{\tau^*} \left(\upsilon_i^* - \overline{\upsilon}_i^*\right) dt \qquad (7)$$

As expected, the transition rate increases with the rates of reactions that must occur more frequently during the transition than they would deterministically. For rate constants that participate in multiple reactions (e.g. dephosphorylations by the same phosphatase), the right hand side of Eq. 7 will contain a summation over all such reactions.

Eq. 7 provides a way to calculate the effect of perturbing rate constants given a single input, the unperturbed optimal path, $\boldsymbol{\upsilon}^*$. This input path can be determined numerically using the efficient geometric minimal action method (gMAM; (16)).

4.3.2 Perturbation of $\mathbf{c}$

Chemical species can be governed by conservation laws (such laws are determined by $\mathbf{E}$). Adding molecules of a species not governed by a conservation law to a system (e.g. the species A in the toy network $A \rightarrow \phi$, $\phi \rightarrow A$) does not change the system's steady states. Therefore, such perturbations will not affect transition times, because the system will relax to an original steady state before any rare transition occurs.

For species that are governed by conservation laws, perturbing concentrations by adding molecules to the system can change the steady states $\mathbf{c}_A^{FP}$ and $\mathbf{c}_B^{FP}$. The optimal path $\boldsymbol{\upsilon}^*$ and the deterministic propensities $\overline{\boldsymbol{\upsilon}}^*$ along the optimal path also change when concentrations are perturbed, similar to perturbing rate constants. (The deterministic propensities $\overline{\boldsymbol{\upsilon}}(t;\mathbf{k},\mathbf{c})$ change because the optimal path in concentration space $\mathbf{c}$ changes according to Eq. 1). We can show that the change in the minimal action is due to the change in deterministic propensities evaluated along the unperturbed optimal path $\boldsymbol{\upsilon}^*$, to the order of $O(\Delta c_i^2)$ (proof in Supplement). Arguments analogous to the perturbation in k_i lead to:

$$\frac{\partial \ln K}{\partial c_i} \approx -V \sum_{j=1}^{N_R} \int_0^{\tau^*} \left(1 - \frac{\upsilon_j^*}{\overline{\upsilon}_j^*}\right) \frac{\partial \overline{\upsilon}_j^*}{\partial c_i} dt \tag{8}$$

where $\frac{\partial \overline{\upsilon}_j^*}{\partial c_i}$ is evaluated by adding molecules to the system at the starting point of the transition, $\mathbf{c}_A^{FP}$, according to Eq. 1 and the predefined rate law. Note that the specific state of the system when the molecules are added is unimportant, since the system will relax to the new steady state before any rare transition occurs, by assumption. For mass

action kinetics, the right hand side of Eq. 8 can be further simplified to

$$V\sum_{j=1}^{N_R}\int_0^{\tau^*} E_{ij}\frac{\upsilon_j^* - \overline{\upsilon}_j^*}{c_i}dt\,.$$

Note there may be multiple ways of perturbing concentrations that achieve the same effect. For example, increasing the concentration of a compound AB by an amount Δc will have the same effect as increasing the concentrations of both species A and B by Δc. This implies, from Eq. 8, that the optimal path $\boldsymbol{\upsilon}^*$ must be such that $\frac{\partial S^*(\mathbf{c})}{\partial c_{AB}} = \frac{\partial S^*(\mathbf{c})}{\partial c_A} + \frac{\partial S^*(\mathbf{c})}{\partial c_B}$, which has been verified numerically for a simple model as a check on the equation's correctness (data not shown).

4.3.3 Transitions between a stable state and a set of other states

The previous equations have been derived for a transition between two fixed points. The same equations apply for a transition from a stable state to a predefined set of states, as long as $\boldsymbol{\upsilon}^*$ is understood to be additionally optimized over all possible endpoints consistent with this set of states, as described algorithmically in (16), because large deviation theory results still hold. The only exception to the applicability of these equations is that Eq. 8 does not directly apply, as derived, to any species that participates in the definition of the set of endpoints. For example, if the transition is complete whenever the concentration of a certain species exceeds a threshold level, Eq. 8 cannot be applied directly to perturbations in the concentration of that species.

4.3.4 Application to a biological system

To test the accuracy of the methods developed above, we apply them to a biochemical reaction network that characterizes a key module in T-cell activation, the Ras-SOS signaling network. This model has been well-studied computationally in conjunction with experiments (21-23). We study a particular version of it as defined in Tables S1 and S4 of (21). This model has 26 reactions (and associated rate constants), 14 species governed by

5 conservation equations, and about 400 molecules in the simulation box. The copy number of individual species, summed over all bound states, is as small at 10. The dynamics do not observe detailed balance.

The main feature of the model is that a key signaling molecule, Ras, can be activated via two distinct pathways, mediated by Rasgrp or by SOS, and deactivated by RasGAP. The activation by SOS is governed by a positive feedback loop: SOS's catalytic activity increases significantly when it is bound to the active form of Ras, RasGTP. This enables the system to exhibit bistability when SOS concentration is at an intermediate level. Meanwhile, at a low SOS level, only one stable state exists, characterized by low level of RasGTP (21). Thus, the model is rich enough to investigate how cells control stochastic transitions between multiple stable states (at intermediate SOS level) and suppress fluctuations from a single stable state (at low SOS level).

We use Eqs. 7 and 8 to predict the sensitivities of the transition time in each of these two cases: in the first case (intermediate SOS), from the lower to the higher RasGTP steady state (which represents stochastic activation); and in the second case (low SOS), from the stable state to a predefined high RasGTP level (which represents spurious Ras activation). To obtain the unperturbed optimal path υ^*, we implemented the gMAM (16). For comparison, we individually calculated the transition times under the unperturbed parameters and under each of the perturbed parameters by trajectory-based simulation; we chose forward flux sampling (FFS; (24)) as the direct simulation method and the RasGTP level as its thresholding parameter. Specifically, we perturbed each of the 26 rate constants by 1%, and we increased the number of each conserved species by 1.

As shown in Fig. 1, our method not only qualitatively predicted key reactions and species, but also provided remarkable quantitative agreement with the direct simulation results. The discrepancies observed in Fig. 1 are due to the finite size of the simulation system, the finite change in rate parameters and initial concentrations, and statistical uncertainties in FFS results. Note that for RasGAP, the species in Fig. 1D to which the

transition time is the most sensitive, an increase of one molecule represents a relatively large (10%) change in concentration, which explains the deviation between the prediction and the direct simulation.

4.4 Discussion

Our technique correctly identifies the key reactions for regulating Ras activation, namely RasGAP activity, SOS activity when RasGTP is bound to it, and Rasgrp activity. The most important species, RasGAP, SOS, and Rasgrp, are, as expected, associated with those key reactions. These predictions are consistent with recent experimental results in T-cell cancers in which different species concentrations were perturbed (23). An interesting prediction that can be tested experimentally is that the relative importance of SOS and Rasgrp switches at a low concentration of SOS (around SOS=5; data not shown), presaged in Fig. 1 by the narrowing of the gap in their importance from SOS=55 to SOS=15.

In addition to these biological findings, the method developed in this chapter has computational and conceptual benefits. Computationally, both direct simulation and our method require a simulation to determine properties of the unperturbed transition (the expected time vs. υ^*). But this is the only simulation required for our method, whereas a trajectory-based approach requires additional simulations to explore the space of all possible perturbation parameters. For the simple network we have studied, this is the difference between 1 (deterministic) simulation and 32 (stochastic) simulations.

Furthermore, Eqs. 4, 7, and 8 give more detailed information than just the overall sensitivities of the transition, because, though the integrand, they provide time-resolved information about when fluctuations must occur and at what points the transition is sensitive to rate or concentration perturbations. This provides the basis to identify coordinated sets of fluctuations that drive the transition and the order in which they occur during the transition, not explored in this work.

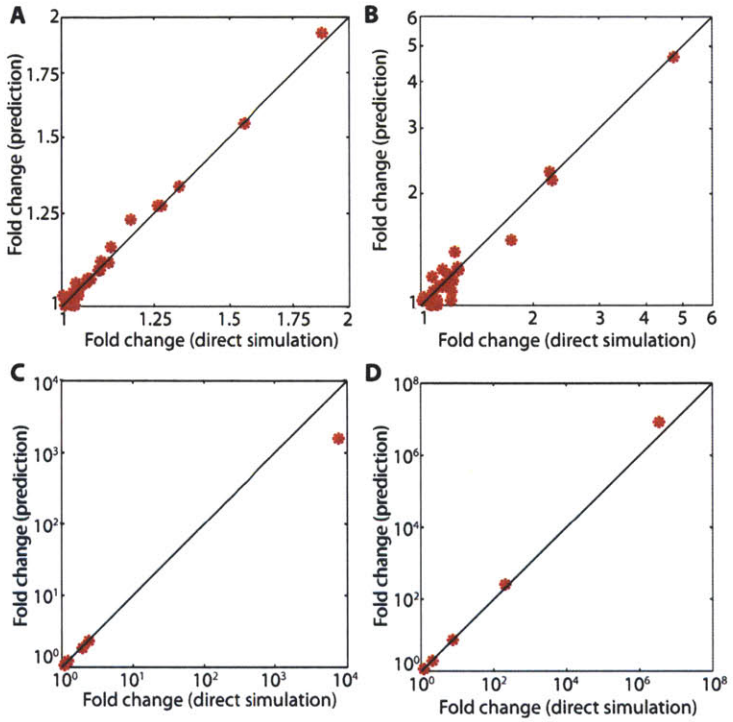

Figure 1: Quantitative consistency between predictions and direct simulation results. (A, B) Fold change in transition rate due to 1% increase of rate constants at (A) SOS = 50 (intermediate) and (b) SOS = 15 (low). Each red dot represents the perturbation of a different rate constant. The direct simulation results are the averages of ten independent FFS runs, and for each FFS run 10^3 points were stored on each surface. For SOS = 15 (low), the transition considered is the stochastic escape from the single stable state to the hyperplane where 60% of Ras molecules are activated. (C, D) Fold change in transition rate when one molecule of each fundamental type is added to the system at (C) SOS = 50 (intermediate) and (D) SOS = 15 (low).

Eq. 7 and 8 suggest general features of reactions most responsible for regulating stochastic transitions. Key reactions are those associated with improbably large fluctuations over a sustained interval of time (rather than short large bursts) to drive the transition against large deterministic propensities opposing it. Note that the probability of a fluctuation in an individual reaction rate is given by Eq. 4 as $S_i^* = \int_0^{\tau^*} dt \left(v_i^* \ln \frac{v_i^*}{\overline{v}_i^*} - v_i^* + \overline{v}_i^* \right)$. Large S_i^* indicates a significant deviation of actual propensity v_i^* from deterministic propensity $\overline{v}_i^*$, and hence large sensitivity in general. Note that S_i^* is convex with respect to $\boldsymbol{v}^*$ while the reaction sensitivity is linear; by

Jensen's inequality, given two reactions with the same individual action, the reaction with fluctuations more evenly distributed along the course of the transition will lead to a larger sensitivity. Also note the first-order approximation $S_i^* \approx \int_0^{\tau^*} \frac{\left(\upsilon_i^* - \overline{\upsilon}_i^*\right)^2}{\overline{\upsilon}_i^*} dt$; hence given the same S_i*, the reaction with larger $\overline{\upsilon}_i$* has a larger sensitivity. This explains why SOS activity becomes less important relative to Rasgrp when the level of SOS decreases, as seen in Figure 1a and b: the decreasing SOS level makes transitions more unlikely (so all sensitivities, including the sensitivity to Rasgrp, roughly increase), but the decreasing deterministic propensity of SOS reactions (because the SOS concentration is reduced), decreases the particular sensitivity to SOS.

An extension of the above features is that the rarer a transition is, the more fragile it is in general to perturbation. This holds even when the measure of fragility is the percentage (not just absolute) change in the transition time. This is confirmed by the difference in the magnitude of sensitivities between Fig. 1a and 1b and between Fig. 1c and 1d.

Finally, as seen in Eqs. 7 and 8, to understand the key components that control stochastic transitions, it is necessary to understand how these transitions occur in the reaction space (as described by $\boldsymbol{\upsilon}$) rather than in the conventional species space (as described by $\mathbf{c}$).

The sensitivity of stochastic transition times to parameter perturbations complements other work, involving different metrics, on sensitivity analysis in both deterministic and stochastic settings (25, 26).

References

1. Raj A & van Oudenaarden A (2008) Nature, Nurture, or Chance: Stochastic Gene Expression and Its Consequences. *Cell* 135(2):216-226.
2. Balaban NQ, Merrin J, Chait R, Kowalik L, & Leibler S (2004) Bacterial persistence as a phenotypic switch. *Science* 305(5690):1622-1625.
3. Kussell E & Leibler S (2005) Phenotypic diversity, population growth, and information in fluctuating environments. *Science* 309(5743):2075-2078.
4. Thattai M & van Oudenaarden A (2004) Stochastic gene expression in fluctuating environments. *Genetics* 167(1):523-530.
5. Thattai M & van Oudenaarden A (2002) Attenuation of noise in ultrasensitive signaling cascades. *Biophys. J.* 82(6):2943-2950.
6. Lestas I, Vinnicombe G, & Paulsson J (2010) Fundamental limits on the suppression of molecular fluctuations. *Nature* 467(7312):174-178.
7. Dickson A & Dinner AR (2010) Enhanced Sampling of Nonequilibrium Steady States. *Annual Review of Physical Chemistry, Vol 61,* Annual Review of Physical Chemistry, (Annual Reviews, Palo Alto), Vol 61, pp 441-459.
8. Bolhuis PG, Chandler D, Dellago C, & Geissler PL (2002) Transition path sampling: Throwing ropes over rough mountain passes, in the dark. *Annu. Rev. Phys. Chem.* 53:291-318.
9. E WN & Vanden-Eijnden E (2010) Transition-Path Theory and Path-Finding Algorithms for the Study of Rare Events. *Annual Review of Physical Chemistry, Vol 61,* Annual Review of Physical Chemistry, (Annual Reviews, Palo Alto), Vol 61, pp 391-420.
10. Touchette H (2009) The large deviation approach to statistical mechanics. *Phys. Rep.-Rev. Sec. Phys. Lett.* 478(1-3):1-69.
11. Faccioli P, Sega M, Pederiva F, & Orland H (2006) Dominant pathways in protein folding. *Phys. Rev. Lett.* 97(10):4.
12. Chan HB, Dykman MI, & Stambaugh C (2008) Paths of fluctuation induced switching. *Phys. Rev. Lett.* 100(13):4.
13. Dykman MI, Mori E, Ross J, & Hunt PM (1994) Large fluctuations and optimal paths in chemical kinetics. *J. Chem. Phys.* 100(8):5735-5750.
14. Maier RS & Stein DL (1993) Escape problem for irreversible systems. *Phys. Rev. E* 48(2):931-938.
15. Vanden-Eijnden E & Heymann M (2008) The geometric minimum action method for computing minimum energy paths. *J Chem Phys* 128(6):061103.
16. Heymann M (2007) The Geometric Minimum Action Method: A Least Action Principle on the Space of Curves. PhD (NYU, New York City).
17. Dykman MI, Schwartz IB, & Landsman AS (2008) Disease extinction in the presence of random vaccination. *Phys. Rev. Lett.* 101(7):4.
18. Khasin M & Dykman MI (2009) Extinction Rate Fragility in Population Dynamics. *Phys. Rev. Lett.* 103(6):4.
19. Khasin M, Dykman MI, & Meerson B (2010) Speeding up disease extinction with a limited amount of vaccine. *Phys. Rev. E* 81(5):11.

20. Liu D (2008) A numerical scheme for optimal transition paths of stochastic chemical kinetic systems. *J. Comput. Phys.* 227(19):8672-8684.
21. Das J, *et al.* (2009) Digital Signaling and Hysteresis Characterize Ras Activation in Lymphoid Cells. (Translated from English) *Cell* 136(2):337-351 (in English).
22. Riese MJ, *et al.* (2011) Decreased Diacylglycerol Metabolism Enhances ERK Activation and Augments CD8(+) T Cell Functional Responses. *J. Biol. Chem.* 286(7):5254-5265.
23. Hartzell C, *et al.* (2011) Effective Synergy between Receptor-input and the Rasgrp1 Oncogene in T cell leukemogenesis.
24. Allen RJ, Warren PB, & ten Wolde PR (2005) Sampling rare switching events in biochemical networks. *Phys. Rev. Lett.* 94(1):4.
25. Gunawan R, Cao Y, Petzold L, & Doyle FJ (2005) Sensitivity analysis of discrete stochastic systems. *Biophys. J.* 88(4):2530-2540.
26. Costanza V & Seinfeld JH (1981) Stochastic sensitivity analysis in chemical kinetics. *J. Chem. Phys.* 74(7):3852-3858.

4A Supplement for Chapter 4

4A.1 Perturbation of **k**:

Let $\mathbf{c}_A^{FP}$ and $\mathbf{c}_B^{FP}$ be the steady states under the rate parameter **k**. Let $\boldsymbol{\upsilon}_{A\to B}^*$ be the optimal path under **k** connecting $\mathbf{c}_A^{FP}$ to $\mathbf{c}_B^{FP}$ and $\tau_{A\to B}^*$ be the corresponding optimal time, so that the minimal action is $S^*(\mathbf{k}) = S\left(\boldsymbol{\upsilon}_{A\to B}^*, \tau_{A\to B}^*; \mathbf{k}\right)$, as defined in Eq. 4 in the main text. Note that here we explicitly include **k** as an argument of S; this reflects the dependence of S on **k** through the deterministic propensities $\bar{\boldsymbol{\upsilon}}^*$, independent of the path $\boldsymbol{\upsilon}$ and the time τ.

Now perturb **k** by a small amount $\Delta\mathbf{k}$ such that the perturbed rate parameter is $\mathbf{k}' = \mathbf{k} + \Delta\mathbf{k}$. Let $\mathbf{c}_{A'}^{FP}$ and $\mathbf{c}_{B'}^{FP}$ be the new steady states under $\mathbf{k}'$ and $\boldsymbol{\upsilon}_{A'\to B'}^{\prime *}$ be the new optimal path from $\mathbf{c}_{A'}^{FP}$ and $\mathbf{c}_{B'}^{FP}$ in time $\tau_{A'\to B'}^{\prime *}$, so that the new minimal action is $S^*(\mathbf{k}') = S\left(\boldsymbol{\upsilon}_{A'\to B'}^{\prime *}, \tau_{A'\to B'}^{\prime *}; \mathbf{k}'\right)$. In what follows, we assume the perturbation in **k** is done by perturbing a single rate constant, k_i. To compute the change in minimal action $S\left(\boldsymbol{\upsilon}_{A\to B}^*, \tau_{A\to B}^*; \mathbf{k}\right) - S\left(\boldsymbol{\upsilon}_{A'\to B'}^{\prime *}, \tau_{A'\to B'}^{\prime *}; \mathbf{k}'\right)$, we develop the following steps. Note the use of * to denote an optimal path, time, or action, and the use of ' to denote quantities calculated under the perturbed rate constants $\mathbf{k}'$.

1. Let $\boldsymbol{\upsilon}_{A'\to A}^{\prime *}$ be the optimal path connecting $\mathbf{c}_{A'}^{FP}$ to $\mathbf{c}_A^{FP}$ in time $\tau_{A'\to A}^{\prime *}$ under $\mathbf{k}'$, and $\boldsymbol{\upsilon}_{B\to B'}^{\prime *}$ be the optimal path connecting $\mathbf{c}_B^{FP}$ to $\mathbf{c}_{B'}^{FP}$ in time $\tau_{B\to B'}^{\prime *}$ under $\mathbf{k}'$. Note that the constructed path $\boldsymbol{\upsilon}_{A'\to B'}' = \left\{\boldsymbol{\upsilon}_{A'\to A}^{\prime *}, \boldsymbol{\upsilon}_{A\to B}^*, \boldsymbol{\upsilon}_{B\to B'}^{\prime *}\right\}$ is a valid path connecting $\mathbf{c}_{A'}^{FP}$ to $\mathbf{c}_{B'}^{FP}$ (through $\mathbf{c}_A^{FP}$ and $\mathbf{c}_B^{FP}$). Since actions are additive and $S\left(\boldsymbol{\upsilon}, \tau; \mathbf{k}'\right)$ achieves its minimum at $\boldsymbol{\upsilon}_{A'\to B'}^{\prime *}$ and $\tau_{A'\to B'}^{\prime *}$, by calculus of variations:

$$S\left(\boldsymbol{\upsilon}_{A'\to B'}^{\prime *}, \tau_{A'\to B'}^{\prime *}; \mathbf{k}'\right) = S\left(\boldsymbol{\upsilon}_{A'\to A}^{\prime *}, \tau_{A'\to A}^{\prime *}; \mathbf{k}'\right) + S\left(\boldsymbol{\upsilon}_{A\to B}^*, \tau_{A\to B}^*; \mathbf{k}'\right) + S\left(\boldsymbol{\upsilon}_{B\to B'}^{\prime *}, \tau_{B\to B'}^{\prime *}; \mathbf{k}'\right) + O\left(\Delta k_i^2\right)$$

2. Note that $S\left(\boldsymbol{\upsilon}_{A'\to A}^{\prime *}, \tau_{A'\to A}^{\prime *}; \mathbf{k}'\right)$ (i.e. the action of the optimal path from $\mathbf{c}_{A'}^{FP}$ to $\mathbf{c}_A^{FP}$ under $\mathbf{k}'$) is $O\left(\Delta k_i^2\right)$, since the minimum action reaches its minimum at steady state $\mathbf{c}_{A'}^{FP}$ (16). Also $S\left(\boldsymbol{\upsilon}_{B\to B'}^{\prime *}, \tau_{B\to B'}^{\prime *}; \mathbf{k}'\right)$ (i.e. the action of the optimal path from $\mathbf{c}_B^{FP}$ to $\mathbf{c}_{B'}^{FP}$ under $\mathbf{k}'$) is zero, since the path will follow the deterministic path into the steady state $\mathbf{c}_{B'}^{FP}$. Hence, the change in minimal action due to the change of steady states is $O\left(\Delta k_i^2\right)$, and the previous equation reduces to:
$$S\left(\boldsymbol{\upsilon}_{A'\to B'}^{\prime *}, \tau_{A'\to B'}^{\prime *}; \mathbf{k}'\right) = S\left(\boldsymbol{\upsilon}_{A\to B}^*, \tau_{A\to B}^*; \mathbf{k}'\right) + O\left(\Delta k_i^2\right)$$

3. Now to compute the sensitivity of minimal action to k_i, we only have to compute $S\left(\boldsymbol{\upsilon}_{A\to B}^*, \tau_{A\to B}^*; \mathbf{k}\right) - S\left(\boldsymbol{\upsilon}_{A\to B}^*, \tau_{A\to B}^*; \mathbf{k}'\right)$, that is, to evaluate the change in

action due to the change in k_i along the original optimal path $\boldsymbol{\upsilon}^*_{A\to B}$. This proves Eq. 6 in the main text.

4A.2 Perturbation of **c**:

Consider perturbing the concentration of species *i* by Δc_i. Assume the concentration of species *i* is governed by conservation equations. Before perturbation, let $\mathbf{c}_A^{FP}$ and $\mathbf{c}_B^{FP}$ denote the steady states, $\boldsymbol{\upsilon}^*_{A\to B}$ denote the optimal path, and $S^*\left(\mathbf{c}_A^{FP}\right) = S\left(\boldsymbol{\upsilon}^*_{A\to B}, \boldsymbol{\tau}^*_{A\to B}; \mathbf{c}_A^{FP}\right)$ denote the minimal action. We suppress the dependence of *S* on **k**, since the latter is held constant; we explicitly include the starting point as one argument, since the deterministic propensity $\bar{\boldsymbol{\upsilon}}^*$ depends on the starting point, as seen in Eq. 1 of the main text. The path in species concentration space **c**(t) evolves on a subspace $\mathbf{C}_0$ with dimension N_S-N_C, where N_C is the number of species conservation equations. After perturbation, let these corresponding quantities be $\mathbf{c}_{A'}^{FP}$, $\mathbf{c}_{B'}^{FP}$, and $S'^*\left(\mathbf{c}_{A'}^{FP}\right) = S\left(\boldsymbol{\upsilon}'^*_{A'\to B'}, \boldsymbol{\tau}'^*_{A'\to B'}; \mathbf{c}_{A'}^{FP}\right)$, respectively. The new path **c**'(t) evolves on a subspace $\mathbf{C}_0$'.

We develop the following steps to compute $S\left(\boldsymbol{\upsilon}^*_{A\to B}, \boldsymbol{\tau}^*_{A\to B}; \mathbf{c}_A^{FP}\right) - S\left(\boldsymbol{\upsilon}'^*_{A'\to B'}, \boldsymbol{\tau}'^*_{A'\to B'}; \mathbf{c}_{A'}^{FP}\right)$:

1. Shift $\mathbf{c}_A^{FP}$ by Δc_i so that its image $\mathbf{c}_{A''}$ lands in the subspace $\mathbf{C}_0$'. Starting from $\mathbf{c}_{A''}$, generate a dynamical path according to $\boldsymbol{\upsilon}^*_{A\to B}$. Note that although $\boldsymbol{\upsilon}^*_{A\to B}$ was optimized on the subspace $\mathbf{C}_0$, it is still a valid sequence of reactions in the subspace $\mathbf{C}_0$'. Furthermore, the resulting path in the species concentration space stays in the subspace $\mathbf{C}_0$', since it starts in this subspace and evolves according to reactions that obey the conservation laws. Denote the endpoint of this path in the subspace $\mathbf{C}_0$' as $\mathbf{c}_{B''}$.

2. We connect $\mathbf{c}_{A'}^{FP}$ to $\mathbf{c}_{A''}$ using the optimal path $\boldsymbol{\upsilon}'^*_{A'\to A''}$, and $\mathbf{c}_{B''}$ to $\mathbf{c}_{B'}^{FP}$ using the optimal path $\boldsymbol{\upsilon}'^*_{B''\to B'}$. Just as in the case of perturbation of **k**, we have:

$$S\left(\boldsymbol{\upsilon}'^*_{A'\to B'}, \boldsymbol{\tau}'^*_{A'\to B'}; \mathbf{c}_{A'}^{FP}\right) = S\left(\boldsymbol{\upsilon}'^*_{A'\to A''}, \boldsymbol{\tau}'^*_{A'\to A''}; \mathbf{c}_{A'}^{FP}\right) + S\left(\boldsymbol{\upsilon}^*_{A''\to B''}, \boldsymbol{\tau}^*_{A''\to B''}; \mathbf{c}_{A''}\right) + S\left(\boldsymbol{\upsilon}'^*_{B''\to B'}, \boldsymbol{\tau}'^*_{B''\to B'}; \mathbf{c}_{B''}\right)$$

and

$$S\left(\boldsymbol{\upsilon}'^*_{A'\to B'}, \boldsymbol{\tau}'^*_{A'\to B'}; \mathbf{c}_{A'}^{FP}\right) = S\left(\boldsymbol{\upsilon}^*_{A\to B}, \boldsymbol{\tau}^*_{A\to B}; \mathbf{c}_{A''}\right) + O\left(\Delta c_i\right)$$

3. To compute the sensitivity of minimal action to Δc_i, we have to compute $S\left(\boldsymbol{\upsilon}^*_{A\to B}, \boldsymbol{\tau}^*_{A\to B}; \mathbf{c}_A^{FP}\right) - S\left(\boldsymbol{\upsilon}^*_{A\to B}, \boldsymbol{\tau}^*_{A\to B}; \mathbf{c}_{A''}\right)$. Note that these two paths in the species concentration space are parallel and point-wise different by Δc_i. To evaluate the change in action, we can simply calculate the action change due to the change of the starting point from $\mathbf{c}_A^{FP}$ to $\mathbf{c}_{A''}$ along the unperturbed optimal path via Eq. 4 in the main text using the pre-defined rate laws. This proves Eq. 8.

Chapter 5

To the nucleus and beyond

"[I] sprinted lickety-
split on my magic Keds
from a crouching start,
scarcely touching the ground
with my flying skin
as I poured it on
for the prize of the mastery
over that stretch of road,
with no one no where to deny
when I flung myself down
that on the given course
I was the world's fastest human.

Stanley Kunitz, "The Testing-Tree"

The previous chapters suggest broad areas of inquiry that merit further study. For example, Chapter 2 highlighted the spatiotemporal aspects of T cell signaling. This chapter probes two additional spatiotemporal aspects of cellular signaling, one temporal problem (how memory effects can arise in T cell signaling) and one spatial problem (how fast signals can propagate through space, for example to the nucleus).

5.1 Memory in T cell signaling can arise from a positive feedback induced hysteresis[1]

In Chapter 4, we briefly introduced the Ras-SOS signaling module, an important module in the translation of pMHC-TCR binding into the ultimate activation of the T cell and other cell signaling systems. As the level of the input SOS increases, the module undergoes two saddle-node bifurcations, so that the system possesses a single stable steady state at low SOS levels (representing an inactive state), two stable steady states at intermediate SOS (representing inactive an active states), and a single stable steady state at high SOS levels (representing an active state) (Fig. 1).

[1] The work in this section has been published in Cell as a small part of "Digital Signaling and Hysteresis Characterize Ras Activation in Lymphoid Cells" (J. Das *et al.*, *Cell* **136**, 337 (Jan, 2009)).

In Chapter 3, we focused on the consequences of the bistability at intermediate SOS, since such bistabilities enable stochastic switching. The bifurcation diagram of the Ras-SOS signaling network also suggests that the network supports hysteresis, or memory. That is, whether the T cell activates at intermediate SOS depends on the state of the cell when it receives stimulus (and therefore the cell's history). If only a basal amount of Ras molecules are active, the T cell will remain inactive, unless it stochastically switches to an active state. If enough RasGTP molecules are already active (the state falls above the separatrix defined by the unstable steady state), however, the T cell will likely activate. Ras levels will be enhanced from their basal levels if the T cell had previously been activated (for example, by having bound an APC that stimulated it very strongly) and this previous encounter was recent enough that the RasGTP had not fully deactivated yet to basal levels (Fig. 2). In the computational model in Fig 2., when RasGTP is initially induced by high levels of SOS and then subsequently restimulated with intermediate levels of SOS, robust restimulation of RasGTP results, provided the restimulation occurs quickly enough. Such hysteresis has been observed experimentally (1).

This hysteresis provides a way for T cells to integrate signals in multiple, successive encounters with moderately stimulating APCs. The implications of this signal integration have been considered by my colleague, Huan Zheng (2).

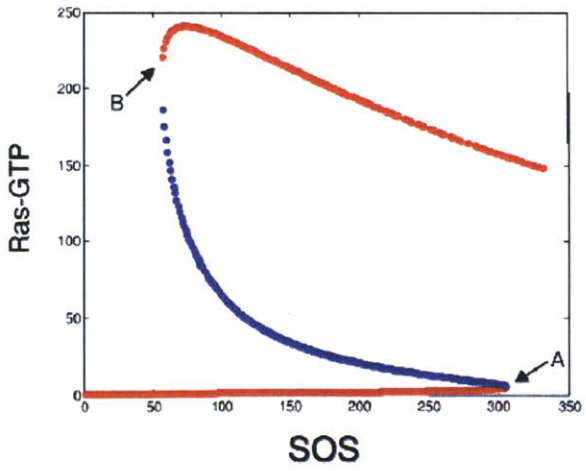

Figure 1: Bifurcation diagram of the Ras-SOS signaling module. Steady states of the mean-field kinetic rate equations show production of low and high concentrations of

RasGTP (characterized by stable fixed points in red) at low and high values of SOS. At intermediate levels of SOS three states arise with unstable fixed RasGTP points shown in blue. A and B denote the saddle-node bifurcations. (Figure and caption adapted from (1)).

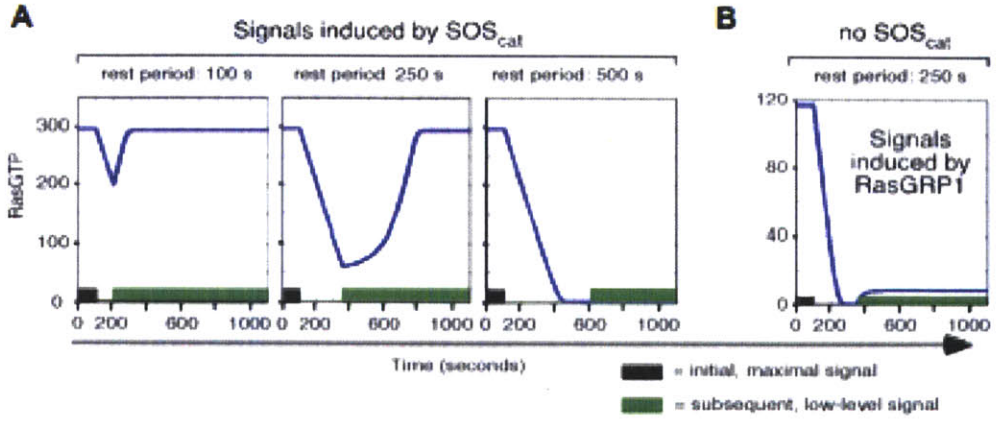

Figure 2: The Ras-SOS signaling module provides a mechanism for T cell signal integration. (A) Modeling serial stimulation. RasGTP (blue line) was initially induced by high levels of SOS (black box, 350 molecules). SOS was removed for 100, 250, or 500 s and subsequent low-level SOS signals were simulated (green box, 150 molecules). Provided that RasGTP levels do not fall below the blue points (Figure 1), robust restimulation is induced by low-level SOS. The results are obtained from mean-field rate equations corresponding to the parameters in Table 1 of Das et al (1).
(B) Lack of sensitized restimulation in the absence of SOS. The model from Fig. 1E in (1) is used to analyze a SOS-deficient state in the same manner as in panel A. RasGRP1 values were set at 100 (black) and 50 (green) molecules of RasGRP1 in the simulation box, respectively. The response to the second stimulus is history independent.

5.2 Signaling Cascades Modulate the Speed of Signal Propagation Through Space[2]

Cells are not mixed bags of signaling molecules. As a consequence, signals must travel from their origin to distal locations. Much is understood about the purely diffusive propagation of signals through space. Many signals, however, propagate via signaling cascades. Here, we show that, depending on their kinetics, cascades speed up or slow down the propagation of signals through space, relative to pure diffusion.

[2] The work in this section has been published in *PLoS One* as "Signaling Cascades Modulate the Speed of Signal Propagation Through Space" (C. C. Govern, A. K. Chakraborty, *PLoS One* **4**, 7 (Feb, 2009)).

We modeled simple cascades operating under different limits of Michaelis-Menten kinetics using deterministic reaction-diffusion equations. Cascades operating far from enzyme saturation speed up signal propagation; the second mobile species moves more quickly than the first through space, on average. The enhanced speed is due to more efficient serial activation of a downstream signaling module (by the signaling molecule immediately upstream in the cascade) at points distal from the signaling origin, compared to locations closer to the source. Conversely, cascades operating under saturated kinetics, which exhibit zero-order ultrasensitivity, can slow down signals, ultimately localizing them to regions around the origin.[3]

Signal speed modulation may be a fundamental function of cascades, affecting the ability of signals to penetrate within a cell, to cross-react with other signals, and to activate distant targets. In particular, enhanced speeds provide a way to increase signal penetration into a cell without needing to flood the cell with large numbers of active signaling molecules; conversely, diminished speeds in zero-order ultrasensitive cascades facilitate strong, but localized, signaling.

5.2.1 Introduction

Signaling cascades, series of molecules that sequentially activate each other, are ubiquitous in cellular systems (3-6). They have long been thought to amplify input signals as each molecule in the cascade can serially activate multiple molecules of a downstream component of the cascade (7, 8). However, doubts have been raised about whether cellular conditions actually allow for this (8). Cascades have also been considered to modulate the duration and timing of signals, filter noise, and otherwise regulate cellular decisions (8-10).

[3] The work in this section considers signal propagation in one dimension. In silico models in two dimensions suggest similar results (data not shown); however, given the importance of dimensionality in diffusion processes, more careful work is needed to draw conclusions in two and three dimensions.

The speed of signal propagation through space is also important. For example, how quickly signals propagate though the cell might affect integration of signals from different receptors on the same cell. Insights into the signal amplitude, duration, and timing at points distal from a signal's source cannot be obtained from computational models that treat the system to be homogenous (or well-mixed).

The influence of cascades on the spatial propagation of signals has been considered before (10-18). Much of this work has focused on the long time behavior of spatially inhomogeneous systems or on the kinetics of particular pathways. In the latter case, for example, many studies have focused on the MAPK cascade, a ubiquitous cellular pathway. The MAPK cascade has been shown to enhance signal penetration into the cell, reducing sharp signaling gradients otherwise caused by phosphatase deactivation of the signal as it travels away from the origin (10, 14). However, according to these studies, simple kinetic considerations do not account for how the cascade enables penetration from the membrane to the nucleus. A more complicated model of the MAPK cascade, involving feedback-induced bistability, has been shown to generate fast-moving signaling waves that might account for long-range propagation (11, 15, 16).

Here, we have examined the mechanistic principles underlying how simple cascades can influence the speed of signal propagation through space regardless of whether the cascade is an intrinsic amplifier or attenuator of signal amplitude.

We find that, depending upon the pertinent kinetic parameters, cascades can either speed up or slow down signal propagation though space in a manner that is largely uncoupled from its impact on features such as amplification of the amplitude. In particular, cascades operating far from saturation can speed signal propagation through the cell. Although phosphatase levels modulating certain kinase cascades have been suggested to be too large for signal penetration into the nucleus, our results may be applicable to kinase cascades over shorter length scales or to other cascaded signaling modules. Additionally, we find that cascades operating under zero-order ultrasensitivity (19), in which the cascaded signal is either completely activated or not active at all, can serve to

slow down signal propagation in a cell, even as the signal is amplified overall. By extending to the spatial domain studies that productively used moment analysis in the temporal domain (8), we provide a way to summarize the complex spatiotemporal behaviors of cascades.

5.2.2 Results and Discussion

5.2.2.1 Simple model of a signaling cascade

We initially model a simple one-level cascade (Figure 3) in which a primary signal, initially localized in space, diffuses away from its origin and activates a secondary, homogenously distributed messenger. Homogenously distributed phosphatases deactivate the signals. In order to reduce the number of competing length scales in the problem, all molecules are assumed to diffuse at identical rates. We neglect many effects that are undoubtedly important, including the effects of scaffolds (8, 20, 21) and feedback regulation (15, 22).

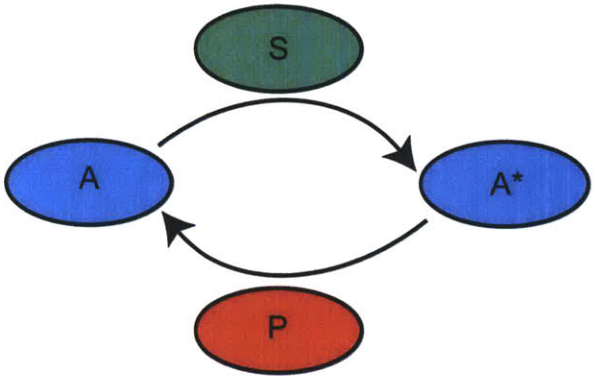

Figure 3: Diagram of a one-level cascade.

Complications arise in modeling the specific geometries involved in cellular signaling. To keep the discussion general to a variety of length scales and signaling contexts, we model a system of infinite extent in all directions from the initial signal. In other words, we imagine that the distance from the origin of the signal to its ultimate target is large

compared to other length scales in the problem. The models have been studied in one dimension.

The primary signal is introduced to the system as a bolus at the origin, as opposed to introduction via a flux, eliminating a time scale in the problem.

Our model differs from more commonly studied models of cascades, in which the primary signal is permanently localized to the origin (10, 12, 14, 17). Under certain conditions, our model of a one-level cascade is similar to a two-level model in which the primary signal is permanently localized. In particular, the common model collapses to our model if the activation of the first mobile messenger is fast compared to its diffusion time and the reaction time scale. We do not focus on the two-level cascade directly because each level of cascading adds complexity to the problem; our goal is merely to determine whether a secondary mobile messenger travels faster or slower than a primary mobile messenger.

We describe the results of relevant modifications to this simple model throughout the discussion.

5.2.2.2 Deterministic formulation of the model

The spatiotemporal evolution of the primary signal, S, and the activated secondary signal, A*, can be described by the following dimensionless (scaled using Table 1) reaction-diffusion equations:

$$\frac{\partial c_S}{\partial t} = \frac{\partial^2 c_S}{\partial x^2} \qquad (1)$$

$$\frac{\partial c_{A^*}}{\partial t} = \frac{\partial^2 c_{A^*}}{\partial x^2} + Da \cdot r\left(c_{A^*}, c_S; \gamma\right)$$

$$c_S(x,0) = \begin{cases} 1 & |x| \le 1 \\ 0 & |x| > 1 \end{cases}$$

$$c_{A^*}(x,0) = 0$$

$$c_{A^*}(\pm\infty, t) = c_S(\pm\infty, t) = 0$$

The rate expression r incorporates the effect of phosphatases through the parameter γ, as detailed below.

Table 1: Scalings in Equation 1

Variable	*Scale*
Distance (x)	Characteristic width of the initial primary signal distribution, L.
Primary signal concentration (c_S)	Characteristic one-dimensional concentration of the primary signal, N_{S0}/L.
Secondary signal concentration (c_{A^*})	Initial concentration of inactive secondary signal, c_{A0}.
Time (t)	Characteristic diffusion time (L^2/D).
Reaction rate	Characteristic reaction time, dependent on the particular kinetics. See examples in text.

The Damkohler number, *Da*, is the ratio of the diffusion and reaction time scales. Specific forms are given below, as part of the discussion on particular kinetics. If all reactions in the system occur on the same time scale, the Damkohler number compares the time scale over which the primary signal diffuses away from its origin to the time scale over which it begins to activate the secondary signal. In this respect, it measures the significance of the primary signal's localization. For example, if the Damkohler number is small (diffusion is fast compared to reaction), the primary signal delocalizes quickly, before it attempts to react.

In this paper, we study two limits of Michaelis-Menten kinetics for the rate expression $r(c_{A^*}, c_S; \gamma)$. If the enzyme kinetics are far from saturation (the Michealis constants are large relative to the secondary signal concentration), it suffices to consider direct reactions between the secondary signal and its activators and deactivators according to mass action kinetics:

$$r(c_{A^*}, c_S; \gamma) = c_S(1 - c_{A^*}) - \gamma c_{A^*} \tag{2}$$

If the enzyme kinetics are saturated (the Michaelis constants are small), the kinetics of the one level cascade become independent of the secondary signal's concentration:

$$r(c_{A^*}, c_S; \gamma) = \frac{c_S(1-c_{A^*})}{\frac{K_m^a}{c_{A0}} + (1-c_{A^*})} - \frac{\gamma c_{A^*}}{\frac{K_m^p}{c_{A0}} + c_{A^*}} \approx c_S - \gamma \quad (3)$$

The expressions in Equations 2 and 3 correspond to Damkohler numbers of $kN_{S0}L/(K_m D)$ and $kN_{S0}L/(c_{A0}D)$, respectively, where k and K_m (assuming, for notational simplicity, identical K_m^a and K_m^p) are the constants corresponding to Michaelis-Menten kinetics.

In both limits of the kinetics, the parameter incorporating phosphatase effects, γ, is $k_p c_p L/(kN_{S0})$, where k_p is the rate constant describing the phosphatase reaction and c_p is the phosphatase concentration. This parameter compares the initial deactivation and activation rates at the signaling origin.

Note that the concentration profile for the primary signal concentration, as described by Equation 1 is just a Gaussian centered at the origin with a variance of *2t*.

To quantify the mean speed of signal propagation, we have analyzed the mean squared displacement of each signal from the origin as a function of time. For the primary signal, S, the mean squared displacement, $\langle x^2 \rangle_S$, is just *2t*. For the secondary signal, A*, it can be calculated from the concentration profile as:

$$\langle x^2 \rangle_{A^*} = \frac{\int_{-\infty}^{\infty} x^2 c_{A^*}(x,t)dx}{\int_{-\infty}^{\infty} c_{A^*}(x,t)dx} \quad (4)$$

The variance of the signal's distribution, along with the overall amount of the signal in the system, serves as a summary of its spatiotemporal evolution. The first passage time distribution, also of interest, is less easily discussed deterministically. Also, it is not as decoupled from other functions of the cascade, such as signal amplification: merely amplifying a signal tends to decrease the first passage time, independent of any effect on the signal's propagation speed.

5.2.2.3 Cascades operating far from saturated kinetics (large Michaelis constants) speed up signal propagation

Numerical solutions for the mean squared displacement of the secondary signal under the kinetics of Equation 2 are presented in Figure 4 for various values of the Damkohler number, $kN_{S0}L/(K_m D)$, without phosphatases ($\gamma=0$). An approximate perturbative solution in the absence of phosphatases, obtained by modeling the initial primary signal as a delta function of unit characteristic length, provides an analytical description for short times and low Damkohler numbers:

$$\left\langle x^2 \right\rangle_{A^*} = 2t \cdot \left(1 + \frac{\sqrt{2\pi}}{20\pi} Da\sqrt{t} + O\left(Da^2\right) \right) \tag{5}$$

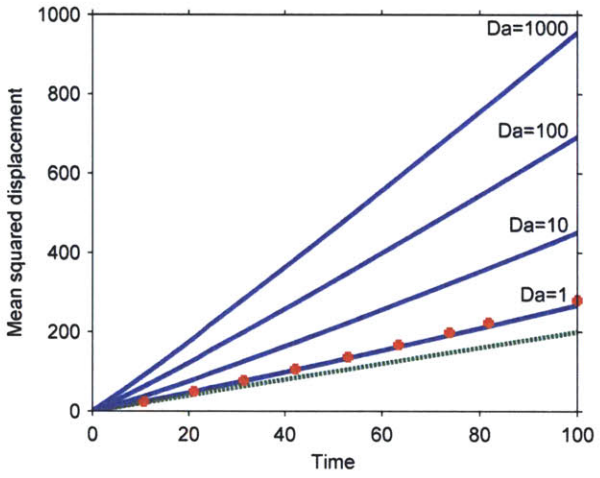

Figure 4: Mean squared displacement of the secondary signal under the kinetics of Equation 2. Dashed line, pure diffusion reference corresponding to the primary signal; solid lines, mean squared displacement of the secondary signal for various Damkohler numbers; squares, approximation for $Da=1$, corresponding to Equation 5.

The numerical and approximate solutions indicate that cascades described by Equation 2 speed up signal propagation; the secondary signal travels faster than the primary. Furthermore, the cascade's effect on the speed of the signal is independent of its effect on

the overall amplitude of the signal: the amplitude can be independently controlled by altering the initial, inactive concentration of the secondary signal, c_{A0}, which does not affect the signal speed. The enhancement of signal speed is negligible when the Damkohler number is negligible (e.g. for fast diffusion or weak primary signals) and increases as the Damkohler number increases. The seemingly linear increase of the secondary signal's mean squared displacement with time admits the possibility of an effective diffusivity.

Both the increased speed of the secondary signal and its dependence on the Damkohler number can be understood by considering the effects of signal localization on serial triggering. Primary signaling molecules initially localized to the origin must compete with each other there to activate a limited amount of secondary signal, constraining any individual molecule's ability to serially activate many secondary signaling molecules. Primary signaling molecules that diffuse away from the origin, on the other hand, encounter less competition and can more readily serially activate many molecules. Serial triggering is enhanced far from the origin, and the distribution of the secondary signal is shifted to greater distances than the primary signal. In the context of signal speed, the result is that the secondary signal moves faster than its predecessor. For example, if the reaction is instantaneous relative to diffusion ($Da>>1$), the secondary signal becomes fully activated wherever there is at least one molecule of the primary signal – potentially quite far from the origin and certainly further at any given time than the primary signal, on average.

Our results also suggest that the greater the disparity between serial triggering at the origin and far away, the greater the enhancement in the signal's speed. Specifically, the speed increases with the Damkohler number, which measures the importance of a signal's localization. When the Damkohler number is high, the primary signal attempts to react before it diffuses away from the origin, and near the origin, its ability to serially trigger is limited.

There are several implications for these results. Directly, by examining the contributions to the Damkohler number, our results suggest that one effect of strongly stimulating a primary signal (increasing N_{S0}) is to generate a quickly moving, not just stronger, secondary signal.

Our results also clarify previous work indicating that cascades help signals penetrate into a cell (10, 14). Specifically, we note that one way cascades help signal penetration is by increasing signal speed. This effect is independent from any overall amplification of the primary signal, which would also contribute to increased penetration. In particular, because of the increased speed, a cascade can help a signal penetrate deep into a cell even if it attenuates the overall level of the signal (Figure 5). Cascades provide a way to increase penetration at any given time without flooding the cell with large numbers of active signaling molecules.

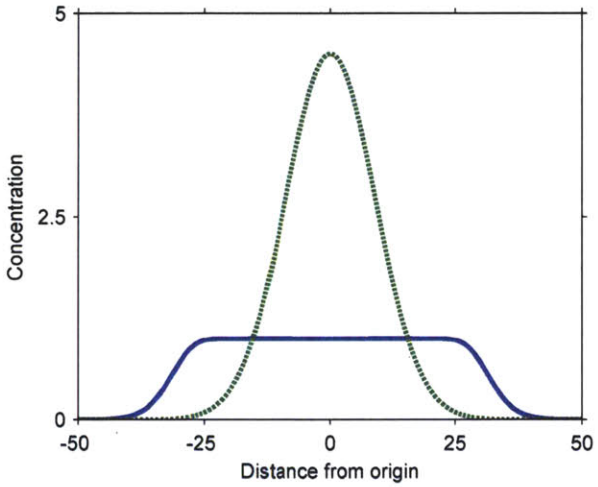

Figure 5: Representative concentration profiles in a cascade that attenuates the overall signal while amplifying the signal far from the origin. Dashed curve, primary signal; solid curve, secondary signal. Parameters (arbitrary units): $Da=1000$; $c_{A0}=1$; $N_{S0}/L=100$; $t=40$. The parameters have been chosen to highlight the limited serial triggering at the origin, where the secondary signal is already, by the figured time, entirely activated.

Another implication of our results is that cascades do not necessarily cause signaling delays. In homogenous systems, cascades lead to delays, because species buried within the chain take time to become activated (8). Heterogeneously, however, the secondary

signal travels faster than the primary signal, so there may be no delay in its arrival at a target.

We investigated several modifications to our simple model to determine whether the basic conclusions continue to hold in more realistic situations. We find that in all cases cascades described by the kinetics in Equation 2 increase the speed of signal propagation.

For example, we considered the effect of adding phosphatases to the system (Figure 6). These molecules homogenously deactivate the primary and secondary signals. Because continual deactivation at the origin enables serial triggering there, the secondary signal slows down in the presence of phosphatases. Consistent with our previous results, however, the secondary signal still moves faster than the primary signal.

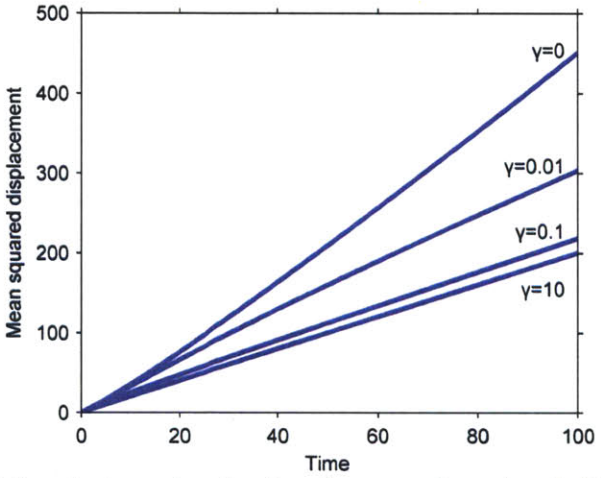

Figure 6: Effect of phosphatases deactivating the secondary signal. The curves indicate the mean squared displacement of the secondary signal for $Da=10$ and various values of the parameter γ. The curve for $\gamma=10$ overlays the purely diffusive curve of the primary signal. Note that γ is a parameter that reflects phosphatase activity at the origin only and so understates phosphatase activity in the system as a whole. Similar results pertain to the effect of phosphatases on the primary signal.

We also investigated multi-level cascades to determine whether speeds continue to be enhanced as more species are added to a signaling chain. We find, consistent with our previous results, that active signaling molecules at all levels of a cascade travel faster than the primary signal (Figure 7). Furthermore, the same basic features that govern signal speed in a one level cascade seem to govern the speeds at each level in a multi-

level cascade. In general, any given step in a multi-level cascade is just a one level cascade in which the primary signal is no longer a simple Gaussian. The language of localization developed above for a Gaussian input, for which the diffusion and reaction time scales determine differences in serial triggering near and far from the origin, broadly translates to multi-level cascades, as suggested by the simulations in Figure 5. If the localization at one level is significant, the next level moves quickly relative to pure diffusion; otherwise, the next level moves almost diffusively. Practically, the consequence for multilevel cascades is that, if signals in the cascade become more and more localized down the chain (e.g. the cascade amplifies signal amplitude, reducing reaction times), the signal travels more and more quickly; if the signals become less localized (e.g. the cascade attenuates signal amplitude), the speeds tend toward pure diffusion.

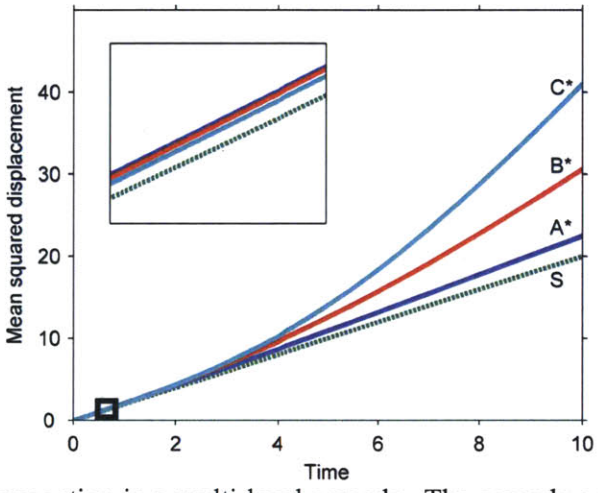

Figure 7: Signal propagation in a multi-level cascade. The cascade ordering is S, A, B, C, with each species activating the species after it in the chain. The parameters have been chosen representatively so that the signal has been amplified at each step by the final time point. (Inset) The cascade at early times, when the signal has not yet been amplified at any level. Note that the species rank, from fastest to slowest, as C*, B*, A*, S at late times (when the signal has been amplified) but as A*, B*, C*, S at early times (when the signal has been attenuated). Parameters: all species are assumed to diffuse at the same rate; the plots correspond to Damkohler numbers of 1 for all levels of the cascade, where the Damkohler number for the ith cascade level is $k_i c_{i-1}^0 L^2 / (K_{mi} D_i)$.

We also interrogated our assumption that the primary signal enters the system instantaneously as a bolus. In many contexts, the primary mobile signal in a cascade is

activated over time by a permanently localized predecessor (e.g. one bound to the membrane). To investigate the consequence of this, we considered a model in which the primary mobile signal is generated at the origin at some constant rate (Figure 8). Consistent with our previous results, the secondary signal travels faster than the primary signal. In addition, we investigated a more detailed model in which the primary mobile signal, initially inactive and homogenously distributed, is activated by a signal on the membrane that decays exponentially over time (Supplementary Figure 1a). Again, the secondary mobile signal travels faster than its predecessor. Furthermore, if the membrane-bound signal decays rapidly, quickly activating the primary signal, the results coincide with those of our simple model (Supplementary Figure 1b).

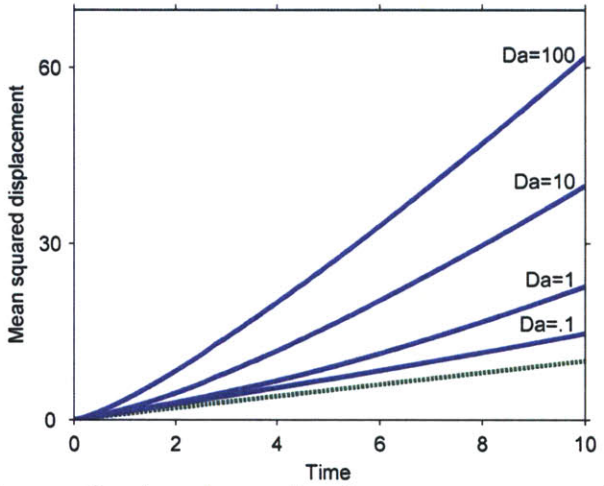

Figure 8: Effect of generating the primary signal at a constant rate at the origin. The results are parameterized by a Damkohler number equal to $kRL^4/(K_m D^2)$, where R is the rate of generation at the origin. Dashed line, primary signal; solid lines, secondary signal for different values of the Damkohler number.

Finally, because the mean-squared-displacement metric is sensitive to the tails of the signals' distributions, we conducted Monte Carlo simulations of our original model with finite, integer particle numbers (Figure 9). As in the deterministic simulations, the secondary messenger travels faster than its predecessor in the cascade. The exact scaling with the Damkohler number was not recovered (not shown), possibly because stochastic effects alter the scaling with the number of particles in the system.

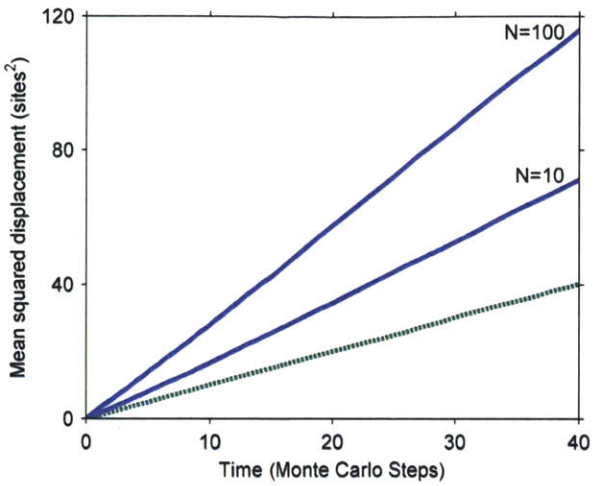

Figure 9: Mean squared displacement of the primary and secondary signals, simulated stochastically. The results are from Monte Carlo simulations on a one-dimensional lattice. At each time step, all molecules hop to adjacent sites and react, if possible, as described in Text S1. Dashed line, purely diffusive reference corresponding to the primary signal; solid lines, secondary signal for different numbers of primary signaling molecules initially at the origin (N). The results are independent of the number of secondary signaling molecules in the system.

In the simple system we investigated, as well as in all the modifications, the cascade serves to speed up the propagation of a signal from its origin. In certain parameter regimes – fast diffusion, slow reaction, strong phosphatases, or weak signals – the difference can be negligible. The kinetics, however, admit the phenomena. In biological systems, in which crowded environments slow down diffusion relative to reaction and phosphatase recruitment is often delayed, the effects we have described are likely to be relevant.

5.2.2.4 Cascades operating under zero-order ultrasensitivity lead to signal localization

Cascades operating under the kinetics of Equation 3 exhibit behavior known as zero-order ultrasensitivity (19): in homogenous systems, the secondary signal is either completely activated or left inactive depending on whether the primary signal exceeds the threshold, γ.

Numerical solutions for the propagation speed of the secondary signal under these kinetics are presented in Figure 10 for various values of the Damkohler number. An approximate solution for the mean squared displacement at large Damkohler numbers is:

$$\left\langle x^2 \right\rangle_{A^*} = -\frac{2}{3} t \cdot \ln\left(4\pi\gamma^2 t\right) \tag{6}$$

This approximation is obtained by assuming that the diffusion time is much slower than the reaction time, so that the secondary signal immediately responds to changes in the primary signal's concentration. In this limiting case, a sharp boundary exists between the complete activation of the secondary signal near the origin, where the primary signal exceeds the threshold, and its complete inactivity further away. The secondary signal's mean squared displacement can then be estimated by tracking this threshold concentration in the Gaussian distribution describing the primary signal. Note that the Damkohler number does not appear in Equation 6 as in this approximation it has been assumed to be infinite for the limiting case.

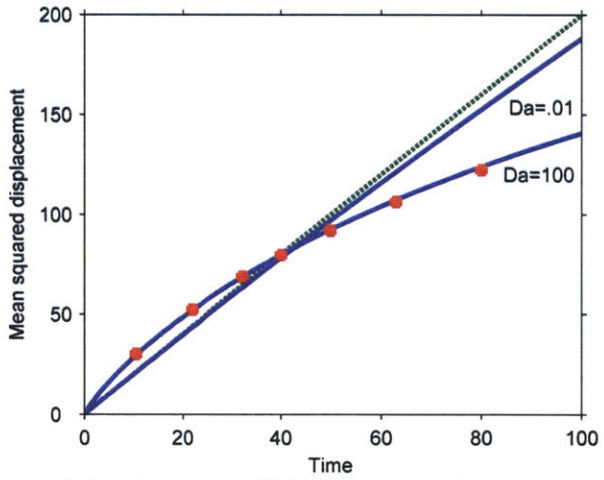

Figure 10: Mean squared displacement of the primary and secondary signals under the kinetics of Equation 3 (zero-order ultrasensitivity). Dashed line, purely diffusive reference corresponding to the primary signal; solid lines, simulation results corresponding to γ=.01 and slow (*Da=100*) and fast (*Da=.01*) diffusion; squares, theoretical prediction for slow diffusion corresponding to Equation 6. Simulations conducted with $K_m/c_{A0} = .01$ (Equation 3).

As indicated by the numerical simulations and by the approximate solution, cascades operating under zero-order ultrasensitivity can both speed up a signal (at early times) and slow it down (at later times). Eventually, the primary signal is nowhere above the

threshold and the secondary signal, after contracting, entirely disappears. Similar to our results in the previous section, when the Damkohler number is small, diffusion dominates and the corrections to pure diffusive motion disappear.

Because the overall concentration of the inactive secondary signal (c_{A0}) appears in the Damkohler number, the signal propagation speed is no longer completely decoupled from the amplification effects of the cascade. In particular, any attempt to drastically amplify the primary signal will promote purely diffusive motion of the secondary signal, because the system's tendency to remove sharp gradients washes out all other effects. The speed and signal amplitude are still independent in the important sense that the signal can be slowed down independently of whether it is also amplified or attenuated, depending on the parameters.

These results have several implications. Like the cascades studied in the previous section, zero-order ultrasensitive cascades can be used to speed up signal propagation. A unique feature of these cascades, however, is that they can also slow down signal propagation, eventually confining the secondary signal to a region around the signaling origin and preventing it from reaching any distant targets or interacting with distant signals. The confinement is accomplished purely by the kinetics of the reactions. The region to which the signal is confined, corresponding to the maximum possible mean squared displacement of the secondary signal, can be approximated as:

$$\left\langle x^2 \right\rangle_{A^*}^{\max} = \frac{1}{6\pi e \gamma^2} \tag{7}$$

As expected, phosphatases shrink the region over which the signal can propagate.

Because they can slow down signal propagation in space without necessarily attenuating a signal, cascades under the kinetics of Equation 3 provide a way for generating strong signals without promoting cross-reactivity with distant signals or interference with distant targets. Other simple mechanisms do not simultaneously localize and amplify the signal. For example, a strongly stimulated, uncascaded signal would necessarily lead to

increased penetration and interference within the cell; a signal localized solely by strong phosphatase activity would be commensurately weakened.

We investigated our simplification that the primary signal enters the system instantaneously as a bolus. If, instead, the primary signal is generated at a constant rate at the origin, the secondary signal moves more slowly than the primary signal at early times and moves more quickly at later times, a temporal order that is opposite that of the original result (Figure 11). If, additionally, phosphatases are added to the system to deactivate the primary signal, the mean squared displacements eventually plateau as a steady state is reached between generation and destruction of the primary signal (Supplementary Figure 2). At long times, the secondary signal will either be more or less localized than the primary signal depending on whether the steady state is reached while the secondary signal moves slower or faster than the primary signal. If the phosphatases are strong and the system quickly reaches steady state, the secondary signal remains more localized than the primary signal; otherwise, it remains less localized. Given that the novel feature of cascades operating under zero-order ultrasensitivity is that they can slow down signal propagation, the relevance of our results in these modified models depends on whether the early period of slowing down is long compared to other signaling processes, such as phosphatase deactivation of the primary signal.

Importantly, once the generation of the primary signal is shut off, the system behaves analogously to our simple model: the secondary signal moves more slowly than the primary signal, contracting as the primary signal dilutes (Figure 12). Thus, the results obtained for our simple model appear to apply to more detailed models on time scales longer than the generation of the primary signal.

We hope that our study adds to the framework for thinking about the role of cascades in signal transduction, especially how cascades influence signal propagation in space.

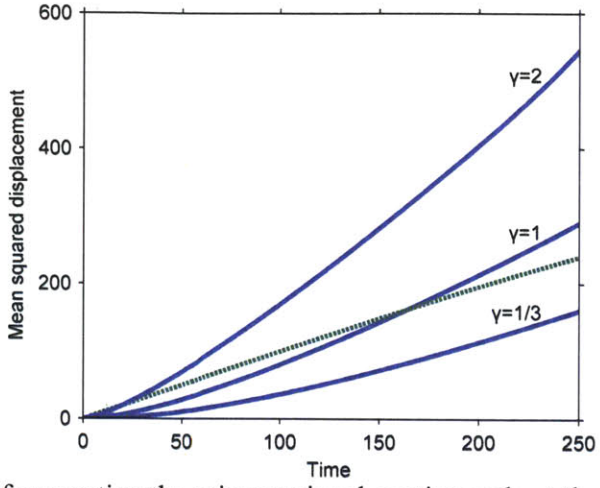

Figure 11: Effect of generating the primary signal continuously at the origin. The results are parameterized by $\gamma = Dk_pc_p/(kRL^2)$, where R is the rate of formation of the primary signal at the origin (see Text S1). The parameters have been chosen so that reactions are fast compared to diffusion (the Damkohler number is approximately infinite). Dashed line, primary signal; solid lines, secondary signal for different values of γ.

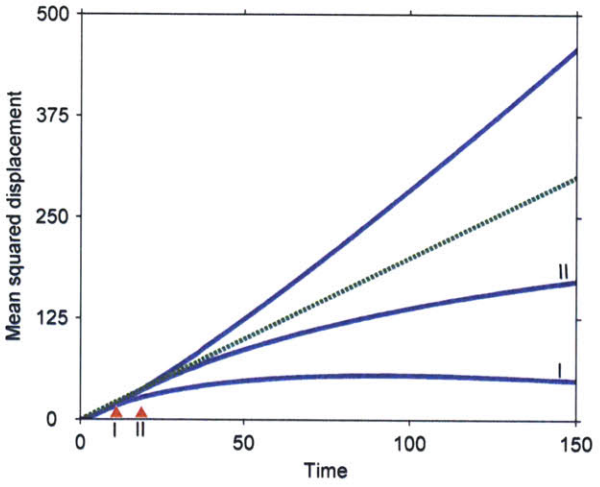

Figure 12: Effect of cutting off generation of the primary signal. Three cases are investigated: the primary signal is not cut off; the primary signal is cut off after a nondimensional time of 5 (I); the primary signal is shut off after a nondimensional time of 10 (II). Dashed line, purely diffusive reference; solid lines, secondary signals corresponding to the three cases. Parameters: $k=1$; $D=1$; $R=10$ (rate of generation at origin); $L=1$; $k_pc_p=1$. See Text S1 for more details.

References

1. Das J, *et al.* (2009) Digital Signaling and Hysteresis Characterize Ras Activation in Lymphoid Cells. *Cell* 136(2):337-351.
2. Zheng H (2010) Multi-scale models of T cell activation. Ph.D. (MIT, Cambridge).
3. Alberts B, *et al.* (2002) *Molecular Biology of the Cell* (Garland, New York).
4. Chang L & Karin M (2001) Mammalian MAP kinase signalling cascades. (Translated from eng) *Nature* 410(6824):37-40 (in eng).
5. Qi M & Elion EA (2005) MAP kinase pathways. *Journal of Cell Science* 118:3569-3572.
6. Lamb TD (1996) Gain and kinetics of activation in the G-protein cascade of phototransduction. *PNAS* 93(2):566-570.
7. Ferrell Jr JE (1996) Tripping the switch fantastic: how a protein kinase cascade can convert graded inputs into switch-like outputs. *Trends in Biochemical Sciences* 21(12):460-466.
8. Heinrich R, Neel BG, & Rapoport TA (2002) Mathematical Models of Protein Kinase Signal Transduction. *Molecular Cell* 9:957-970.
9. Thattai M & van Oudenaarden A (2002) Attenuation of noise in ultrasensitive signaling cascades. (Translated from English) *Biophysical journal* 82(6):2943-2950 (in English).
10. Kholodenko BN (2006) Cell-signalling dynamics in time and space. *Nat Rev Mol Cell Biol* 7(3):165-176.
11. Kholodenko BN (2003) Four-dimensional organization of protein kinase signaling cascades: the roles of diffusion, endocytosis and molecular motors. *Journal of Experimental Biology* 206(12):2073-2082.
12. Brown G, C. & Kholodenko BN (1999) Spatial gradients of cellular phospho-proteins. *FEBS letters* 457(3):452-454.
13. Kholodenko BN (2002) MAP kinase cascade signaling and endocytic trafficking: a marriage of convenience? *Trends in Cell Biology* 12(4):173-177.
14. Naka T, Hatakeyama M, Sakamoto N, & Konagaya A (2006) Compensation effect of the MAPK cascade on formation of phospho-protein gradients. *BioSystems* 83:167-177.
15. Markevich NI, Tsyganov MA, Hoek JB, & Kholodenko BN (2006) Long-range signaling by phosphoprotein waves arising from bistability in protein kinase cascades. *Mol Syst Biol* 2.
16. Slepchenko BM & Terasaki M (2003) Cyclin Aggregation and Robustness of Bio-switching. *Mol. Biol. Cell.* 14(11):4695-4706.
17. van Albada SB & ten Wolde PR (2007) Enzyme Localization Can Drastically Affect Signal Amplification in Signal Transduction Pathways. *PLoS Computational Biology* 3(10):1925-1934.
18. Stelling J & Kholodenko B (2009) Signaling cascades as cellular devices for spatial computations. *Journal of Mathematical Biology* 58(1):35-55.
19. Goldbeter A & Koshland DE (1981) An amplified sensitivity arising from covalent modification in biological systems. *Proceedings of the National Academy of Sciences* 78(11):6840-6844.

20. Pawson T (2007) Dynamic control of signaling by modular adaptor proteins. (Translated from English) *Curr. Opin. Cell Biol.* 19(2):112-116 (in English).
21. Kortum RL & Lewis RE (2004) The molecular scaffold KSR1 regulates the proliferative and oncogenic potential of cells. (Translated from English) *Mol. Cell. Biol.* 24(10):4407-4416 (in English).
22. Kholodenko BN (2000) Negative feedback and ultrasensitivity can bring about oscillations in the mitogen-activated protein kinase cascades. (Translated from eng) *European journal of biochemistry / FEBS* 267(6):1583-1588 (in eng).

5A. Supplement for Chapter 5

5A.1 Description of modifications to the simple model

Several modifications to our basic model are discussed in the text. These are explicitly enumerated below in more detail.

(1) The primary signal is constantly generated at the origin.

$$\frac{\partial c_S}{\partial t} = \frac{\partial^2 c_S}{\partial x^2} + \delta(x) \qquad \text{(S1)}$$

$$\frac{\partial c_{A^*}}{\partial t} = \frac{\partial^2 c_{A^*}}{\partial x^2} + Da \cdot r\left(c_{A^*}, c_S; \gamma\right)$$

$$c_S(x,0) = c_{A^*}(x,0) = 0$$

$$c_{A^*}(\pm\infty, t) = c_S(\pm\infty, t) = 0$$

The Damkohler number corresponds to those in the main text, except that c_s is scaled by RL^2 / D, where R is the rate of generation at the origin. Specifically, for kinetics far from saturation, $Da = kRL^4 / \left(K_m D^2\right)$; for zero-order ultrasensitive kinetics, it is $kRL^4 / (c_{A0} D^2)$. The parameter γ is $Dk_p c_p/(kRL^2)$.

(2) The primary signal is constantly generated at the origin; phosphatases homogenously deactivate the primary and secondary signals.

$$\frac{\partial c_S}{\partial t} = \frac{\partial^2 c_S}{\partial x^2} + \delta(x) - Da_p c_s \qquad \text{(S2)}$$

$$\frac{\partial c_{A^*}}{\partial t} = \frac{\partial^2 c_{A^*}}{\partial x^2} + Da \cdot r\left(c_{A^*}, c_S; \gamma\right)$$

$$c_S(x,0) = c_{A^*}(x,0) = 0$$

$$c_{A^*}(\pm\infty, t) = c_S(\pm\infty, t) = 0$$

$$Da_p = \frac{k_p c_p L^2}{D}$$

The Damkohler number Da and the parameter γ are as described in the first scenario.

(3) The primary mobile signal is generated at the origin by an exponentially decaying signal (I) permanently localized to the origin.

$$\frac{\partial c_S}{\partial t} = \frac{\partial^2 c_S}{\partial x^2} + Da_1 e^{-\frac{t}{\tau_{decay}}} \cdot (1 - c_s) \cdot \delta(x) \tag{S3}$$

$$\frac{\partial c_{A^*}}{\partial t} = \frac{\partial^2 c_{A^*}}{\partial x^2} + Da_2 \cdot r(c_{A^*}, c_S; \gamma)$$

$$c_S(x,0) = c_{A^*}(x,0) = 0$$

$$c_{A^*}(\pm\infty, t) = c_S(\pm\infty, t) = 0$$

$$Da_1 = \frac{k_s N_I L}{K_m^s D}$$

$$Da_2 = \frac{k_a c_{S0} L^2}{K_m^a D}$$

In these equations, N_I is the initial amount of the signal I in the region of size L; c_{S0} is the initial amount of inactive S in the system; τ_{decay} is the ratio of the decay time of I to the diffusion time.

For kinetics far from saturation (Equation 2 in the main text), we also conducted stochastic simulations with finite particle numbers. These were simple Monte Carlo simulations on a one dimensional grid with no excluded volume. The grid was initialized with N_{S0} molecules of the primary signal at the origin and the requisite number of inactive secondary signaling molecules randomly distributed throughout the system to achieve a number concentration of c_{A0}. At each time step, every molecule was given a chance, in random order, to hop to an adjacent site and, separately, to react, if possible. (This corresponds to a case of commensurate reaction and diffusion propensities.)

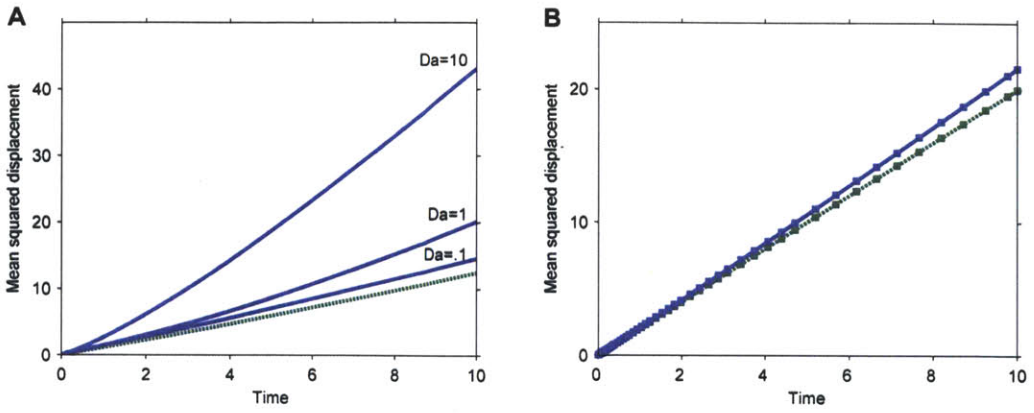

Fig. S1: Effect of primary signal activation by a decaying, immobile signal. Simulations correspond to Equation S3. (a) Slow decay (τ_{decay} = 10). Dashed line, primary signal (a representative curve is shown for clarity; the three cases are within 10% of this curve); solid lines, secondary signal. The Damkohler numbers of the first and second steps were chosen to be identical for the simulations. (b) Fast decay (τ_{decay} = .001). Parameters chosen so that the primary signal is generated in an initial burst (Da_1 = 1000; Da_2 = 1). Dashed line, primary signal; solid line, secondary signal; squares, simulations corresponding to the original model (Equation 1 in the main text) with the initial bolus of signal (N_{S0}) set to the amount of primary signal eventually generated in the case of fast decay.

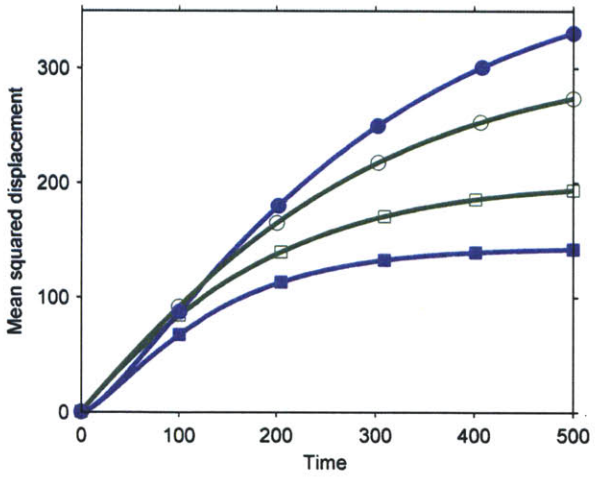

Fig. S2: The effect of phosphatases that deactivate the primary signal. Lines with squares, Da_p = 0.01; lines with circles, Da_p = 0.005; open symbols, primary signal; closed symbols, secondary signals. Other parameters: Da = 1.5; γ = 0.67.

Chapter 6

Conclusions and outlook

"Yes, she thought, laying down her brush
in extreme fatigue, I have had my vision."

Virginia Woolf, "To the Lighthouse"

Chapters 2 through 4 of this thesis span three different biological problems at three different scales of the immune system, ranging from individual molecular interactions to the population of T cells acting in concert. The projects recruit different techniques from engineering and physical sciences to understand these biological problems, including random walks and diffusion (chapter 2), decision theory and statistical inference (chapter 3), and large deviation theory (chapter 4).

In this conclusion, we seek to situate the three projects in larger areas of inquiry, which suggest constructive frameworks for applying techniques from engineering and the physical sciences to consider new problems in T cell immunology. One of these frameworks – spatiotemporal aspects of signaling – was introduced in Chapter 5.

6.1 Spatiotemporal aspects of signaling

Cells are not well-mixed bags of signaling molecules. Molecules are produced in different locations than their targets, setting up concentration gradients. Molecules cluster in rafts or islands. Organelles inside the cell, importantly the nucleus, provide structure.

Neither are cells static. Molecules diffuse on membranes and in the cytoplasm; they react with each other to form new species. Cytoskeletal motion provides driven transport of

membrane bound species; molecular motors drive motion of molecules in the cytoplasm. Entire cells migrate.

These length and time scales interact with each other to influence cellular responses. Understanding these interactions provides a key to understanding the complex spatiotemporal function of cellular signaling networks. In Chapter 2, we demonstrated how a competition between a time scale set by the on-rate between pMHC and TCR and a diffusive time scale relating to their separation led to biologically important consequences.

Consideration of these different scales, via scaling analysis, can suggest the different physical processes or structures that are relevant to any particular biological phenomenon. More broadly, however, explicit enumeration of all these possible scales generates hypotheses for predicting new mechanisms and explaining puzzling experimental data.

6.2 How cells gather and use information to make decisions

The diversity of length and time scales in immunological problems complicates mechanistic studies. Underneath its mechanistic complexity however, the immune system has two essential tasks: to collect information about what is self and what is foreign and to use that information to make decisions about the nature of its responses. From this viewpoint, the immune system is a group of statisticians playing games, communicating over telephone lines filled with static.

As previewed in Chapter 3, a variety of theories have been developed which can address such representations of biological systems, including information theory and decision theory (statistical inference). These powerful theories constitute systematic ways to confront the immune system's complexity. By thinking about the immune system's features in terms of how they affect the collection, transfer, and use of information, it

may be possible to advance a unifying framework that informs more detailed computational models and experimental work.

For example, there are important immunological questions pertaining to information collection and transfer. T cells have information about whether they should activate in specific contexts only because of developmental processes that shape a host's T cell repertoire. How are these developmental processes designed to encode information in the T cell interactions? This approach may elucidate the role of "mistakes" in these developmental processes, which has not been understood (that is, how do these "mistakes" affect the information transferred in later interactions?), and may clarify the interplay between developmental processes and post-development, peripheral processes (e.g. T regulatory cells; how does this interplay affect information transfer in T cell-APC interactions). Also, how do less context-specific sources of information (e.g. from innate immunity and cytokines) compensate for imperfect information in T cell interactions? Information theory has been used productively in biological contexts by Leibler and Bialek, for example.

Furthermore, the decisions that the immune system makes take many forms. In addition to decisions by effector cells about whether to activate (studied in Chapter 3), cells in the immune system must make lineage commitment decisions (e.g. effector and memory subsets). Because the information transmitted by the immune system is imperfect and incomplete, these are decisions under uncertainty. Moreover, these interactions are analogous to a game among different players in the immune system (different clonotypes of T cells, different cell types) and, less subtly, between the host and pathogen. How do immunodominant responses emerge? How are memory responses designed? How does the immune system confront rapidly mutating viruses like HIV? Each of these questions has to do with the decisions that T cells make. Applications of decision theory, including game theory, also have been useful in biological contexts. For example, Nowak and others have used game-theoretic techniques to investigate mechanisms that maintain biodiversity in ecosystems.

In this context, Chapter 3 is just one example of how such theories can illuminate T cell biology.

6.3 The surprising predictability of the unpredictable

Over the past several decades, the importance of stochasticity in reaction networks has been emphasized. Operating with small copy numbers over finite time scales, biological conditions are prime for stochastic effects. The limitations of approximations that neglect some or all of these fluctuations – the most famous is the deterministic approximation, which neglects all of them – have become apparent.

But when must stochastic fluctuations be considered? When do they change the qualitative biological function of a system, rather than just contributing to biologically irrelevant small fluctuations around otherwise deterministic behavior?

Furthermore, when the stochastic behavior does qualitatively differ from the deterministic behavior, with what accuracy must the stochastic fluctuations be considered to correctly capture the behavior of the system? Solutions to the master equation, either analytical or computational, capture all fluctuations, but do all possible fluctuations need to be considered?

Chapter 4 introduces a technique which neglects all but one fluctuation, the most probable fluctuation. Applying this technique to a biological system demonstrated how surprisingly predictable the unpredictable can be. Although many fluctuations are possible, only one occurs with appreciable probability, and it can be predicted without explicitly considering all fluctuations. Biological systems may not be as unpredictable as their small copy numbers might suggest.

That is, even though biological systems operate with small copy numbers over finite times, the entropy of biological systems (in state or trajectory space) may be small

enough to permit approximation. How the details of the reaction network and the copy numbers affect the entropy is a question that does not seem to be fully explored.

One appealing aspect of this approach is that explicit consideration of all possible fluctuations yields far more information than is usually useful. Biologically relevant questions often are related to the average time of a transition or the probability it will occur, or the average state of a system; the variance is also often of use. But rarely is the full distribution relevant, if only because such data is rarely available experimentally for comparison or prediction. Not only is wasted information wasted computation, explicit simulation of all fluctuations can often occlude the essential features of a phenomenon, burying them in pools of data. As we begin to understand how we can approximate the complex behavior of stochastic biological systems, we maybe able to gain more qualitative insight.